博士論文

Study on Ratcheting Occurrence Conditions of Piping under Seismic Loads

(地震荷重下の配管ラチェット発生条件に関する研究)

呂　金其

Jinqi LYU

Contents

Abstract

The accident occurred on March 11, 2011, at the Fukushima Daiichi nuclear power plant, which was followed by a massive earthquake and tsunami, was one of the most severe nuclear accidents in history. This accident has impacted the use of nuclear energy all over the world.

One of the essential lessons learned from the Fukushima Daiichi nuclear accident is that the mitigation of accident consequences for beyond design basis events (BDBEs), which are assumed to occur due to extreme conditions, becomes essential. Operation experiences indicate that events that are outside of the design basis may result in severe consequences. Those events, which are categorized as BDBEs, have a low likelihood of occurrence and are characterized by large uncertainties. The consideration of BDBEs is an essential component of the defense approach in ensuring nuclear safety. Requirements and required functions are different between design basis events (DBEs) and BDBEs. Requirements for DBEs are safety, availability, and serviceability; therefore, any failure should be prevented. However, requirements for BDBEs are safety and resilience; therefore, limited failure locations are allowable, and failure consequences should be mitigated. For BDBEs, the prediction of actual failure phenomena is necessary to find weak points and determine effective countermeasures. The design guided by conventional approaches may be feasible and reasonable; however, it is too conservative for BDBEs and is not optimal in terms of cost and performance. Therefore, conservative methods are not suitable to predict actual failure locations and their order under BDBEs.

Countermeasures for BDBEs require the best strength evaluation methods of nuclear power plant components. Therefore, it is necessary to clarify the dominant failure modes under different extreme loads, which includes the identification of probable failure modes as well as the occurrence conditions of these failure modes. The current study focuses on ratcheting, which is one dominant failure mode of piping under seismic loads. The strain accumulating in the direction of the applied stress causes the occurrence of ratcheting and may cause more severe failures of structures consequently (e.g., collapse). Therefore, it is essential to identify the occurrence conditions of ratcheting, as considered in many design criteria. Those criteria require

the structures to remain below the defined ratcheting boundaries. However, current methods determining the ratcheting boundary only considers the constant pressure load with varying thermal loads. They are not suitable for the progressive deformation due to excessive seismic loads, especially when considering the mitigation of accident consequences under BDBEs. Therefore, investigating the ratcheting behavior under excessive vibrations with reasonable accuracy is necessary for engineering reference.

Two types of models were included in this study: the beam model and the piping model. The beam model was under consideration to identify the basic mechanisms of the occurrence conditions of ratcheting due to strong vibrations and compare thermal ratcheting (the Bree diagram and the Yamashita diagram) with vibration ratcheting. The analyses of the piping model were extended to the mechanisms to realistic structures. These two models are closely connected. For example, for a hollow cylinder, if the wall thickness is much less than the mean radius, the effects of curvature may be neglected. Therefore, the thin cylinder may be regarded as a two-dimensional beam model. The characteristic of seismic loads is ambiguous so that the classification of seismic load characteristics with frequency effect was also under consideration. Besides, this study also tried to propose countermeasures against ratcheting for engineering reference.

Chapter 2 focused on clarifying the ratcheting mechanism of beams subjected to the combination of gravity and seismic loads. Thermal ratcheting was compared to clarify the characteristics of seismic loads. Seismic ratcheting occurred due to the combination of load-controlled load (e.g., gravity) and alternative cyclic accelerations. The criterion to judge the occurrence condition of ratcheting was decided to be 1% plastic strain accumulated during 100 cycles of sinusoidal waves at the root part of the specimen. The material was decided to be the lead alloy due to the realization of ratcheting by the small size shaking table in the laboratory and safety concerns during experiments. Besides, the stress-strain curve of the lead alloy has a similar trend to the steel but much smaller yield stress. Dynamic inelastic finite element analyses were performed on a beam-shaped model under different loading conditions. FINAS/STAR did the finite element analyses (FEA) with the aid of the mesh generation by FEMAP. Three types of vibrations were

applied to the beam model: sinusoidal excitations, superposition of two sinusoidal acceleration excitations, and seismic excitations. Experiments were carried out to validate the analytical analyses of the seismic excitations partially. Characteristics of seismic loads between load-controlled and displacement-controlled properties were studied from the viewpoint of the frequency ratio of forcing frequencies to natural frequencies. All the results were placed in a non-dimensional diagram, which was similar to the Bree diagram, to clarify ratcheting occurrence conditions.

In Chapter 3, experimental and numerical analyses were performed on bent solid bars, which represented piping. Two types of loads were applied to the piping model. The first one was the external compressive force at the ends of the piping model, which acted as the load-controlled force and caused primary bending stress. The second load was cyclic accelerations from the shaking table, acting as the source of alternating dynamic loads. The nonlinear stress-strain curve of the Pb99%-Sb1% alloy, which was from the tensile test at room temperature at the authors' laboratory, was applied in numerical analyses. Both kinematic and isotropic hardening rules were included in this study. The piping models were divided into two categories: the piping model without additional supports (Piping-N) and the piping model with three supports in the medium part (Piping-S). For the piping model, the criterion of ratcheting it was determined to be a 0.5% plastic strain at the extrados of the elbow accumulated during 50 sinusoidal cycles. Characteristics of seismic loads were studied from the viewpoint of the frequency ratio of the forcing frequency over the natural frequency of the piping model. Besides, the effect of supports on the occurrence of ratcheting was also considered in this chapter.

Chapter 4 focused on the comparison of the ratcheting occurrence conditions between the beam model and the piping model, together with the Bree diagram and the Yamashita diagram. This chapter proposed one normalized vibration ratcheting diagram to show and compare ratcheting occurrence conditions with different materials and shapes. The final chapter presented the general conclusions on the occurrence of ratcheting. In addition, countermeasures against ratcheting were also proposed in this chapter.

Keywords

Ratcheting, Seismic load, Frequency ratio, Support, Gravity, Piping, Beam

List of Figures

List of Tables

Chapter 1. Introduction

On March 11th, 2011, a catastrophic earthquake and tsunami caused one of the most severe nuclear accidents ever experienced in history at the Fukushima Daiichi nuclear power plant. This accident has influenced the nuclear industry profoundly all over the world. Addressing the accident, both in terms of its immediate or long-term consequences and the application of corrective actions from lessons learned to prevent a recurrence of such accident, became necessary for the whole nuclear industry in all countries with nuclear power plants [1][2][3][4][5][6][7].

1.1 Requirements after Fukushima Daiichi nuclear accident

1.1.1 Design basis events (DBEs) and beyond design basis events (BDBEs)

Understanding and using lessons learned from applicable service experience is a significant part of good design. One essential lesson learned from the Fukushima Daiichi nuclear accident is that the mitigation of accident consequences for beyond design basis events (BDBEs), which possibly occur under excessive seismic loads, becomes essential [8][9][10].

1.1.1.1 Design basis events (DBEs)

“Design basis events (DBEs)” causes accident conditions regulated by established design criteria and conservative methodologies. Those conditions should make sure that releases of radioactive material should be kept within acceptable limits. This concept has been applied in many standards or codes for many years. The requirements for DBEs have been established and are thought to be very conservative to avoid severe accidents [11]. Nuclear power plant operation experiences show that during the lifetime, the events defined within the DBEs have some probabilities of occurrence. However, the consequences of DBEs are usually within acceptable limits [12].

1.1.1.2 Beyond design basis events (BDBEs)

On the other hand, operation experiences also indicate that the events, which are beyond the design basis, would result in terrible consequences. Those accidents are thought to have a low likelihood of occurrence and are characterized by large uncertainties. Those events are called "beyond design basis events" (BDBEs). The consideration of BDBEs is an essential part of the defense approach in ensuring nuclear safety.

Requirements and required functions are different between DBEs and BDBEs, as shown in Table 1-1 [13]. Requirements for DBEs are safety, availability, and serviceability; therefore, any failure should be prevented. However, requirements for BDBEs are safety and resilience; therefore, limited failure locations are allowable, and failure consequences should be mitigated.

Table 1-1 Comparison between DBEs and BDBEs

	DBEs	BDBEs
Requirements	Failure prevention for safety, availability, and serviceability.	Failure mitigation for safety and resilience.
Performance	Any failure modes should not occur. Easy inspection is required.	Unstable failure modes, such as fractures, should not occur. The sequence of chain failure should be verified. Limited failure locations are allowable.
Failure modes	Stable failure modes (deformation, fatigue, etc.) and unstable failure modes (fracture, collapse, etc.).	Unstable failure modes (fracture collapse, etc.), chain failure.
Risk assessment	Focus on probability.	Find relatively weak points. Focus on consequent damage.
Performance evaluation and evaluation method	Conservative evaluation for assumed failure modes. Focus on each component.	Best estimation for actual failure modes. Focus on the system failure sequence.
Performance improvement	Risk-informed optimization of design, fabrication, and maintenance (graded approach).	Fracture control, according to the failure mode sequence. Risk-informed combination of fracture control with accident management.

Performance and related failure modes are different according to requirements. Under DBEs, any failure modes, including stable and unstable failure modes, should be prevented. Design codes for DBEs provide conservative allowable limits. Also, it is required to add enough margin to the actual strength of the nuclear power plant components to avoid any failure. Therefore, the exceedance of those limits does not mean actual failures. On the other hand, for BDBEs, only unstable failure modes (fracture, collapse, etc.) are not allowed.

Consideration of failure modes is also different between DBEs and BDBEs (Figure 1-1). Under BDBEs, stable failure modes (e.g., deformation and local boundary failure) can extend to unstable failure ones (e.g., the collapse). Such chain failure sequences should be blocked. Therefore, it is essential to understand their ultimate behavior and take reasonable countermeasures according to the strength estimation of the components to avoid the severe failure of structures [14]. The objectives of risk assessment are also different. Viewpoint for DBEs focuses on probability. In contrast, the purpose of BDBEs is to find relatively weak points with attention to consequent damage [13].

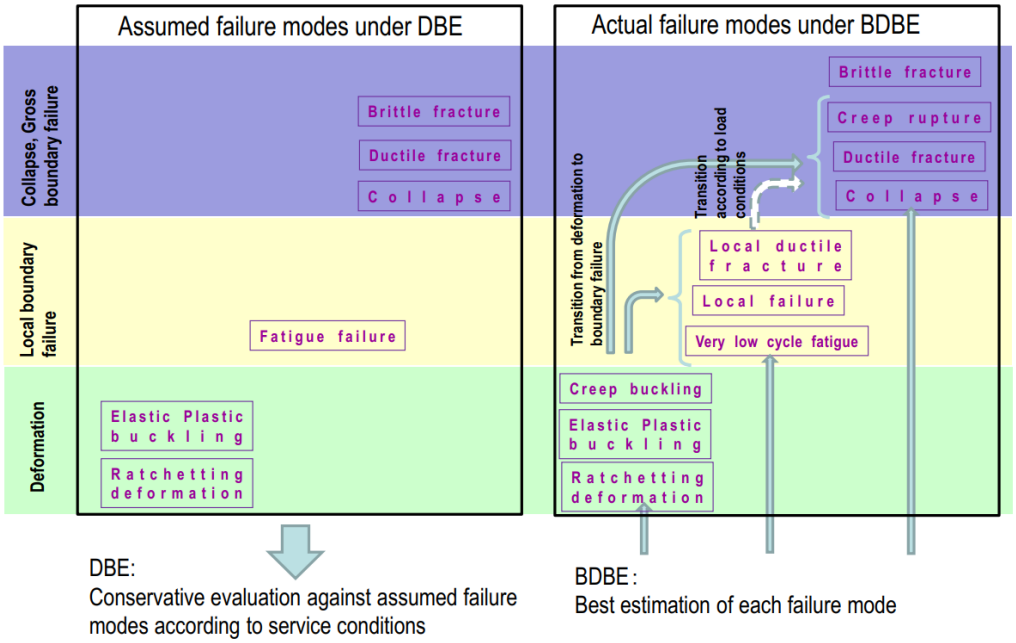

Figure 1-1 Different considerations of failure modes between DBEs and BDBEs

1.1.1.3 Design extension conditions (DECs)

One subset of BDBEs is known as design extension conditions (DECs). The definition of DECs was introduced in IAEA Specific Safety Requirements No. SSR-2/1 (Rev. 1) to improve the safety and security of nuclear power plants by improving the plant's capability to withstand the conditions caused by BDBEs [15]. In IAEA SSR-2/1 (Rev. 1), DECs are accident conditions that are not included for DBEs. Instead, DECs are considered in the design process for the firmness of facilities by best estimate methodologies (Figure 1-2).

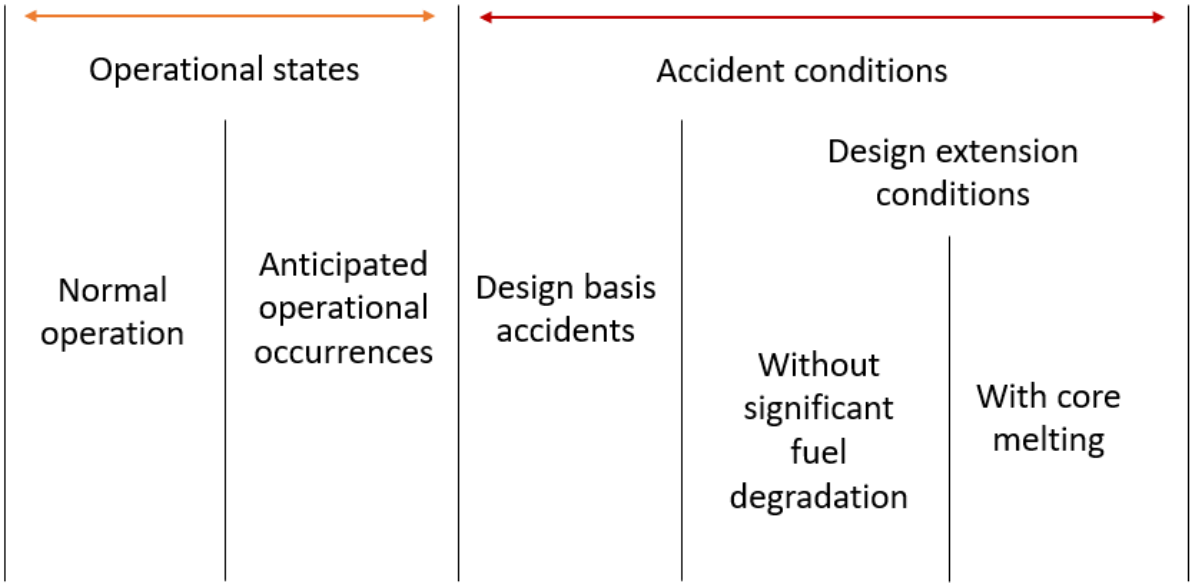

Figure 1-2 Revised definitions of plant states in IAEA SSR-2/1 (Rev. 1)

Under DECs, releases of radioactive material should be kept within acceptable limits [16]. Requirement 5.28 of IAEA SSR-2/1 (Rev. 1) specifies that the DECs shall be used to define the design specifications for safety concerns and the design of all aspects essential to safety. Considering DECs help to prevent some severe conditions from arising. If they do arise, the consideration of DECs can also contribute to control them within acceptable limits and to mitigate their consequences. DECs could include severe accident conditions. Besides, plant states cover DECs in IAEA SSR-2/1 (Rev. 1). In contrast, in IAEA Safety Standards Series No.

NS-R-1 published in 2000, the whole part of BDBEs was not included in the design basis [17]. The difference between SSR-2/1 (Rev. 1) and NS-R-1 is shown in Figure 1-3.

IAEA, NS-R-1, "Safety of Nuclear Power Plants: Design," 2000.

<table>
<tr><td colspan="2">Operational States</td><td colspan="3">Accidental Conditions</td></tr>
<tr><td rowspan="2">Normal Operation</td><td rowspan="2">Anticipated Operational Occurrence</td><td rowspan="2">Design Basis Accidents</td><td colspan="3">Beyond Design Basis Accidents</td></tr>
<tr><td>No core degradation</td><td>Severe Accidents</td></tr>
<tr><td>1st level DiD</td><td>2nd level DiD</td><td>3rd level DiD</td><td colspan="2">4th level DiD</td></tr>
<tr><td colspan="3">Included in the design basis</td><td colspan="2">Beyond design basis</td></tr>
</table>

IAEA, SSR-2/1 (Rev. 1), "Safety of Nuclear Power Plants: Design," 2016.

<table>
<tr><td colspan="2">Operational States</td><td colspan="3">Accidental Conditions</td><td rowspan="3">Conditions practically eliminated</td></tr>
<tr><td rowspan="2">Normal Operation</td><td rowspan="2">Anticipated Operational Occurrence</td><td rowspan="2">Design Basis Accidents</td><td colspan="2">Design Extension Conditions</td></tr>
<tr><td>Without fuel degradation</td><td>With fuel degradation</td></tr>
<tr><td>1st level DiD</td><td>2nd level DiD</td><td>3rd level DiD</td><td>3rd or 4th level DiD</td><td>4th level DiD</td><td></td></tr>
<tr><td colspan="4">Included in the design basis</td><td colspan="2">Beyond design basis</td></tr>
</table>

Figure 1-3 Comparison between SSR-2/1 (2016) and NS-R-1 (2010)

The consideration of DECs is supposed to enhance the safety features based on the engineering judgment and the probabilistic assessment [18]. The engineering judgment derives from research results, lessons learned from accidents, and operating experiences. The application of probabilistic insights is vital in recognition of DECs.

When designing pieces of equipment for DECs, the loads are often treated similarly as those for DBEs. However, according to the definition of DECs in IAEA SSR-2/1 (Rev. 1), the best estimate methodology for determining environmental conditions is also necessary. Stress limits

that are used to justify the feasibility of equipment are supposed to be less conservative than those used for design basis conditions. The judgment of feasibility would be decided according to reasonable expectations for the performance of the equipment. Besides, IAEA SSR-2/1 (Rev. 1) also requires that external hazards should be considered in the design by assuming appropriate amplitudes, load combinations, and margins for equipment under design basis conditions.

1.1.2 Defence in depth

Defence in depth (DiD) is a concept applied to optimize nuclear safety for many years. It is used in the design of nuclear facilities, the assessment of such designs, and all aspects of their regulation [19]. For example, the IAEA SSR-2/1 (Rev. 1) sets a specific requirement for the design: “Requirement 7: Application of defence in depth. The design of a nuclear power plant should incorporate defence in depth. The levels of defence in depth should be independent as far as is practicable.”

Table 1-2 Levels of defence in depth for new nuclear power plants

Level of Defence (Approach 1)		Objective	Essential design means	Essential operational means	Level of Defence (Approach 2)	
Level 1		Prevention of abnormal operation and failures	Conservative design and high quality in the construction of normal operation systems, including monitoring and control systems	Operational rules and normal operating procedures	Level 1	
Level 2		Control of abnormal operation and detection of failures	Limitation and protection systems and other surveillance features	Abnormal operating procedures/emergency operating procedures	Level 2	
Level 3	3a	Control of design basis accidents	Engineered safety features (safety systems)	Emergency operating procedures	Level 3	
	3b	Control of design extension conditions to prevent core melt	Safety features for design extension conditions without core melt	Emergency operating procedures	4a	Level 4
Level 4		Control of design extension conditions to mitigate the consequences of severe accidents	Safety features for design extension conditions with core melt. Technical Support Centre	Supplementary emergency operating procedures/severe accident management guidelines	4b	
Level 5		Mitigation of radiological consequences of significant releases of radioactive materials	On-site and off-site emergency response facilities	On-site and off-site emergency plans	Level 5	

The DiD concept has been reinforced after the Fukushima accident with a revised description of all five levels. The introduction of the DECs represents the main difference with the original definitions in INSAG-10 [10]. The description of the levels of DiD for the design of nuclear power plants is presented in Table 1-2 [18]. Since currently there is a discrepancy with the association of DECs without fuel degradation, DECs are placed in the 3rd or 4th level of DiD. From the table, it is evident that provisions should be implemented in the design to eliminate the possible severe failures, reduce the possibilities, and deal with their consequences.

1.1.3 Risk reduction approaches

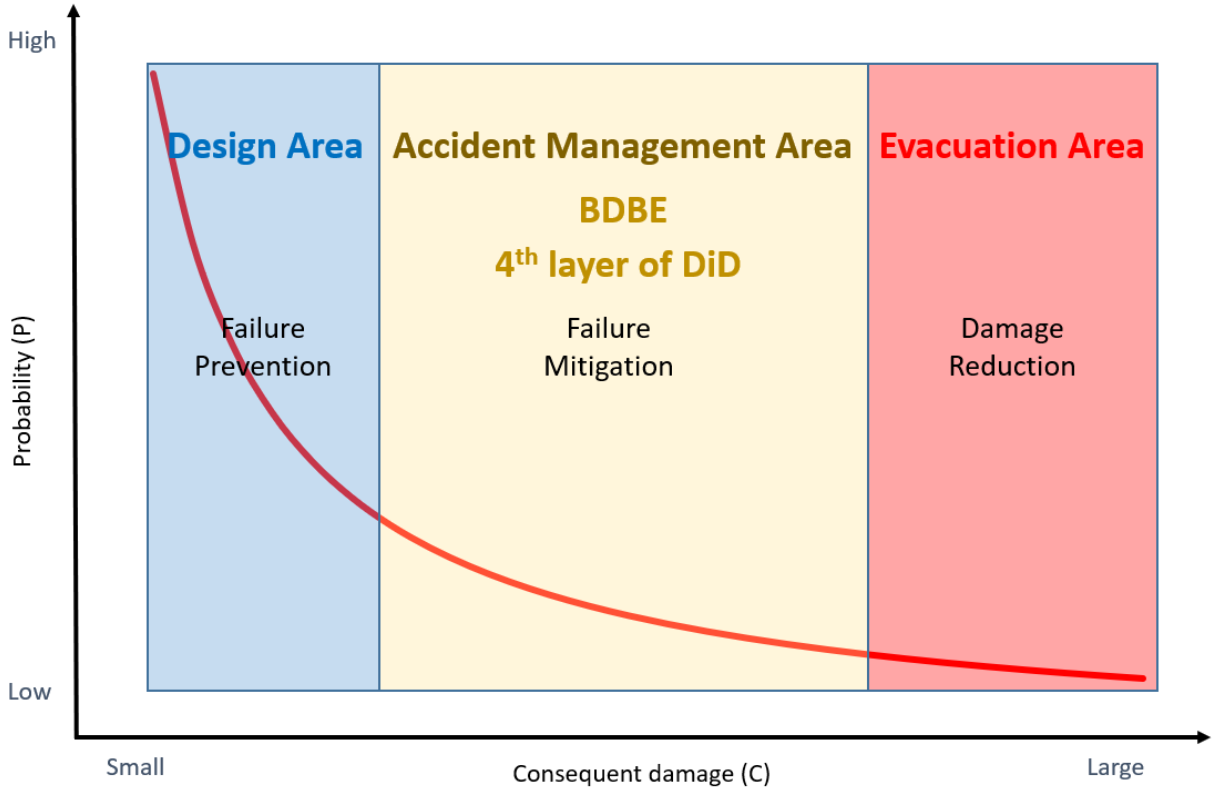

Figure 1-4 Risk reduction scheme

Efficiencies of risk reduction approaches are different according to risk stages [5]. Therefore, multi-stage countermeasures become suitable according to the performance of each level. The relationship between probability (P) and consequent damage (C) is shown in Figure 1-4. There

are three risk stages in this figure – design area, accident management area and evacuation area. The design area has higher risk probabilities with lower consequent damages. Therefore, at this level, the reduction of probabilities by failure prevention is efficient. In contrast, a suitable way for the evacuation area is the reduction of consequent damage. The intermediate region is accident management, where BDBEs would occur. This area is categorized as the 4th layer in the concept of Defence in Depth.

1.1.4 Fracture control

Previous efforts in the structural strength field mainly focused on the design area. There are few suitable approaches applied to the beyond design area. Therefore, there is a large gap between the design area and the beyond design area in structural strength fields [20]. Unlike the conventional design approaches for DBEs, understanding the ultimate failure modes, and conducting adequate countermeasures based on the rational strength estimation of the components under BDBEs are necessary to prevent the severe failures of structures [14].

The concept of fracture control has been proposed and applied to mitigate the accident consequences of nuclear power plants from the viewpoint of structure and material fields [13] [20]. An example is shown in Figure 1-5. For piping under excessive earthquakes, the ratcheting deformation and crack initiation consume considerable vibration energy. That consumption can help to avoid the collapse or break of pipes. Therefore, severe failures can be prevented by energy release due to prior small-scale failures. One key issue for fracture control is the identification of failure locations with their failure modes, which means adequate consideration of failure modes is necessary. Fracture control requires relative strength evaluation for different failure modes, which is more feasible than conducting the precise strength evaluation for different failure modes. When the order of failure locations and modes can be identified, fracture control becomes available to enable effective accident management [13].

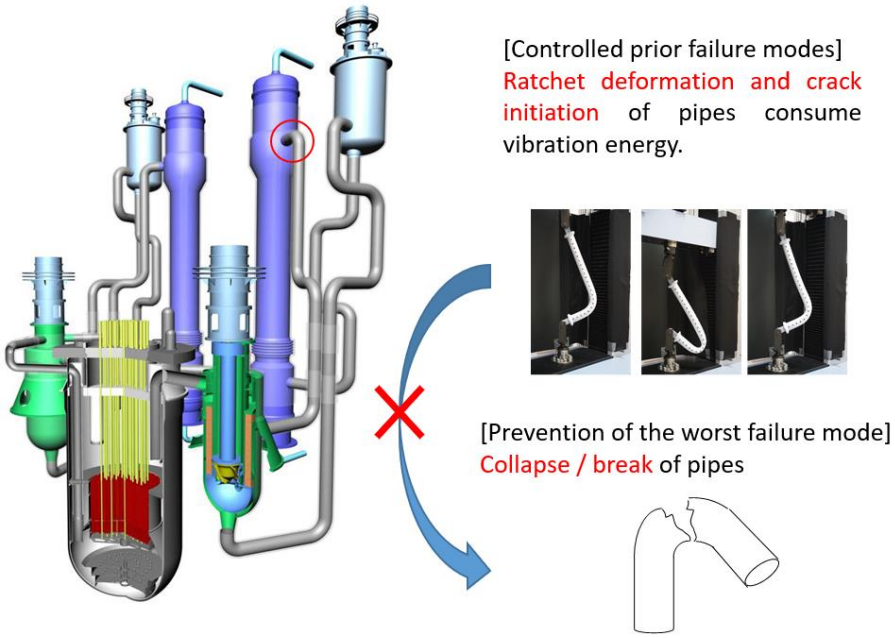

Figure 1-5 Prevention of collapse and break of pipes under excessive earthquake

1.2 Seismic loads and related failure modes

The 2011 earthquake off the Pacific coast of Tōhoku increases the researcher's interest in the seismic safety of nuclear power plant facilities [21]. Typically it is impossible to predict the occurrence time and intensity of natural disasters [22][23]. Therefore, when designing structures, the expectation of deforming beyond the elastic limit during infrequent devastating vibrations in earthquake-prone regions with adequate margins introduced at different stages of design, analysis, qualification, and construction is included. Thus, for nuclear power plants built in areas where strong earthquakes frequently occur, the inelastic response is necessary to study [24].

1.2.1 Adequate consideration of failure modes

The Fukushima accident reinforced the need for the capability to safely withstand the full range of external and internal events to which it is supposed to be exposed [19]. IAEA SSR-2/1 (Rev. 1) requires the identification of external hazards. The evaluation of their effects, especially the assumed events and generated loads, are also necessary for the design. Causation and likelihood

should be under consideration in possible assumptive hazards. Besides, an adequate margin should be provided against external hazards. The safety margins to be taken depends on specific attributes of these hazards. The important factors include the possibility of causing disastrous accidents and the uncertainties in the assessment. Combinations of events, such as a tsunami following an earthquake, should also be taken into consideration.

According to the different requirements shown in Table 1-1, the structural strength, which is defined as the strength to satisfy the required performance, is also different. Design codes for DBEs provide a conservative allowable limit. Therefore, the exceedance of those limits does not mean actual failure. In contrast, for BDBEs, the prediction of actual failure phenomena is necessary to find weak points and determine effective countermeasures. Conservative methods are not appropriate to predict practical failure locations and their occurrence sequences. According to IAEA SSR-2/1 (Rev. 1), strategies for BDBEs require precise estimate methodologies based on practical failure phenomena in the design process. For DECs with significant fuel degradation, the uncertainties are highly possible to exceed those for DBEs. Therefore, safety margins should be expanded for DECs.

In terms of structural design, nuclear power plant components need to be enhanced to mitigate severe accidents and eliminate accident sequences that may cause a large radioactive release [25]. For previse estimation, it is necessary to elucidate failure modes under extreme loads such as high temperature, high pressure, and excessive earthquakes. Since such events are rare, it is significant for designers to know the dominant failure modes at extreme loads. Predicting and controlling severe nuclear accident modes requires the identification of possible failure modes and the clarification of occurrence conditions of such failure modes [26].

1.2.2 Load-controlled stress and displacement-controlled stress

Stresses can be classified into two types related to failure modes (Figure 1-6): load-controlled stress (primary stress) and displacement-controlled stress (secondary stress) [27]. The main characteristic of load-controlled stress is that plastic instability occurs without the additional

external force. The representative load-controlled stresses are internal pressure and dead weight. In contrast, for displacement-controlled stress, plastic deformation does not grow indefinitely unless the external load is increased. One example of displacement-controlled stress is thermal stress. Seismic loads are thought to have both load-controlled and displacement-controlled characteristics. Therefore, it is essential to clarify the features of seismic loads to avoid related failure modes.

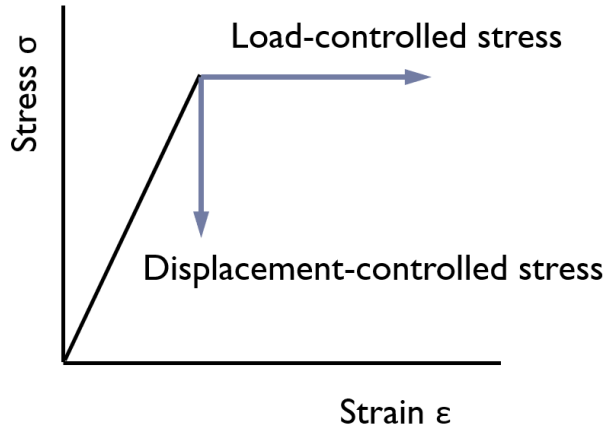

Figure 1-6 Difference between load-controlled and displacement-controlled stress

1.2.3 Nuclear power plants under seismic loads

One requirement of the design for nuclear facilities is earthquakes, and other external events will not endanger the safety of the plant [28].

1.2.3.1 Seismic evaluation in codes

Many codes and specifications include seismic evaluation in the design progress of nuclear power plant components. For example, ASME B&PV III NB-3592.3 required that an analysis, when required by the Design Specification, shall be performed based on static forces resulting from equivalent earthquake acceleration acting at the centers of gravity of the extended masses [29]. In addition, EPRI provides guidelines for the safety of the nuclear power plant under earthquakes [30]. The guidelines provide for pre-earthquake planning and progressive response

to an earthquake. The responses include recommended immediate actions, as well as post-shutdown and longer-term actions.

1.2.3.2 Failure modes under seismic loads

There are many studies on failure modes under seismic loads, and more or less, those studies have found that low cycle fatigue failure, collapse, ratcheting, and their combinations are probable failure modes. However, it is found that the occurrence conditions of those failure modes are not clear yet.

Experimental evaluations showed that the types of failure modes caused by seismic loads are collapse, brittle fracture, low cycle fatigue, and so on [31]. Besides, fatigue ratcheting and ratcheting buckling are also important failure modes for pipe structures.

Figure 1-7 Setup in JNES tests [32]

Japan Nuclear Energy Safety Organization (JNES) conducted tests for several types of nuclear reactor facilities by one large-scale shaking table (Figure 1-7). They found that the main failure modes were low cycle fatigue and ratcheting [32].

Electric Power Research Institute (EPRI) performed the component tests focusing on the dynamic behavior and failure mode of pressurized piping components (Figure 1-8). They found that among 32 failed cases, the failure mode of 30 cases is fatigue with ratcheting. The failure mode of the rest two is collapse with ratcheting [33].

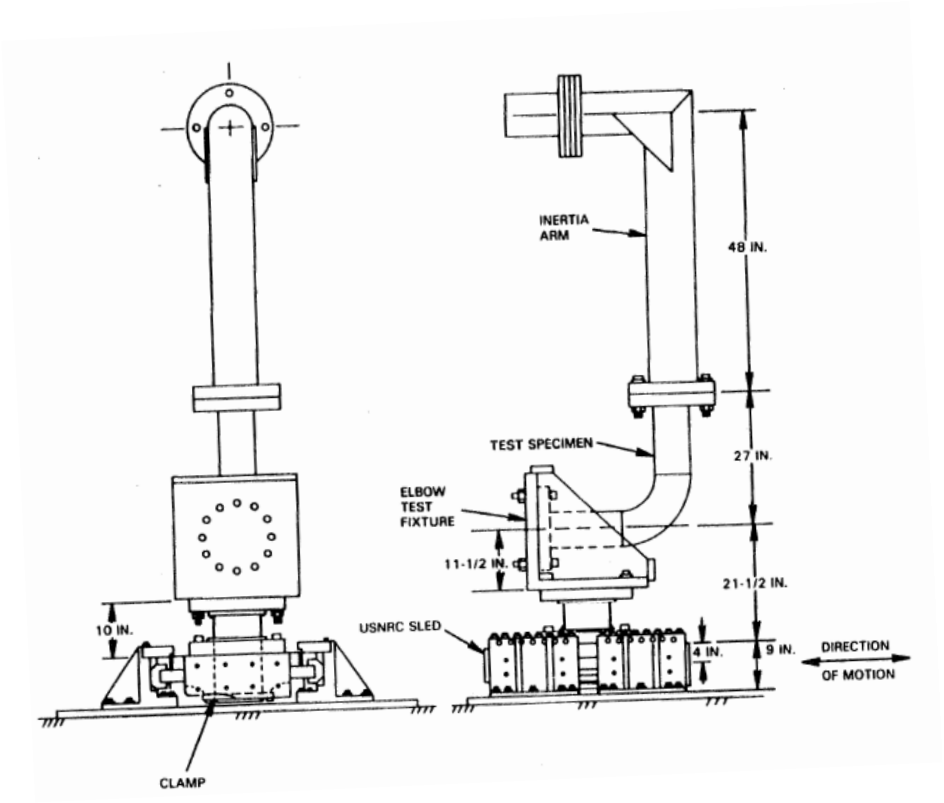

Figure 1-8 Setup in EPRI tests [33]

1.2.4 Failure modes of piping systems

The piping system is one crucial part of nuclear power plants and is thought to be the vulnerable components under extreme seismic events. Unlike the DBEs, BDBEs require the best estimation

methods against seismic loads. For this purpose, knowing the dominant failure modes of the structure is essential to make adequate preparation for seismic loads.

ASME B&PV III NB-3622.3 mentioned that: Piping shall be arranged and supported so that vibration will be minimized. The designer shall be responsible, by design, and by observation under startup or initial service conditions, for ensuring that the vibration of piping systems is within acceptable levels [29].

Plastic-collapse is one postulated failure mode under seismic loads in the conventional design rules. In contrast, the fatigue failure is the most probable failure mode from the various previous studies on piping systems made of steel even when input accelerations were much higher than the design allowed limit [33][34][35][36]. Failure mode other than fatigue failure may occur under the extreme loading condition, although it is rare [33].

National Research Institute for Earth Science and Disaster Resilience (NIED) conducted experiments on failure behaviors of elbow pipes made of simulation materials to clarify the possible failure modes under beyond design level seismic loads. The strength of the simulation materials was much lower than that of the steel; therefore, the experiments under the extreme loading condition were enabled with the existing testing facilities. That research found that the most typical failure mode from shaking table tests was the ratchet and subsequent collapse (Figure 1-9). Several factors, such as the configuration of the piping system, input frequency, additional mass weight, input acceleration level, were thought to affect the failure modes [37]. The experimental results indicated that it was crucial to understanding the structure's ultimate behavior when treating BDBEs, and the investigation procedure using simulation materials was effective to investigate the ultimate behavior of piping systems.

Initial status | After first excitation (ratchet) | Final status (collapse)

Figure 1-9 Typical failure process of the inverted type specimen (ratchet and subsequent collapse) [37]

1.3 Literature review on ratcheting

Ratcheting is a progressive incremental inelastic deformation or strain which can occur in a component that is subjected to variations of mechanical stress, thermal stress, or both [29]. There are many studies on ratcheting [38][39][40][41]. Ratcheting is one possible failure mode under excessive earthquakes. Since ratcheting is possible to lead to rupture ultimately, it is essential to clarify the loading conditions which enable ratcheting to occur. Pressurized piping systems are the most basic structures in nuclear power plants and are normally subjected to variable thermal and mechanical loads with cyclic nature. As described in Section 1.1, for BDBEs, the ratchet is acceptable, and collapse should be prevented [13].

However, current methods determining the ratcheting boundary only consider the constant pressure load with varying thermal loads such as the Bree diagram. They are not suitable for the progressive deformation due to the excessive seismic load, especially when considering the mitigation of accident consequences for BDBEs. Therefore, investigating the ratcheting behavior under excessive vibrations with reasonable accuracy is necessary for engineering reference.

In this section, the Bree diagram, and the Yamashita diagram, which were referred to in this research, were introduced.

1.3.1 Cylinder model (the Bree diagram, membrane-bending ratcheting model)

The Bree diagram describes the ratcheting mechanism of a pressurized cylinder (Figure 1-10) subjected to cyclic thermal stress (Figure 1-11). In this diagram, various regimes of structural behavior were clarified as with magnitudes of the thermal stress and pressure stress. Thermal ratcheting occurred due to the combination of load-controlled stress (primary membrane stress) and displacement-controlled stress (secondary bending thermal stress). Bree diagram is now applied in the ASME code for class-1 components for the light water reactor as well as the fast breeder reactor at the evaluated temperature [42].

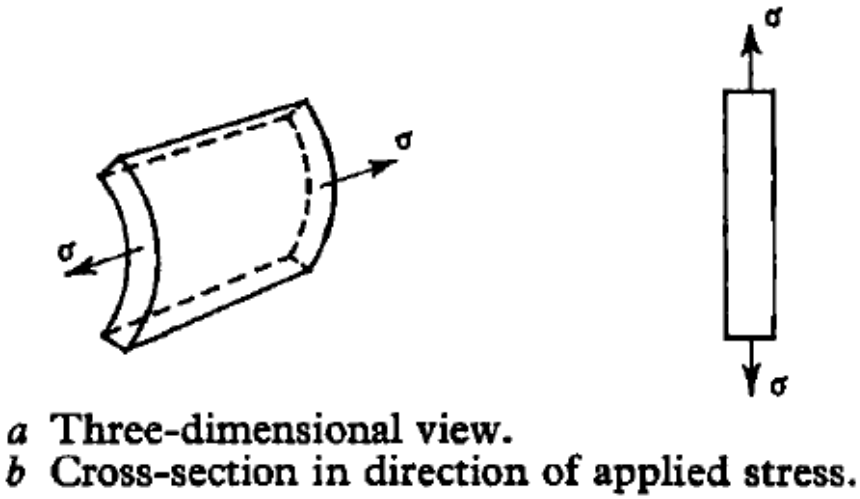

a Three-dimensional view.
b Cross-section in direction of applied stress.

Figure 1-10 Uniaxial stress model of a cylinder [43]

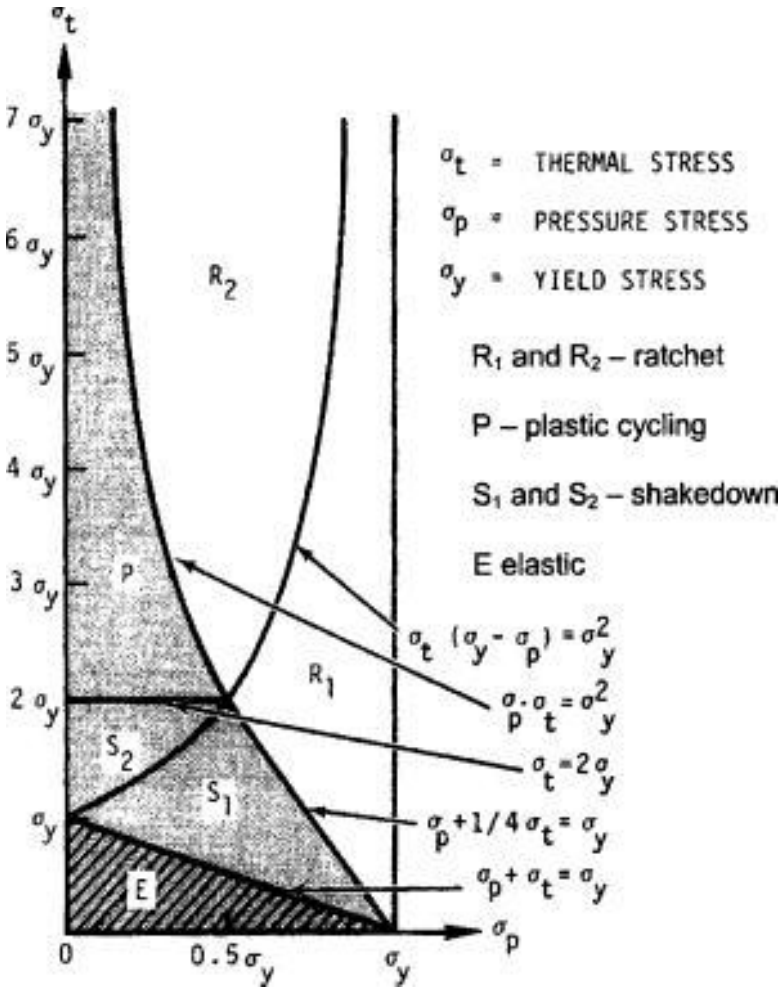

Figure 1-11 Bree diagram [43]

Though in this study, the specimen was subjected to vibrations, the Bree diagram was referred to and compared to investigate the difference between thermal ratcheting and vibration ratcheting. If dividing the pressure stress (σ_p) and the thermal stress (σ_t) by the yield stress (σ_y), the Bree diagram can be transformed to be a non-dimensional form, as shown in Figure 1-12. In this figure, the X value is the ratio of the pressure stress to the yield stress (Equation 1-1), and the Y value is the ratio of the peak of elastic thermal stress to the yield stress (Equation 1-2). The non-dimensional form is also used in this research.

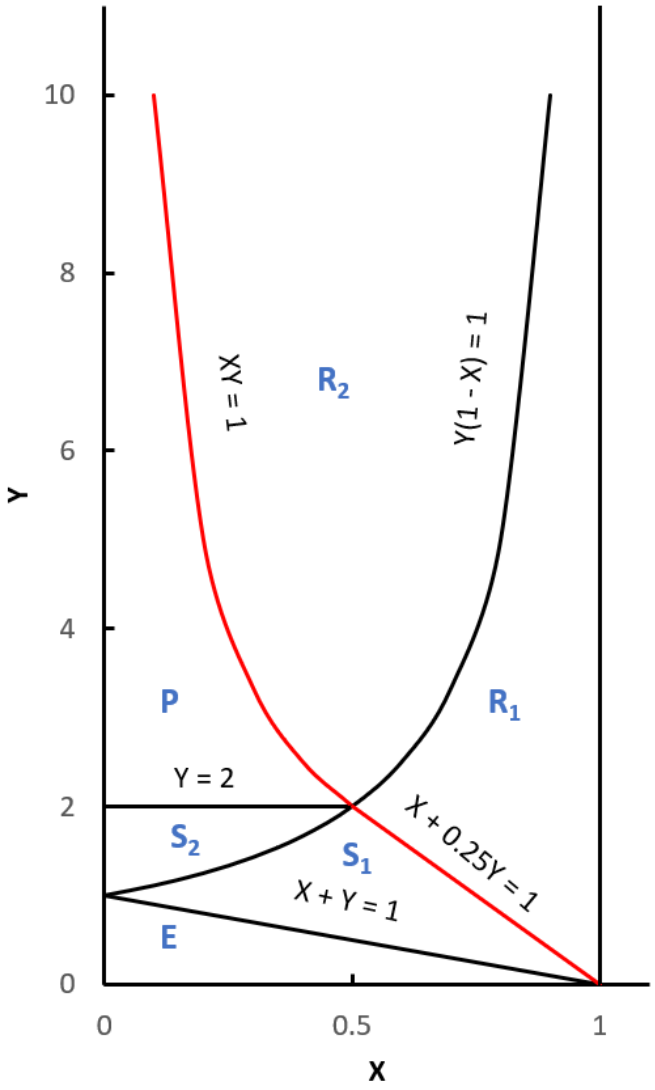

Stress regime	Can behavior
R_1 and R_2	Ratcheting
S_1 and S_2	Shakedown after first half-cycle
P	Plastic cycling
E	Elastic

Figure 1-12 Bree diagram in non-dimensional from

$$X = \frac{\sigma_p}{\sigma_y} = \frac{Pressure\ stress}{Yield\ stress} \qquad \text{Equation 1-1}$$

$$Y = \frac{\sigma_t}{\sigma_y} = \frac{Thermal\ stress}{Yield\ stress} \qquad \text{Equation 1-2}$$

1.3.2 Beam model (the Yamashita diagram, bending-bending ratcheting model

A similar theoretical ratcheting study for beam (Figure 1-13), which is known as the "bending-bending" ratchet diagram (Figure 1-14), was conducted by Yamashita et al. The primary bending stress was from the uniformly distributed constant lateral force. The secondary bending stress was due to cyclic lateral deflection [44]. There are many similarities between Bree diagram and Yamashita's "bending-bending" ratchet diagram. At some point, the "bending-bending" ratchet diagram is one kind of extension of the Bree diagram.

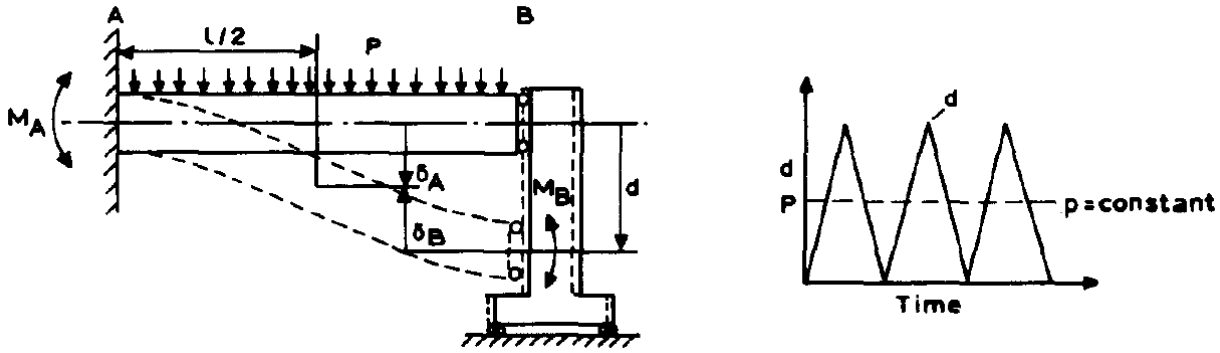

Figure 1-13 Rectangular-beam model for ratcheting [44]

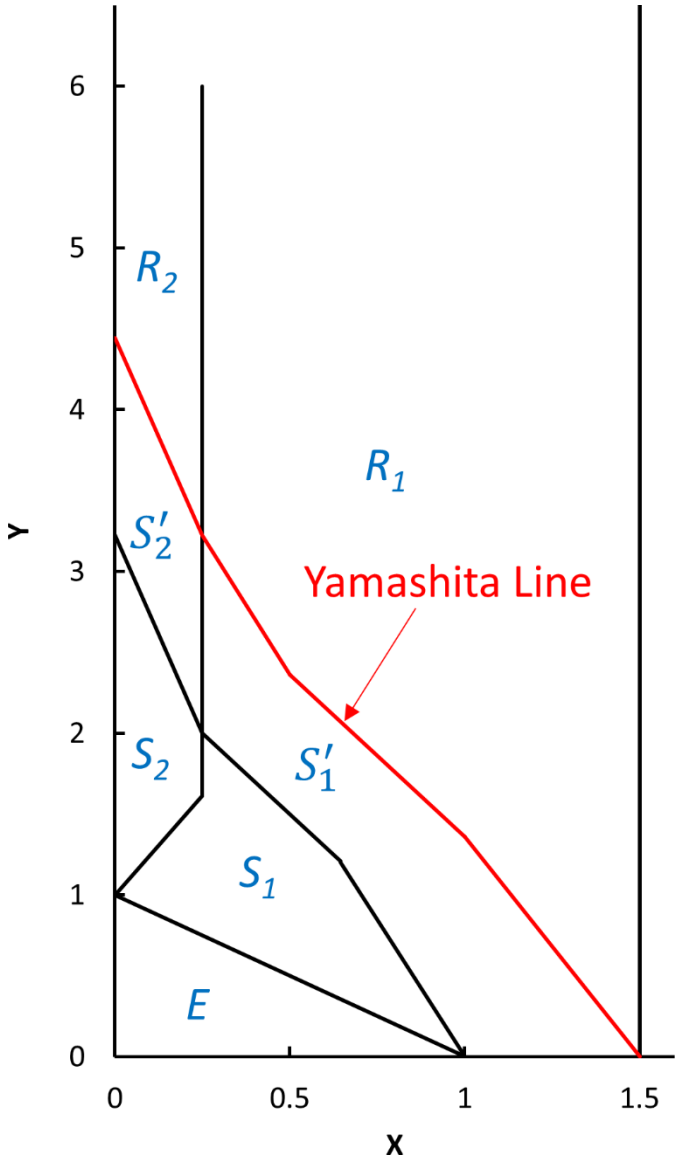

Stress regime	Beam behavior
R_1 and R_2	Ratcheting
S_1 and S_2 S_1' and S_2'	Shakedown after first half-cycle
E	Elastic

Figure 1-14 Ratchet diagram for a rectangular beam [44]

1.4 Objectives of this research

Countermeasures for BDBEs require the best estimation of the strength of nuclear power plant components. Therefore, it is necessary to clarify the possible failure modes due to extreme loads, which includes the recognition of reasonable failure modes and the occurrence conditions of those failure modes. The current study focuses on ratcheting, which is one common failure mode of piping under extreme earthquakes. The strain accumulates in one direction with the combination of a constant load and cyclic loads. Ratcheting may lead to severer failures of structures consequently (e.g., collapse). Therefore, it is essential to identify the occurrence conditions of ratcheting, as considered in many design codes such as ASME Boiler and Pressure Vessel Code Section Ⅲ [45], JSME code [46], and RCC-MR [47]. Those criteria require the structures to remain below the defined ratcheting boundaries [48]. However, current methods determining the ratcheting boundary only considers the constant pressure load with cyclic thermal loads. They are not suitable for the ratcheting evaluation due to the excessive seismic load, especially when considering the mitigation of accident consequences for BDBEs. Therefore, investigating the ratcheting behavior under excessive vibrations with reasonable accuracy is necessary for engineering reference.

Piping is sensitive to seismic loads in nuclear power plants. This study deals with two types of models: beam and piping models. The objective of the beam model is to identify the basic mechanisms of the occurrence conditions of ratcheting due to strong vibrations. The mechanisms would be compared with the conventional thermal ratcheting models (the Bree diagram and the Yamashita diagram). The objective of the study of the piping model is to extend the basic mechanisms to realistic structures.

Through the comparison of the above two models, this study will clarify the basic mechanisms of seismic ratcheting related to vibration frequency. Furthermore, a frequency-dependent ratcheting diagram will be proposed based on the above basic mechanisms.

1.5 Outline of the thesis

There are two types of models in this study: beam and piping models. The beam model was under consideration to identify the basic mechanisms of the occurrence conditions of ratcheting due to strong vibrations and compare thermal ratcheting (the Bree diagram and the Yamashita diagram) with vibration ratcheting. The analyses of the piping model were to extend the basic mechanisms to realistic structures. These two models are closely connected. The characteristic of the seismic load is ambiguous so that the classification of seismic load characteristic with frequency effect is also under consideration. In addition, this study also tries to propose countermeasures against ratcheting for engineering reference.

Chapter 2 focuses on clarifying the ratcheting mechanism of beams subjected to the combination of gravity and seismic loads. The analogy between vibration ratcheting and thermal ratcheting was taken into consideration to investigate the characteristics of seismic loads. Seismic ratcheting occurred under the combined effect of load-controlled load (e.g., gravity) and alternative cyclic accelerations. The criterion to judge the occurrence condition of ratcheting was decided to be 1% plastic strain accumulation during100 cycles of sinusoidal waves at the root part of the specimen. Dynamic inelastic finite element analyses were performed on a beam-shaped model under different loading conditions. FINAS/STAR did the finite element analyses (FEA) with the aid of the mesh generation by FEMAP. There were three types of vibrations in this chapter: sinusoidal excitations (it is called “SIN” excitations later), superposition of two sinusoidal acceleration excitations (it is called “SIN+SIN” excitations later), and seismic excitations. Experiments were carried out to validate the analytical analyses of the seismic excitations partially. Extreme loading conditions such as larger input accelerations are necessary to conduct an in-depth investigation of failure behaviors under BDBEs. However, it is difficult to realize those conditions for steel models due to the limitation of the performance of testing facilities and safety concerns during experiments. Thus, an experimental method using specimens made of simulation materials instead of steel pipes to investigate failure modes under seismic loads with several reasonable assumptions was applied in this study. Characteristics of seismic loads between load-controlled and displacement-controlled properties were studied from the viewpoint of the frequency ratio of input loads to the natural frequencies. All the results were

shown in a diagram similar to the Bree diagram to clarify the occurrence conditions of ratcheting. Results showed that the lower frequency load had a relatively lower Y value, which means ratcheting is highly possible to occur. With lower frequency input, the load acts like load-controlled stress. With higher frequency input, the load acts like displacement-controlled stress. In addition, it is meaningful to use simple SIN waves instead of the complicated seismic wave to judge the occurrence of ratcheting if the major frequency of the seismic wave is the same as the SIN wave.

In Chapter 3, experimental and numerical analyses were performed on bent solid bars, which represented piping models in this study. Similar to the beam model, considering the limitation of the shaking tables at the authors' laboratory and the safety concerns, the material of the piping specimens used was also lead alloy. There were two types of loads applied to the piping model. The first one was the external compressive force at the ends of the piping model, which acted as the load-controlled force and caused primary bending stress. The second load was cyclic accelerations from the shaking table, acting as the source of alternating dynamic loads. The nonlinear stress-strain curve of the Pb99%-Sb1% alloy, which was from the tensile test at room temperature at the authors' laboratory, was applied in numerical analyses. Both kinematic and isotropic hardening rules were included in this study. The piping models were divided into two categories: the piping model without additional supports (Piping-N) and the piping model with three supports in the medium part (Piping-S). The criterion of ratcheting was determined to be a 0.5% plastic strain at the extrados of the elbow accumulated during 50 sinusoidal cycles. The load-controlled and displacement-controlled properties were studied from the viewpoint of the frequency ratio of the harmonic force frequency over the natural frequency of the piping model. In addition, the effect of supports on the occurrence of ratcheting was also considered. Results show that the resonance effect was evident in the piping model compared with the beam model due to the limited plastic area in the piping model. At higher frequency, ratcheting was easier to occur in the piping with supports because additional supports increased natural frequencies and decreased frequency ratio. In terms of the occurrence of ratcheting, sometimes providing more supports does not mean increasing the safety of piping. The vibration with a lower frequency

ratio showed load-controlled characteristics. In contrast, the vibration with a higher frequency ratio has displacement-controlled characteristics.

Chapter 4 focused on the comparison of the ratcheting occurrence conditions between the beam model and the piping model, together with the Bree diagram and the Yamashita diagram. This chapter proposed one normalized vibration ratcheting diagram to show and compare ratcheting occurrence conditions with different materials and shapes. The final chapter presented the general conclusions on the occurrence of ratcheting. In addition, countermeasures against ratcheting were also proposed in this chapter.

Chapter 2. Ratcheting of Beam Models

This chapter studied the ratcheting mechanism of the beam model under the combination of gravity and vibration loads. The analogy between vibration ratcheting and thermal ratcheting was considered to clarify the characteristics of seismic loads.

Beams are fundamental structures in nuclear power plants and are often subjected to cyclic mechanical loads such as thermal or seismic stresses [49]. However, the occurrence of ratcheting under seismic loads is not clear because seismic loads are thought to contain both load and displacement controlled characteristics [31]. The current criterion defines the failure mode for the pipes in nuclear power plants as collapse [50], which means the leakage caused by the cracks [31]. The seismic probabilistic risk assessment (PRA) usually treats the failure modes under severe seismic loads as collapse. However, this assumption is not appropriate when considering the best estimation to think about countermeasures against BDBEs. This chapter concentrated on the analogy between vibration ratcheting and thermal ratcheting; the latter was described by the Bree diagram or the Yamashita diagram, as shown in Section 1.3. Seismic ratcheting occurred under the combined load-controlled load (e.g., gravity) and alternative cyclic vibrations. Dynamic inelastic finite element analyses were performed on a beam with different loading schemes. There were three types of vibration waves in this chapter: sinusoidal acceleration excitations ("SIN" excitations), the superposition of two sinusoidal excitations ("SIN+SIN" excitations), and seismic excitations. Experiments were carried out to validate the analytical studies. Properties of seismic loads were considered from the viewpoint of the frequency ratio of the forcing frequencies to the system natural frequencies. All the results were placed in a non-dimensional diagram similar to the Bree diagram to describe the detailed occurrence conditions of ratcheting.

Part of this work in this chapter, especially the ratcheting of the beam model under SIN loads, was done by previous laboratory members and published already [26]. That work was repeated in this study with the agreement from previous laboratory members since it was fundamental for further researches in this study and could help to distinguish the characteristics of seismic loads.

2.1 Methods for ratcheting analyses of beam models

Experimental and numerical analyses have equally essential roles in mechanics. In this study, experiments were conducted to validate numerical results partly and verify the ratcheting characteristics. Detailed numerical analyses were applied to obtain precise ratcheting boundaries at different loading schemes.

2.1.1 Experimental methods for the beam model

Extreme loading conditions, such as large input accelerations, are necessary to conduct an in-depth investigation of failure behaviors under BDBEs. However, it is difficult to realize those conditions due to the limitation of the performance of experiment facilities and safety concerns during experiments. Thus, a method using specimens made of simulation materials instead of steel to investigate failure modes under seismic loads was applied in this study. Figure 2-1 shows the beam model in experiments. The material was lead-antimony (Pb-Sb) alloy [51][52][53][37]. The stress-strain curves of lead-antimony alloys, including pure lead, are shown in Figure 2-2. The carbon steel, which is widely used in industry, is referred. The curves of Pb-Sb alloys have a similar tendency as that of carbon steel. However, the yield stress is much smaller comparing to carbon steel [52]. Those characteristics in the stress-stain curves indicate that it is reasonable to use the Pb-Sb alloy to simulate the components made of steel. Therefore, experiments under the extreme loading condition can be simulated with the existing testing facilities using the simulation materials.

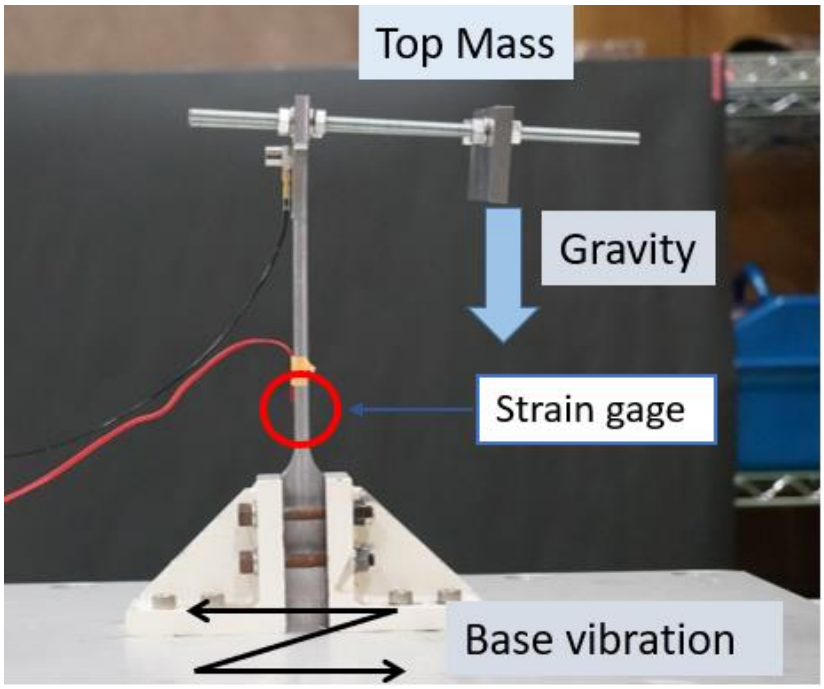

Figure 2-1 Experiment setup of the beam model

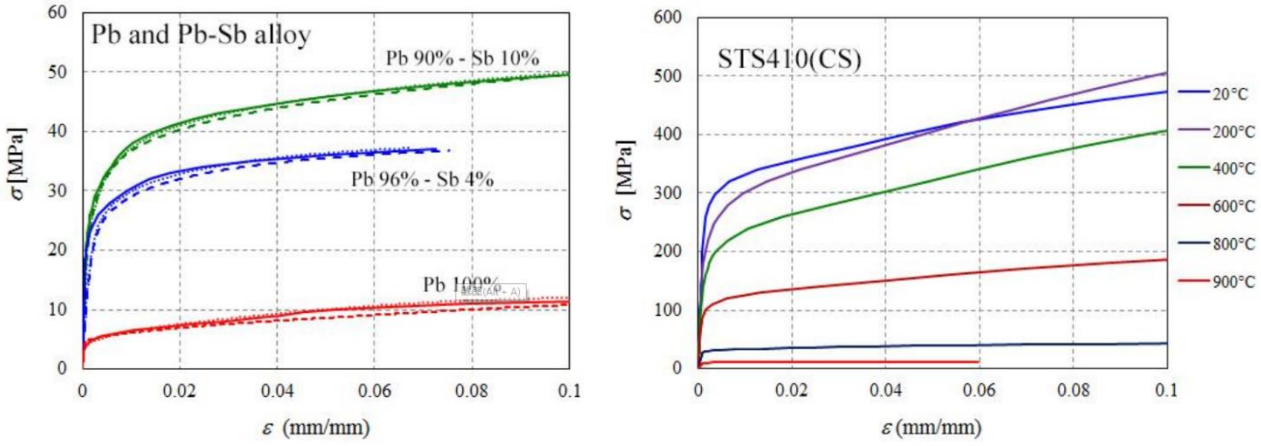

Pb-Sb alloys (at 23°C) Carbon Steel

Figure 2-2 Stress-strain curves of Pb-Sb alloys and carbon steel [51]

The cross section of the beam model was 6 mm × 13 mm, with the length as 140 mm (Figure 2-3). As shown in Figure 2-1, one end of the rectangular beam model was fixed to the shaking table. The gravity of the top mass provided the load-controlled load. The top mass and length

were decided according to different ratcheting conditions. The dynamic loads were from the skating table.

Figure 2-3 Specimen in experiments

2.1.1.1 Material tests

Tensile tests (Figure 2-4) at the author's laboratory provided the material parameters, as shown in Table 2-1.

Figure 2-4 Tensile test at the laboratory

Table 2-1 Material parameters (Pb99%-Sb1%) from the tensile tests

	Symbol	Unit	Value
Modulus of elasticity	E	GPa	19.15 (23°C)
Yield strength	σ_y	MPa	8.5 (23°C)
Poisson's ratio	ν	-	0.36
Density	ρ	kg/m^3	11,340
Length	l	mm	140
Width	d	mm	13
Height	h	mm	6

2.1.1.2 Experiment facilities

The high-performance shaking table used in this research was made by SAN-ESU CO., LTD, as illustrated in Figure 2-5. The model type is SPTD-8KS-85L-5T and is one-direction movable. This shaking table, with the size as 800 mm × 600 mm, and the load capacity as 19.6 kN, can reproduce recorded earthquakes time-histories within its capacities. Research can change the platform according to different test conditions. This shaking table can achieve the maximum acceleration as 20.0 G. The working frequency varies from 0.1 Hz to 100 Hz. The controller, shown in Figure 2-6, can load sinusoidal, shock, and seismic waves to the shaking table.

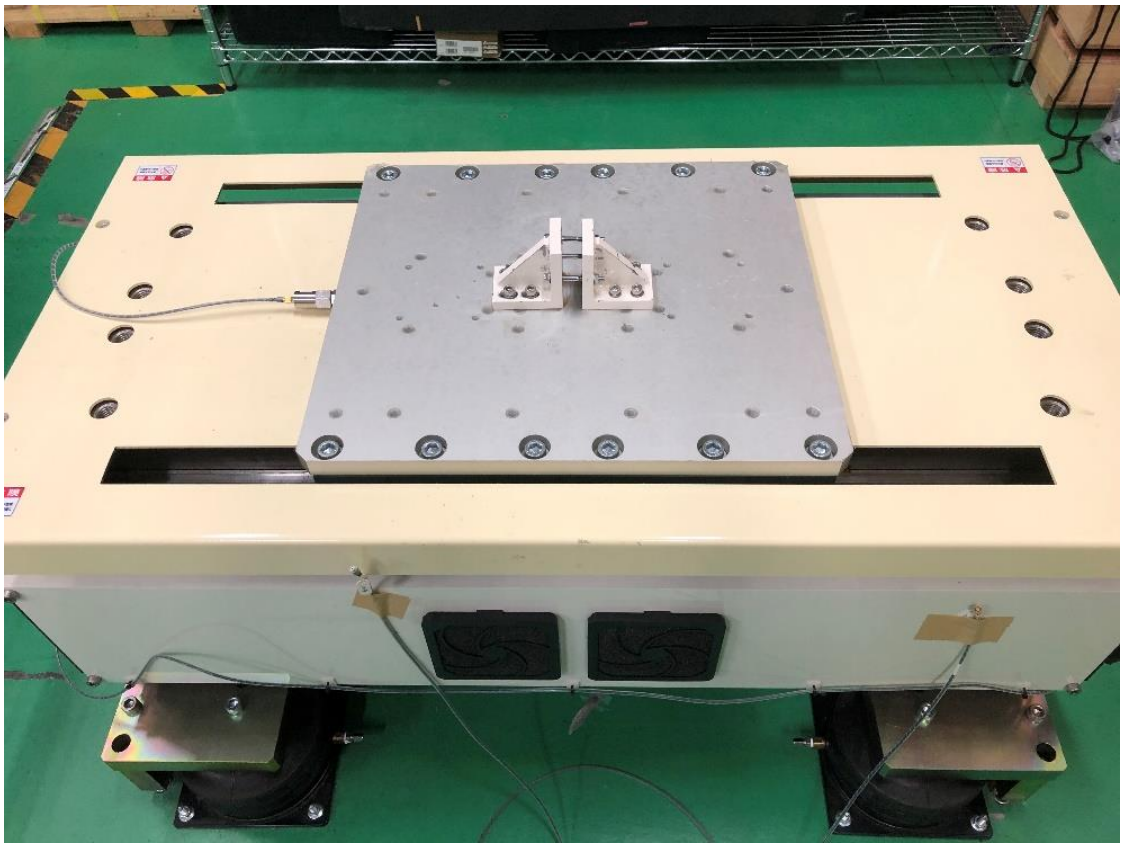

Figure 2-5 Shaking table used in this research

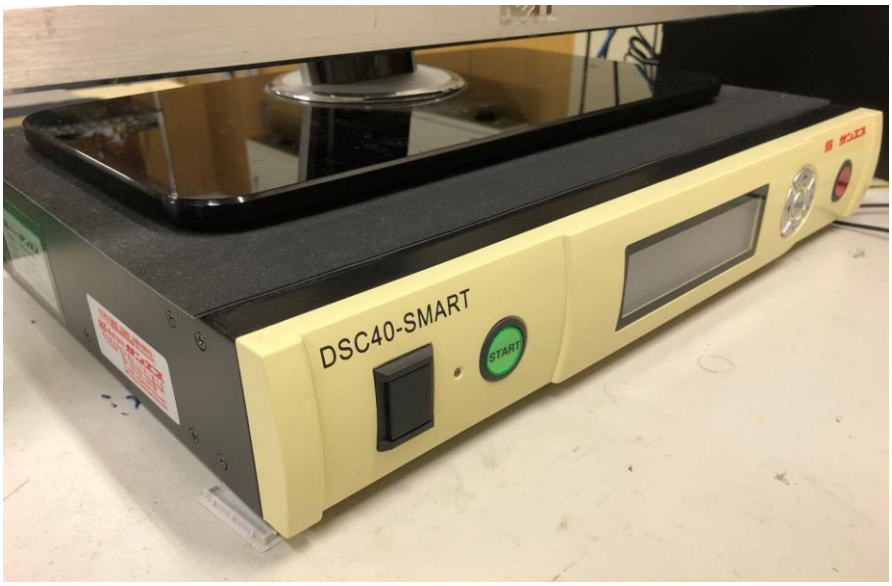

Figure 2-6 Controller of the shaking table

Several accelerometers, velocity sensors, and displacement sensors were used in experiments to measure motions and vibrations (Figure 2-7). SAN-ESU CO., LTD also provided most sensors. The types included IEPE SA-122L, P51C, and so on.

Figure 2-7 One accelerometer used in experiments

Strain gauges were also applied to measure the strain of some parts of specimens (Figure 2-8). It was produced by Kyowa Electronic Instruments Co., Ltd. The type was KFEL-2-120-C1L3M2R and could measure strain with the range from 1.05% to 3.05%.

Figure 2-8 Strain gauge used in experiments

The data logger (Figure 2-9) is used to measure the strain during experiments. It was produced by KEYENCE CORPORATION.

Figure 2-9 Datalogger used in experiments

2.1.1.3 X and Y parameters in experiments

One diagram, with non-dimensional primary and secondary stress parameters X and Y, was used to show the ratcheting occurrence conditions for loads with different schemes (forcing frequency, top mass, amplitude). The concept of parameter X and Y is similar to that introduced in Section 1.3.1. The parameter X was the ratio of bending stress caused by gravity to the material yield stress. Similarly, Y is the ratio of bending stress caused by maximum accelerations to the material yield stress.

$$X = \frac{\sigma_g}{\sigma_y} \quad \text{Equation 2-1}$$

$$Y = \frac{\sigma_i}{\sigma_y} \quad \text{Equation 2-2}$$

where σ_y is the material yield stress; σ_g is the bending stress caused by the gravity of the top mass; σ_i is the bending stress caused by the peak floor acceleration.

The bending stresses were calculated according to the following equations:

$$\sigma_g = \frac{M_g}{Z} \quad \text{Equation 2-3}$$

$$\sigma_i = \frac{M_i}{Z} \quad \text{Equation 2-4}$$

where M_g and M_i represent the moments caused by gravity and inertia force; Z is the section modulus as below:

$$Z = \frac{b * h^2}{6} \quad \text{Equation 2-5}$$

Where h and b are the width and height of the beam rectangular cross section.

The calculation of M_g and M_i is shown in Equation 2-6 and Equation 2-7. Similar calculations were conducted in numerical analyses.

$$M_g = m_{mass} * l_{mass} * g + m_{rod} * l_{rod} * g \quad \text{Equation 2-6}$$

$$M_i = m_1 * l_1 * a + (m_2 + m_{mass} + m_{rod}) * l_2 * a \qquad \text{Equation 2-7}$$

The geometrical parameters are shown in Figure 2-10, which is a simplified structure of specimen in experiments. “a” is the maximum value of the input acceleration waves.

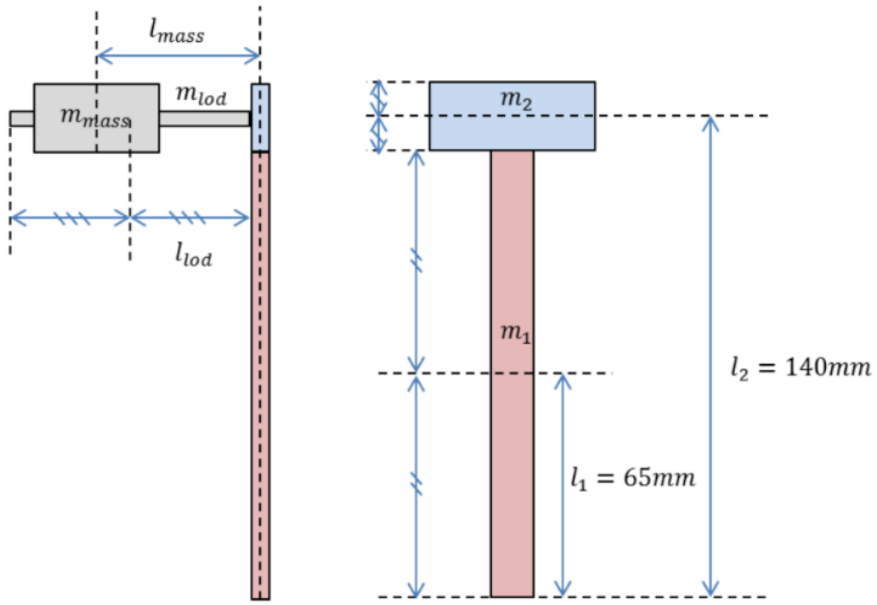

Figure 2-10 Geometrical parameters in experiments

2.1.2 Numerical methods for the beam model

Although the experimental investigation is necessary to illustrate the mechanism of ratcheting, the facility capabilities, experimentation cost, and safety concerns limit the experimental conditions. Therefore, numerical methods are suitable to find the specific inelastic behavior of structures suffering from strong earthquakes. In this research, finite element analyses helped predict ratcheting behavior with proper constitutive models.

In numerical analysis, FINAS/STAR [54] was used for the finite element analyses (FEA). The finite element method (FEM) is widely applied in approximating a continuous system as a multi-degree-of-freedom system. Through this method, plenty of small elements replace the original

continuous system geometry. The conditions (displacement, force, etc.) within the element can be described with approximation functions. By assuming the displacement approximation function that satisfies the constitutive equation and compatibility condition, the approximate solution to the original system can be achieved. FEMAP performed the mesh generation [55].

Table 2-2 shows the geometrical and material parameters in FEM. It is necessary to mention that the material in FEM was inconsistent with that in experiments since this research was sustained for six years, and the specimen was updated according to different conditions. However, since the ratcheting occurrence conditions were shown in the non-dimensional X-Y diagram, the effect of the material difference was negligible. Elastic-perfectly plastic analyses were performed to the model shown in Figure 2-11. The beam model also contained two types of loads similar to experiments. The first one was the gravity load from the top mass at the free end of the beam and weight of the beam model. This load provided load-controlled stress (primary stress). The second one was from the vibrations of the shaking table and acted as cyclic dynamic loads. As described in Section 1.2.3, seismic loads exhibit both load-controlled and displacement-controlled characteristics; therefore, later sections would focus on the distinction between the two stress types from the viewpoint of the frequency ratio. The forcing frequency, the amplitude of input accelerations, and the weight of top mass were adjusted according to different ratcheting occurrence conditions.

Table 2-2 Material and geometrical parameters In numerical analysis

	Symbol	Unit	Value
Modulus of elasticity	E	GPa	16
Yield stress	σ_y	MPa	5
Poisson's ratio	ν	-	0.44
Mass density	ρ	kg/m^3	11,340
Length	l	mm	140
Width	d	mm	13
Height	h	mm	6

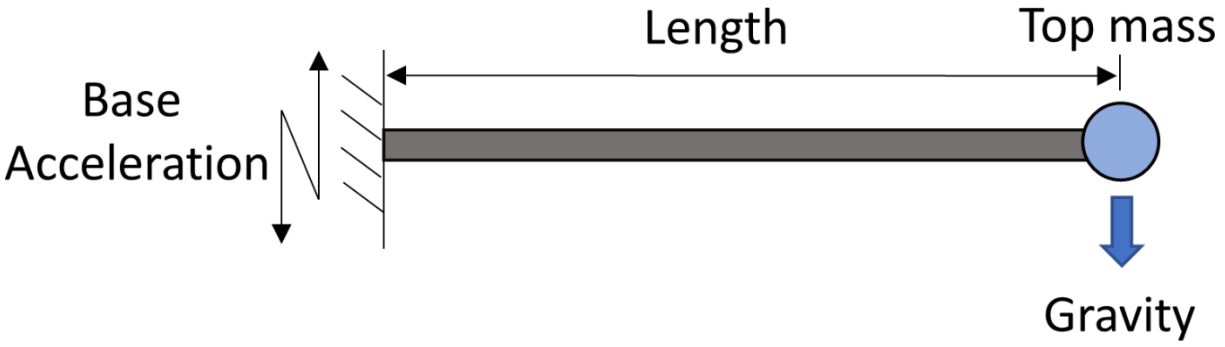

Figure 2-11 Beam model with loading conditions in numerical analyses

2.1.2.1 X and Y in the numerical approach

Same as experimental analyses, the non-dimensional X-Y diagram was also applied in the numerical approach to show the ratcheting occurrence conditions. Figure 2-12 illustrates the meaning of the parameter X and Y in numerical analyses. The stress statically equivalent to the stress due to gravity was the numerator in the calculation of X. In terms of Y, the stress due to inertia force was included.

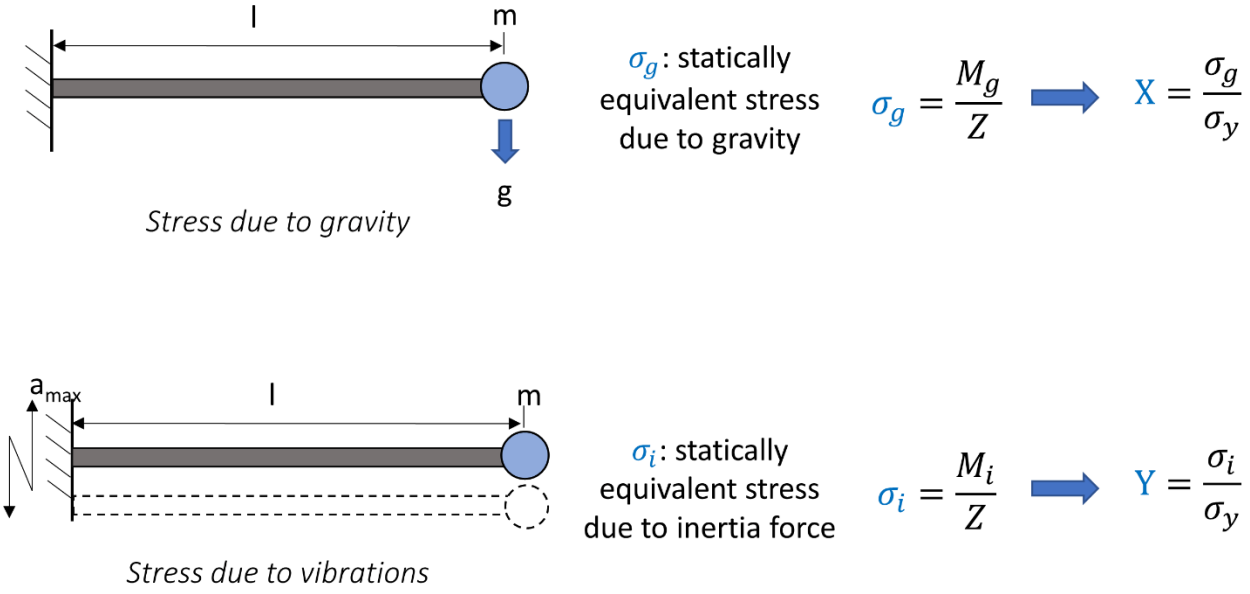

Figure 2-12 Explanation of the parameter X and Y in numerical analyses

The calculation and definition of X and Y are similar to those in experimental analyses. The detailed calculations of M_g and M_i in numerical analyses are a little different from those in experiments due to the differences in setting, as below:

$$M_g = m_{top} * l * g + m_{beam} * \frac{l}{2} * g \qquad \text{Equation 2-8}$$

$$M_i = m_{top} * l * a + m_{beam} * \frac{l}{2} * a \qquad \text{Equation 2-9}$$

Where the "l" is the beam length, and "a" is the static equilibrium acceleration of input vibration waves.

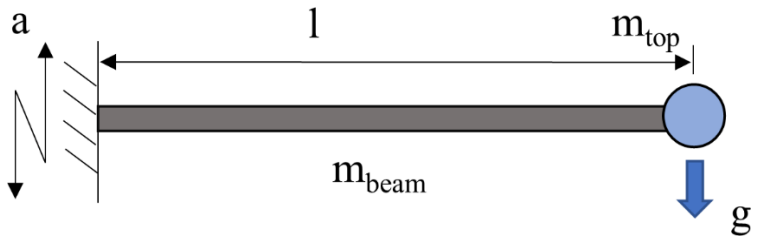

Figure 2-13 The detailed model parameters of the specimen in numerical analyses

2.1.3 Natural frequency and frequency ratio

If a system contains N degrees of freedom, accordingly, there are N natural frequencies associated with mode shapes [56]. In the current research, only the first natural frequency was considered since the participation factor of the rest frequencies was negligible.

In this study, "fn" meant the beam specimen's natural frequency. For example, "1.0 fn" meant that the forcing frequency (the frequency of input waves) was the same as the specimen's natural frequency. The frequency ratio (fr) was defined as the ratio of the forcing frequency to the specimen's natural frequency by the following equation:

$$fr = \frac{f_i}{f_n} \qquad \text{Equation 2-10}$$

Where f_i is the frequency of input sinusoidal wave, and f_n is the specimen's natural frequency in the elastic region.

2.1.4 Input waves

There were three types of input waves in this research: SIN, SIN+SIN, and seismic waves. They were loaded as a base excitation at the fixed end of the beam model.

2.1.4.1 SIN waves

Harmonic components with a wide range of frequencies constitute the seismic excitation. Therefore, it is meaningful to consider the response to harmonic motion firstly. Harmonic excitations are always encountered in engineering systems, such as unbalanced rotating machinery. Besides, understanding the response of structures to harmonic excitation provides insight into how the system responds to earthquakes. In this research, for convenience, sinusoidal waves were named as "SIN" excitations, as shown in Equation 2-11.

$$a = A\sin(\omega t) = A\sin(2\pi f \cdot t) \qquad \text{Equation 2-11}$$

Figure 2-14 shows the part of sinusoidal input waves with different frequencies. In this figure, "50 g" means that the top mass is 50g; "fn" means the specimen's natural frequency, as discussed in Section 2.1.3. There were 100 sinusoidal cycles in one input wave. Different waves were loaded to clarify the effect of additional masses, the forcing frequencies, and the acceleration levels of the input sinusoidal waves.

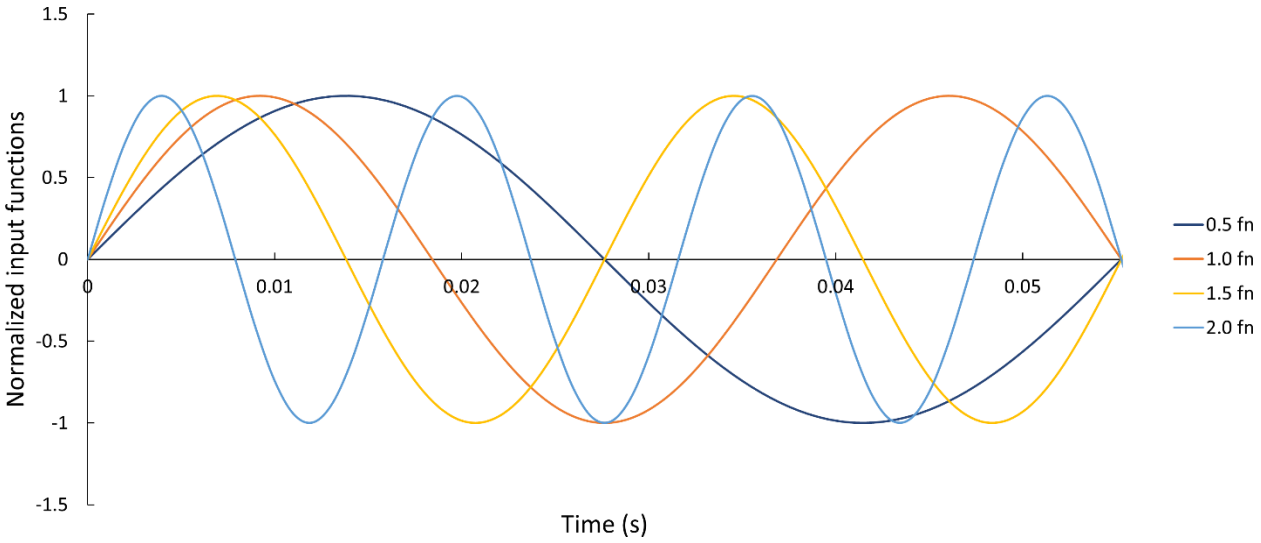

Figure 2-14 Input SIN waves with different frequencies (normalized to [-1, 1], 50 g, 0.5 fn)

2.1.4.2 SIN+SIN waves

Two sinusoidal acceleration waves made up the SIN+SIN excitation wave, as shown in Equation 2-12 and Figure 2-15. Therefore, there were two frequencies in one SIN+SIN excitation wave. The SIN+SIN wave was also cyclic, and the two components had the same amplitude. The main objective of loading SIN+SIN waves was to find out which frequency contributed more to the occurrence of ratcheting.

$$a = A(\sin(\omega_1 t) + \sin(\omega_2 t)) \qquad \text{Equation 2-12}$$

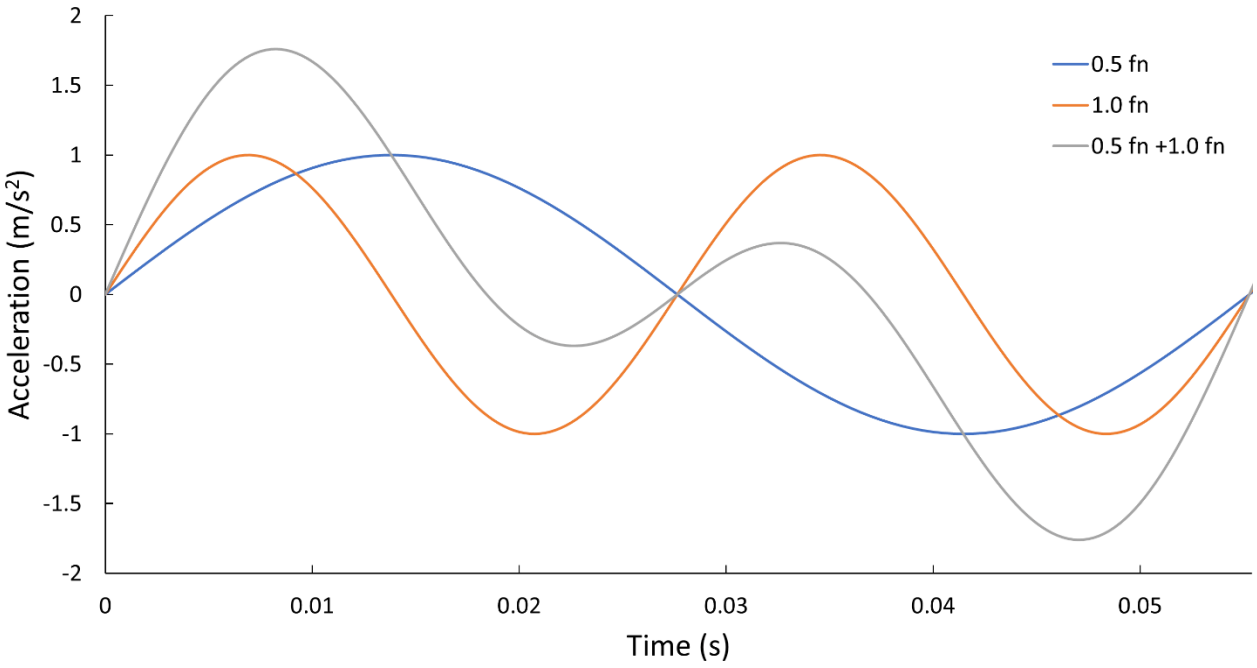

Figure 2-15 SIN wave and SIN+SIN wave

2.1.4.3 Seismic waves

Analyzing the response of structures to earthquakes was one of the essential purposes of this research. The seismic wave used in this study was the vertical component of one of the Kumamoto earthquake waves, which occurred on April 15, 2016, in the Kumamoto region, Kyushu Island, Japan [57]. The seismic data were downloaded from the Resilience National Research Institute for Earth Science and Disaster[58]. The accelerogram and the Fourier spectrum are displays in Figure 2-16 and Figure 2-17, respectively. Damping was taken equal to 5%. In order to decrease the calculation time, only the part with larger acceleration amplitudes (20 seconds) was loaded to the shaking table. It is worthwhile to notice that the region around 4 Hz, which we named it "Sensitive Region" (Figure 2-17) in this study, had a much larger Fourier amplitude. The magnitude and the dominant frequency of the seismic wave were adjusted according to the research targets. For example, "0.5 fn" means that the dominant frequency of the seismic wave was the half of the specimen's natural frequency (Figure 2-18); "1.0 fn" means that the dominant frequency of the seismic wave was the same as the specimen's natural frequency (Figure 2-19).

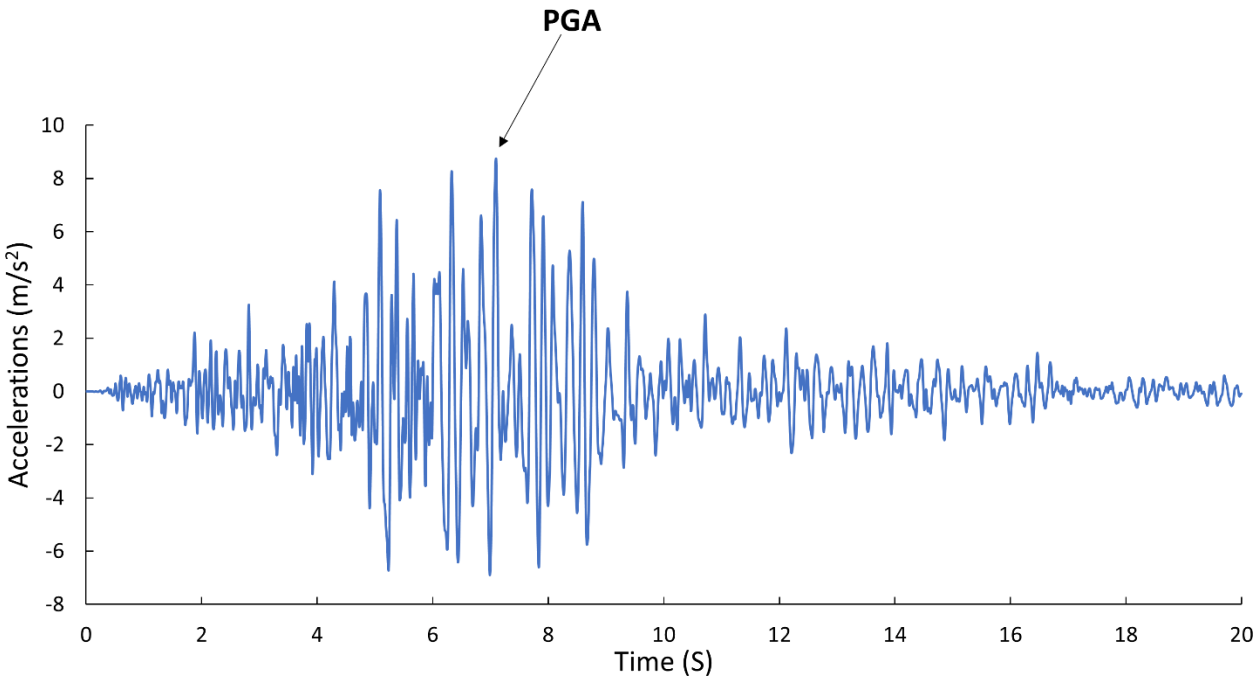

Figure 2-16 Accelerogram of the vertical component of the 2016 Kumamoto earthquake waves

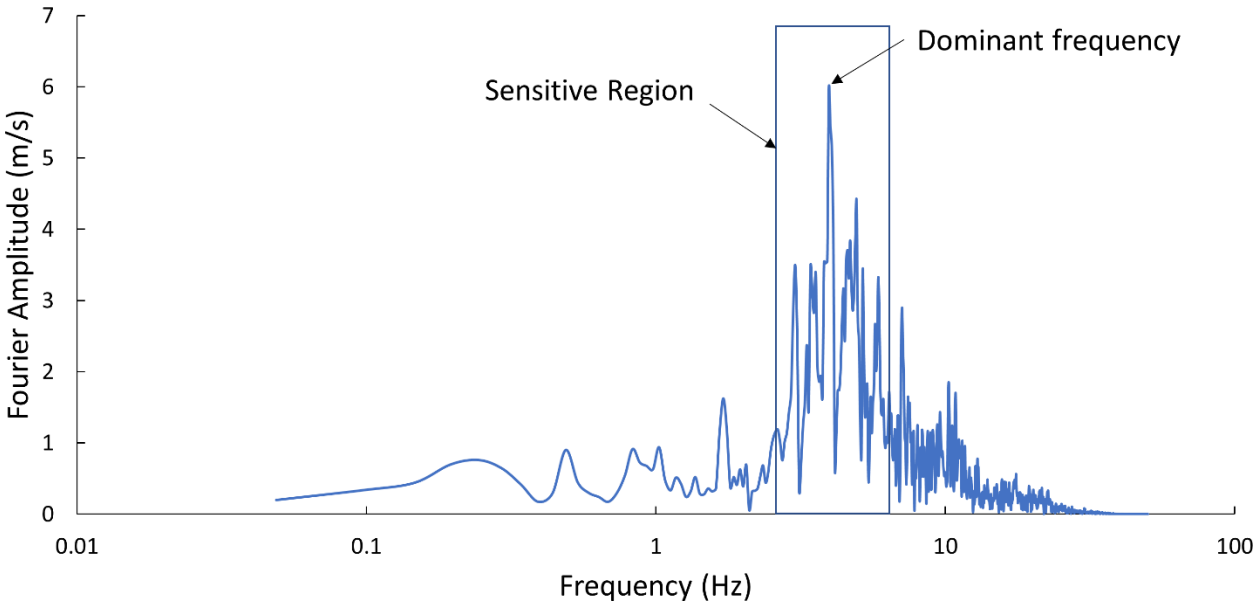

Figure 2-17 Fourier spectrum of the vertical component of the 2016 Kumamoto earthquake waves

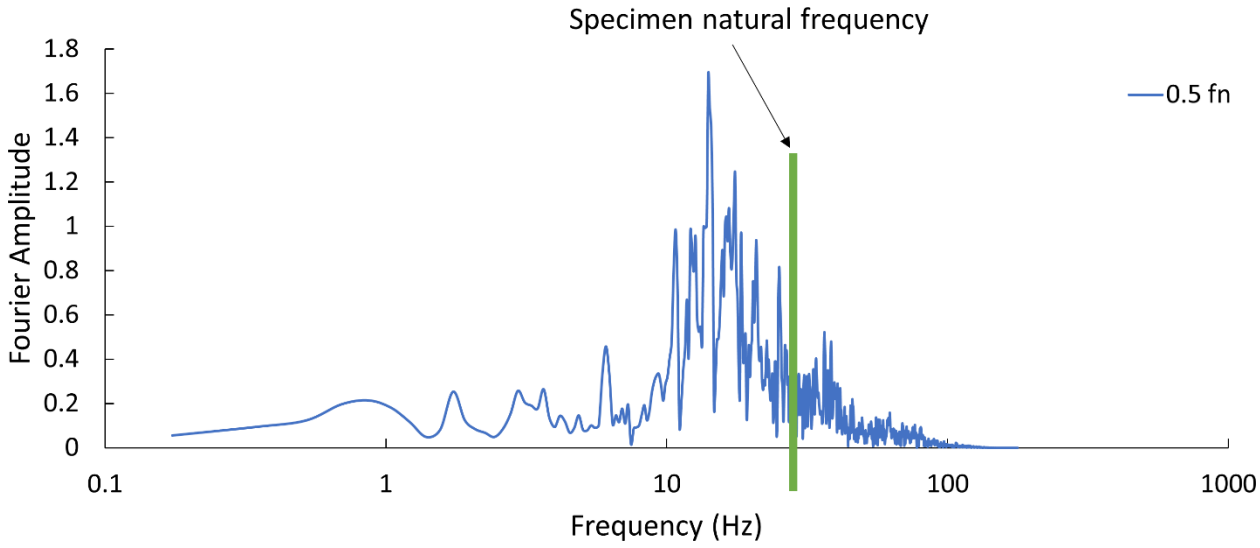

Figure 2-18 Definition of frequency ratio of seismic loads (0.5 fn)

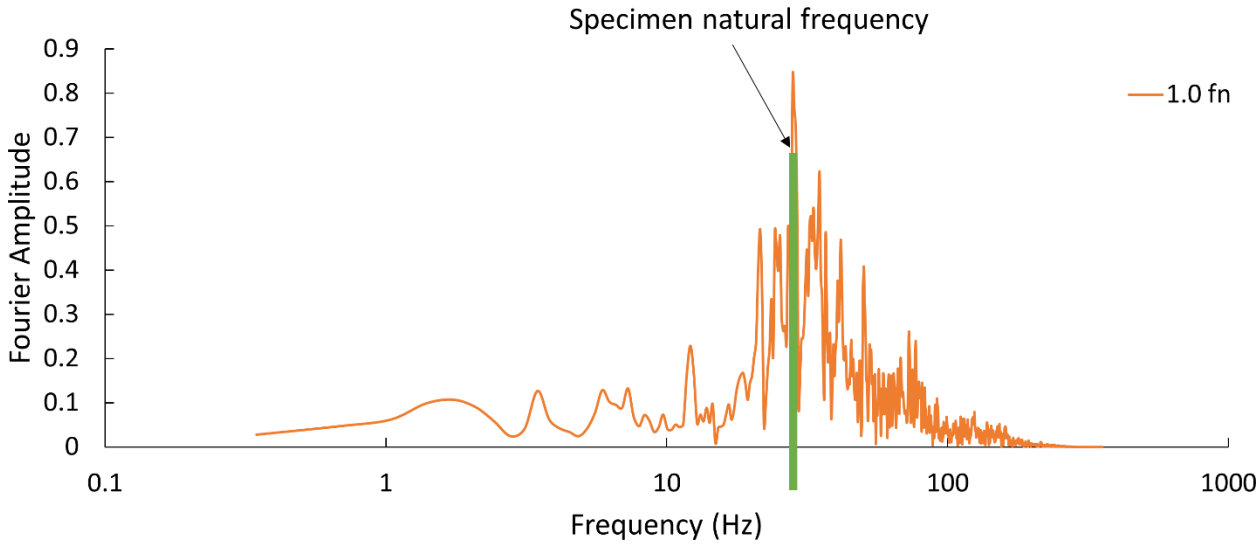

Figure 2-19 Definition of frequency ratio of seismic loads (1.0 fn)

2.1.5 Criteria for ratcheting

It is necessary to define the occurrence conditions of ratcheting to get clear ratcheting boundaries. According to the definition, ratcheting occurs due to cyclic accumulation of plastic deformation. However, the deformation is not suitable to judge the occurrence of ratcheting. Considering the

size of different components, the strain, which is the elongation per unit length, is a better choice. The number of cycles is also an important factor; therefore, the total strain is also not suitable. It means that the criteria should consider the number of repetitions and the limit of total strain. When nuclear power plant components work at extreme conditions such as the high temperature, the yield stress decreases, and creep occurs; therefore, limited plastic deformation is acceptable. In addition, under BDBEs, ratcheting is allowed in order to release some deformation or pressure. In this study, for the beam model under SIN and SIN+SIN loads, the criterion of ratcheting was decided to be the 1% plastic strain accumulated in 100 cyclic vibrations. For the beam model under seismic vibrations, since the amplitude of different wave peaks were different, the criterion was decided to be the 0.2% plastic strain accumulated in one seismic wave. One strain gauge was attached to the root part of the specimen in experiments (Figure 2-1) since the largest strain occurred in this position. Accordingly, the strain at the root part of the specimen in numerical analyses was also recorded.

One typical strain increment of the beam root part in numerical analysis is shown in Figure 2-20. The top mass was 166 g, and the frequency ratio, which was described in Section 2.1.3, was 1.5. Though the difference between the two amplitudes was relatively smaller, the phenomenon was totally different. When the amplitude was 12 m/s^2, the accumulated strain was minimal (0.2%) after 100 cycles. In contrast, it increased to 1% quickly with the amplitude equal to 14 m/s^2. The yielding occurred in the first cycle and accumulated continuously in the same direction in the rest cycles. From the figure, it is clear that if the amplitude of input accelerations is larger than the threshold value, the strain will accumulate, and finally, ratcheting occurs.

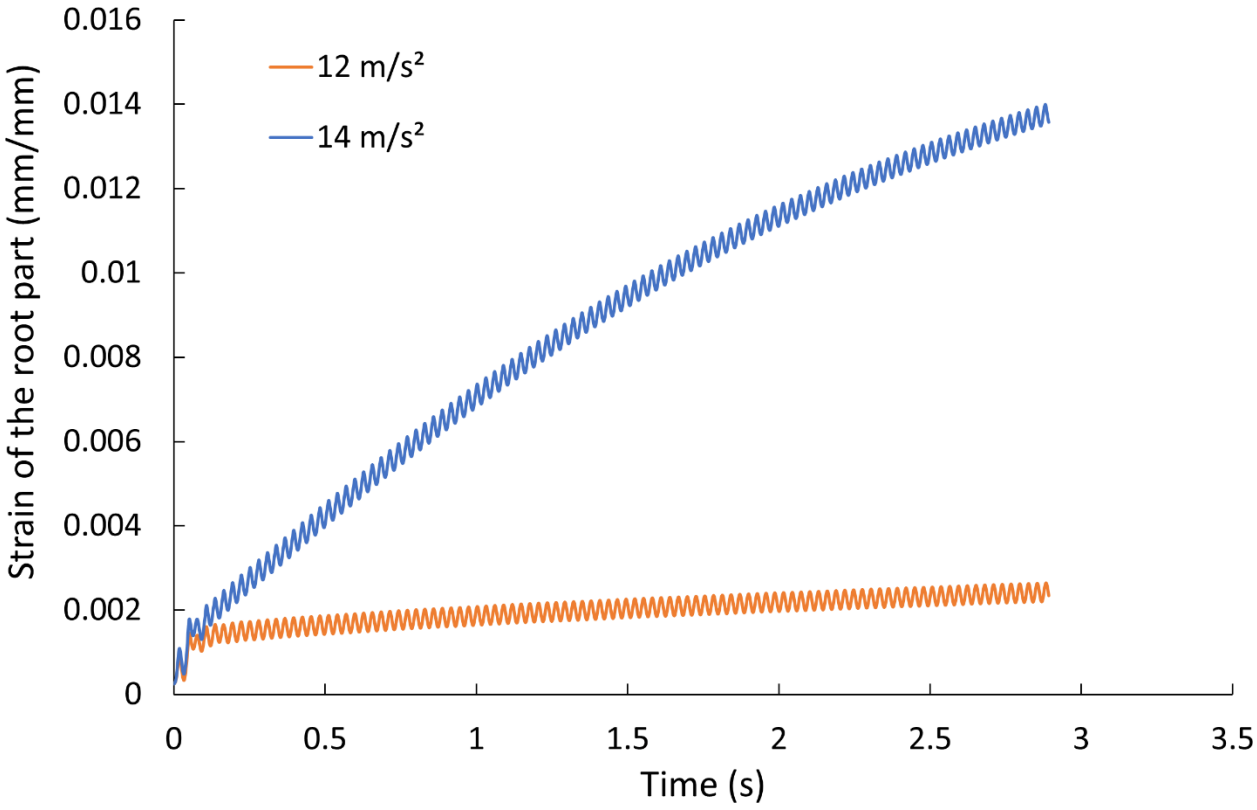

Figure 2-20 Strain increment in numerical analysis (166 g, 1.5 fn)

2.2 Beam models under SIN loads

2.2.1 Experimental results of the beam model under SIN loads

Experimental conditions for ratcheting of beam models under SIN loads are shown in Table 2-3. There were four different top masses with different X values. The forcing frequencies varied from 0.5 fn to 2.0 fn for each X value.

The non-dimensional X-Y diagram (Figure 2-21) demonstrates the experimental results with four different forcing frequencies (0.5, 1.0, 1.5, and 2.0 fn). Those lines mean the ratcheting boundaries, and ratcheting occurs in the area above those lines. All lines have a similar trend to the ratcheting line proposed by Yamashita et al. If showing the ratcheting occurrence conditions in the frequency ratio (fr) as in Figure 2-22, evident frequency-dependent characteristics can be found among the lines. Loads with lower forcing frequencies, such as 0.5 fn and 1.0 fn, had

relatively smaller Y value. It means that in such a case, ratcheting occurred more easily, even with low amplitude accelerations.

Table 2-3 Experimental conditions for ratcheting of beam models under SIN loads

Case #	Steady bending stress		Natural frequency (Hz)	Input	
	Top additional mass (kg)	X		Frequency ratio	Frequency (Hz)
1	0.245	0.3272	15.625	0.5	7.81
2				1.0	15.63
3				1.5	23.43
4				2.0	31.25
5	0.340	0.5121	11.718	0.5	5.85
6				1.0	11.72
7				1.5	17.58
8				2.0	23.44
9	0.530	0.7369	9.375	0.5	4.69
10				1.0	9.38
11				1.5	14.06
12				2.0	18.75
13	0.805	1.0623	8.790	0.5	4.39
14				1.0	8.79
15				1.5	13.16
16				2.0	17.58

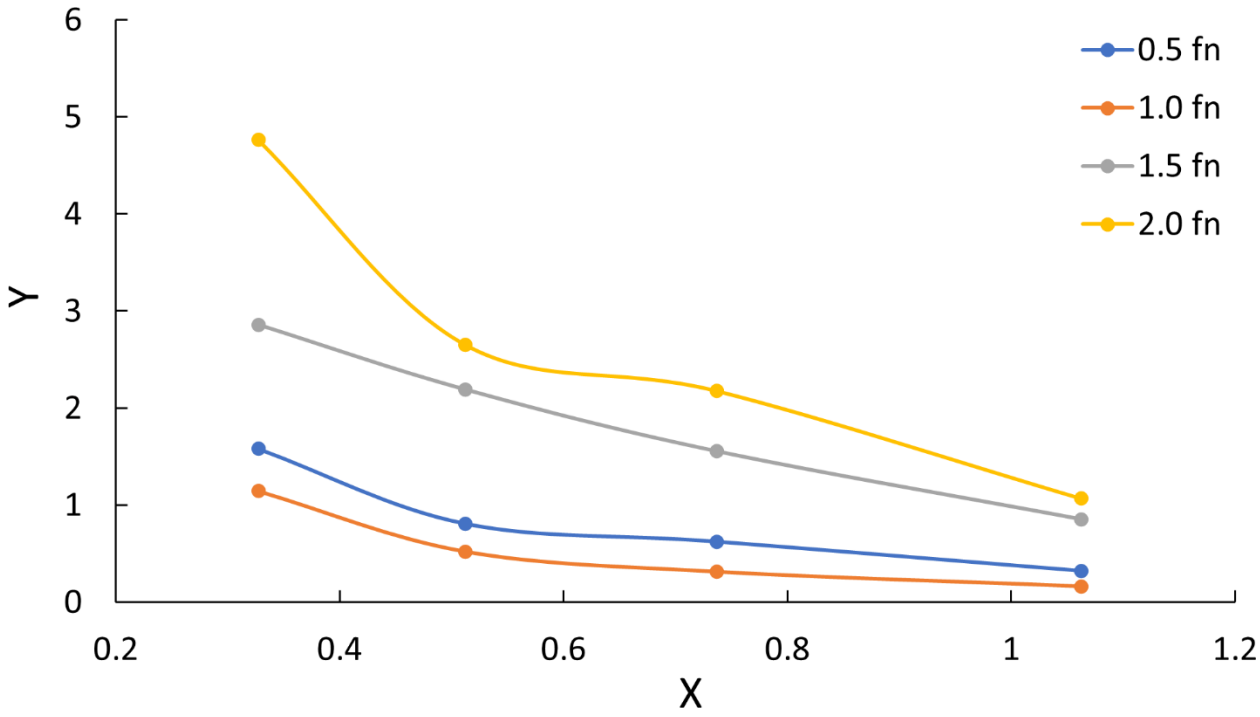

Figure 2-21 Ratcheting diagram of experiments with four different forcing frequencies (0.5, 1.0, 1.5 and 2.0 fn)

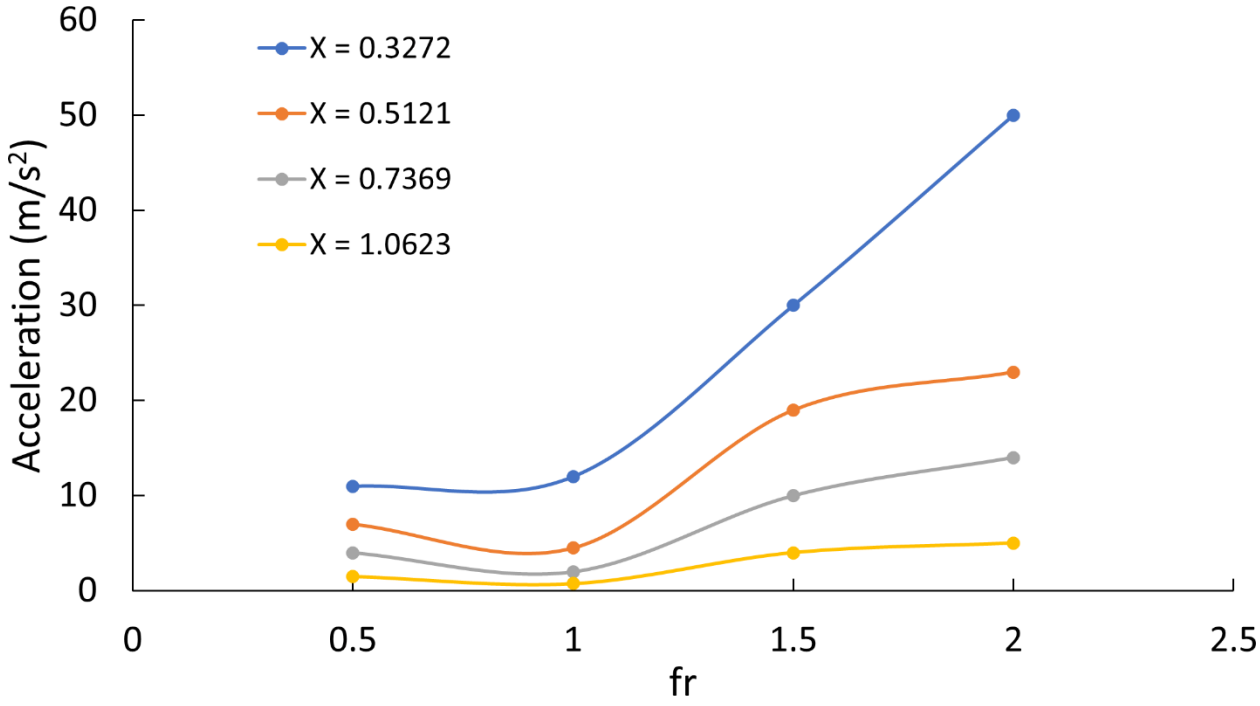

Figure 2-22 Frequency-dependent characteristics in experimental results

2.2.2 Numerical results of the beam model under SIN loads

The analysis conditions for SIN input accelerations are summarized in Table 2-4. There were eight different top masses with different X values. The forcing frequencies varied from 0.5 fn to 2.0 fn for each X value.

Table 2-4 Analysis conditions for ratcheting of the beam model under SIN loads

Case No.	Steady bending stress		Natural frequency (Hz)	Input frequency (Hz)	
	Top additional mass (kg)	X		Frequency ratio	Exact value (Hz)
1	0.000	0.218	59.600	0.5	29.800
2				0.75	44.700
3				1.0	59.600
4				1.5	89.400
5				1.75	104.300
6				2.0	119.200
7	0.050	0.394	36.185	0.5	18.092
8				0.75	27.138
9				1.0	36.185
10				1.5	54.277
11				1.75	63.323
12				2.0	72.369
13	0.080	0.500	30.815	0.5	15.408
14				0.75	23.111
15				1.0	30.815
16				1.5	46.223
17				1.75	53.927
18				2.0	61.631
19	0.100	0.570	28.330	0.5	14.165
20				0.75	21.247
21				1.0	28.330
22				1.5	42.495
23				1.75	49.577
24				2.0	56.660
25	0.166	0.803	23.048	0.5	11.524
26				0.75	17.286
27				1.0	23.048
28				1.5	34.572

29				1.75	40.334
30				2.0	46.096
31	0.223	1.003	20.277	0.5	10.138
32				0.75	15.207
33				1.0	20.277
34				1.5	30.415
35				1.75	35.484
36				2.0	40.553
37	0.279	1.201	18.342	0.5	9.171
38				0.75	13.757
39				1.0	18.342
40				1.5	27.513
41				1.75	32.099
42				2.0	36.684
43	0.336	1.401	16.850	0.5	8.425
44				0.75	12.637
45				1.0	16.850
46				1.5	25.275
47				1.75	29.487
48				2.0	33.700

The ratcheting diagram for the SIN waves with the numerical method is shown in Figure 2-23. The collapse line and the ratcheting line of Yamashita et al. 's model (it is called the "Yamashita line" later) are included for reference. The collapse line means the occurrence of the theoretical plastic collapse of the rectangular beam if the elastic stress reaches the 1.5 times of yield stress. Therefore, if one ratcheting boundary is close to the collapse line, the static load caused by the top mass creates 1.5 times of yield stress. This load is a load-controlled load according to the definition. The Yamashita line was also referred to in the ratcheting diagram. The secondary stress of Yamashita's model was purely displacement-controlled stress; therefore, in the same X-Y diagram, if one ratcheting boundary is close to the Yamashita line, the characteristic is close to the displacement-controlled stress.

In Figure 2-23, if the forcing frequency is relatively smaller, such as 0.5 fn, 0.75 fn, 1.0 fn, the ratcheting boundaries are close to the collapse line. According to the above description, those loads had load-controlled characteristics. In contrast, the waves with higher frequencies, such as

1.75 fn, are close to the Yamashita line. Therefore, those loads showed displacement-controlled characteristics. In conclusion, the characteristics of dynamic loads profoundly depend on their frequencies.

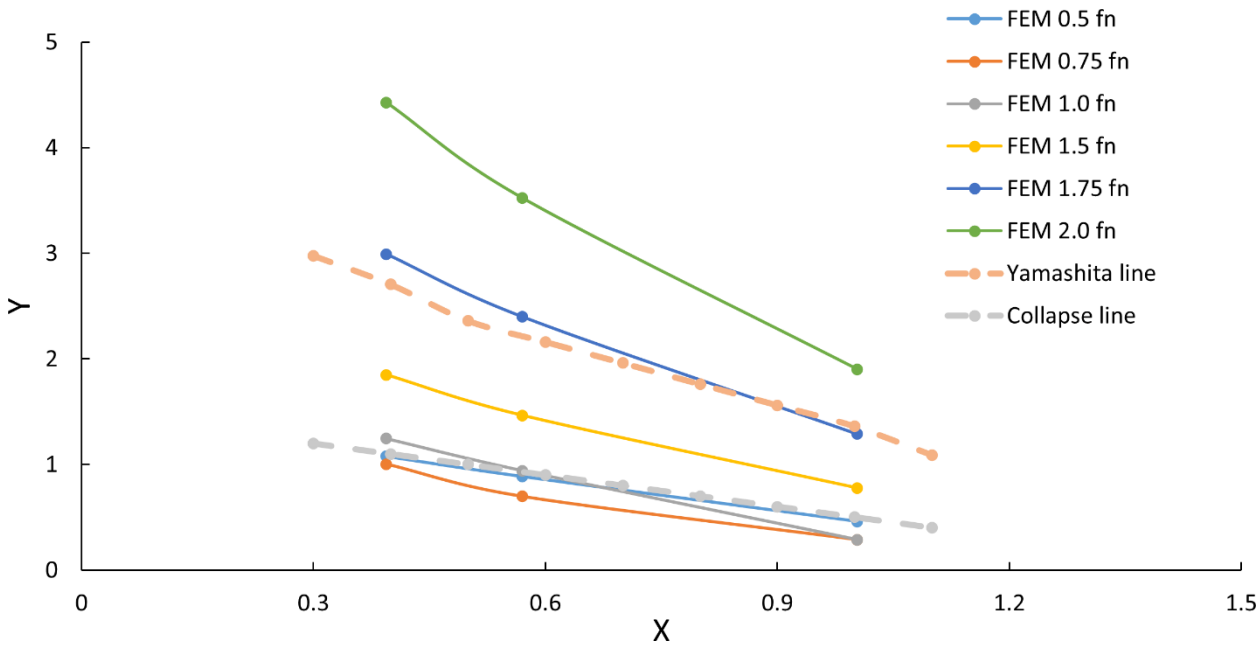

Figure 2-23 Ratcheting diagram for the SIN accelerations in numerical analyses

Lines in Figure 2-23 illustrate the ratcheting boundaries under loads with different forcing frequencies. Ratcheting occurs in the area above one particular boundary. It is evident that, with the same top mass, ratcheting occurred easily for the loads with lower forcing frequencies. This phenomenon was due to the phase delay between load and displacement (Figure 2-24). With lower forcing frequencies, the movement of the shaking table varied slowly; the displacement was generally in phase with the applied excitation. Therefore, there was a small delay, and the load was close to the static load, and more energy was transferred from the shaking table. In contrast, with a higher forcing frequency, the excitation quickly varied, and the displacement was almost of opposite phase relative to the applied excitation. Therefore, the delay was considerable, and energy could not be fully transferred to structures from the input vibrations. In addition, the occurrence of ratcheting was also strongly affected by the resonance effect. Sizeable plastic deformation was caused in the procedure of ratcheting occurrence. Due to the plastic

deformation, the beam model became moderate, and the resonance frequency shifted to the smaller value rather than the natural frequency in elastic conditions. Therefore, in Figure 2-23, due to the resonance effect, 0.75 fn is the lowest case, followed by 0.5 fn and 1.0 fn. In the case of the frequency higher than 1.0 fn, structures hardly responded to external acceleration due to the phase delay.

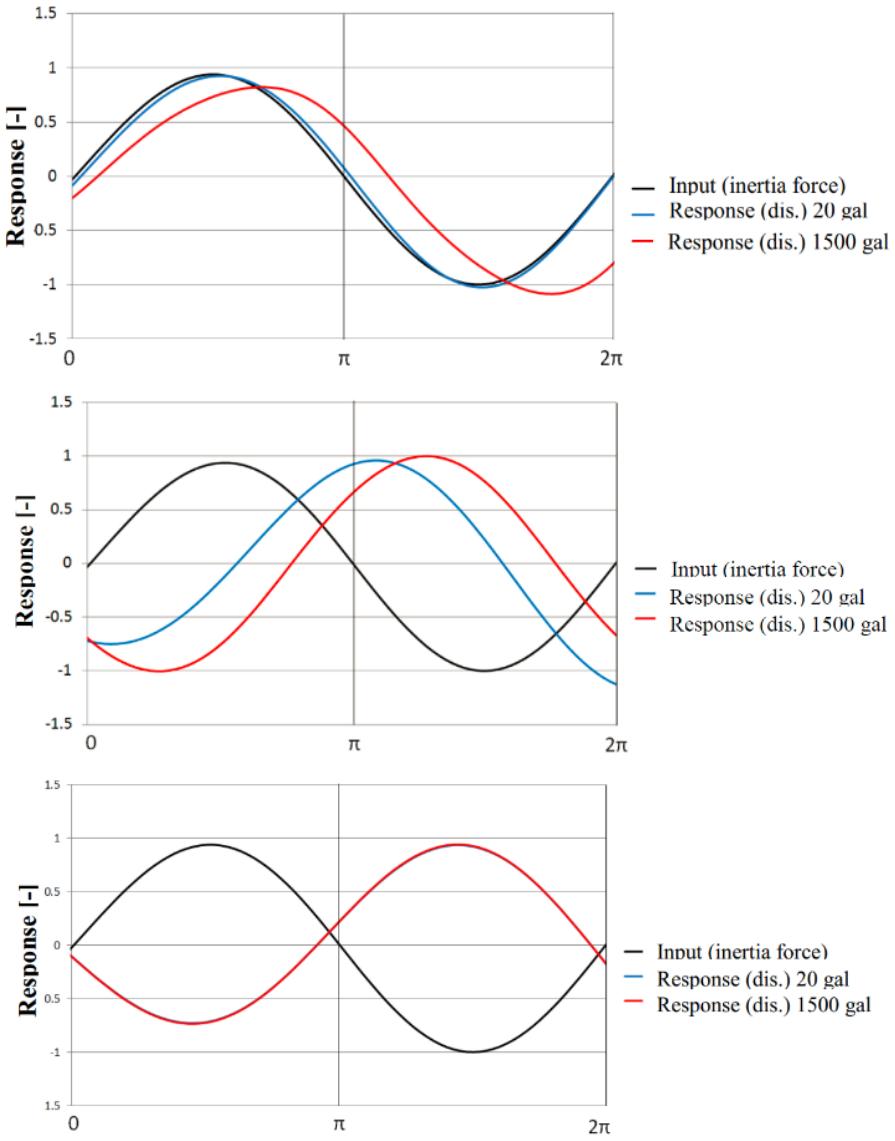

Figure 2-24 The phase shift at 0.5 fn, 1.0 fn, and 1.5 fn respectively

Figure 2-25 shows the ratcheting occurrence conditions in the frequency ratio. The whole region is divided into two parts: the pseudo load-controlled region and the pseudo displacement-controlled region. The word "pseudo" means that the loading vibrations are not purely load-controlled or displacement-controlled loads. The boundary is decided to be 1.25 fn according to the slope of those curves. Before 1.25 fn, the curves increase slowly. In contrast, after 1.25 fn, a sharp growth appears. The resonance effect is not evident in the beam model since the plastic deformation occurred in most parts of the beam model. Figure 2-26 shows the typical deformation of the beam model after vibrations.

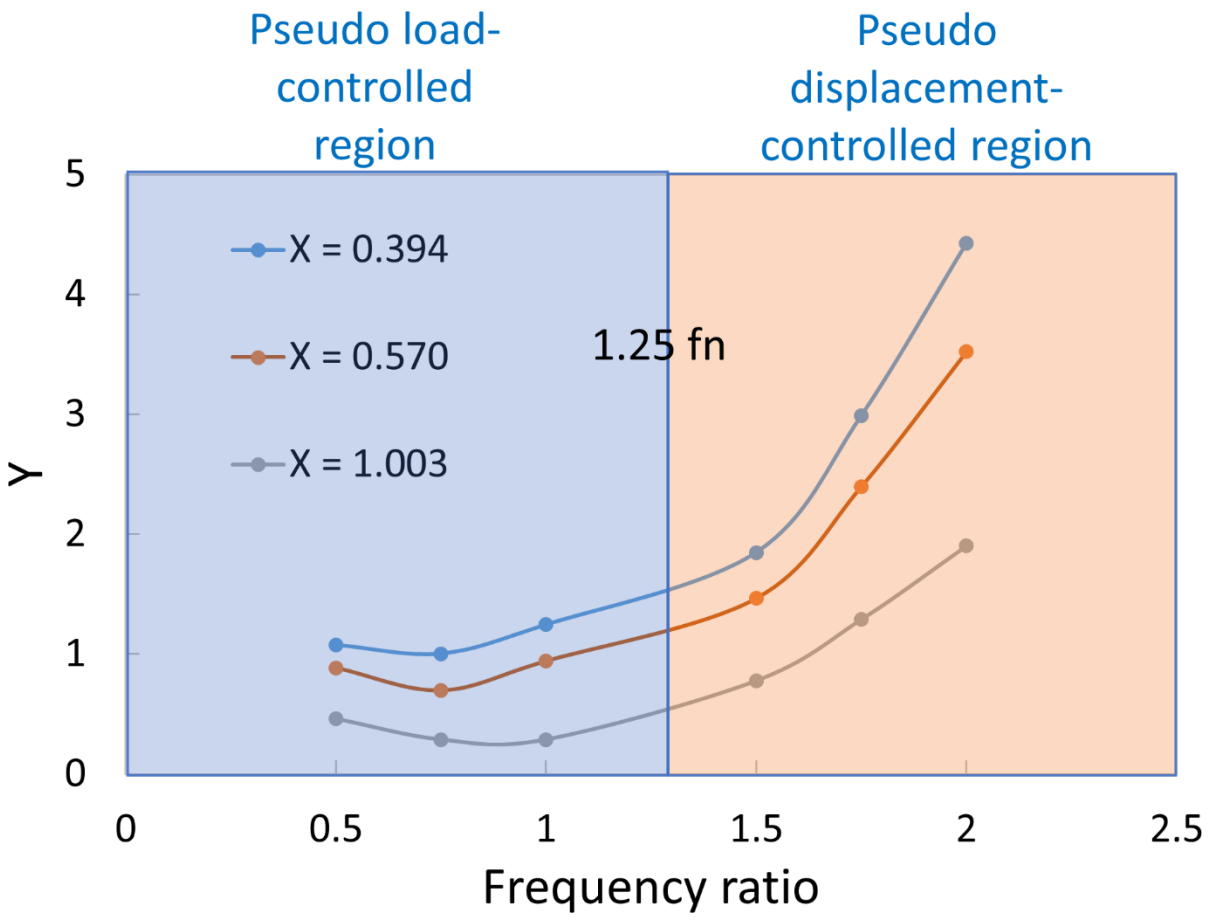

Figure 2-25 Two parts of the beam model according to the frequency ratio

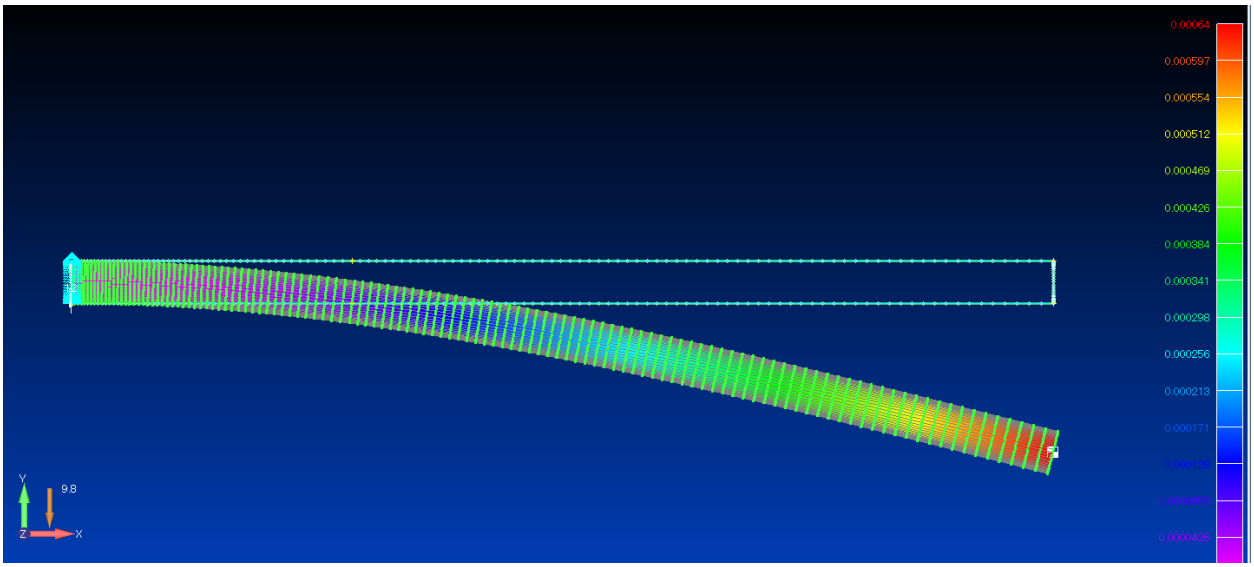

Figure 2-26 Deformation after vibrations

2.2.3 Comparison between experimental and numerical analyses

Four figures from Figure 2-27 to Figure 2-30 compare the numerical and experimental analysis results under SIN load waves with different frequencies. The trend of experimental results agrees well with FEA results. With the increment of X, Y decreases. This phenomenon means that the top mass contributed to the occurrence of ratcheting. In general, experimental results validated the FEM results under SIN excitations.

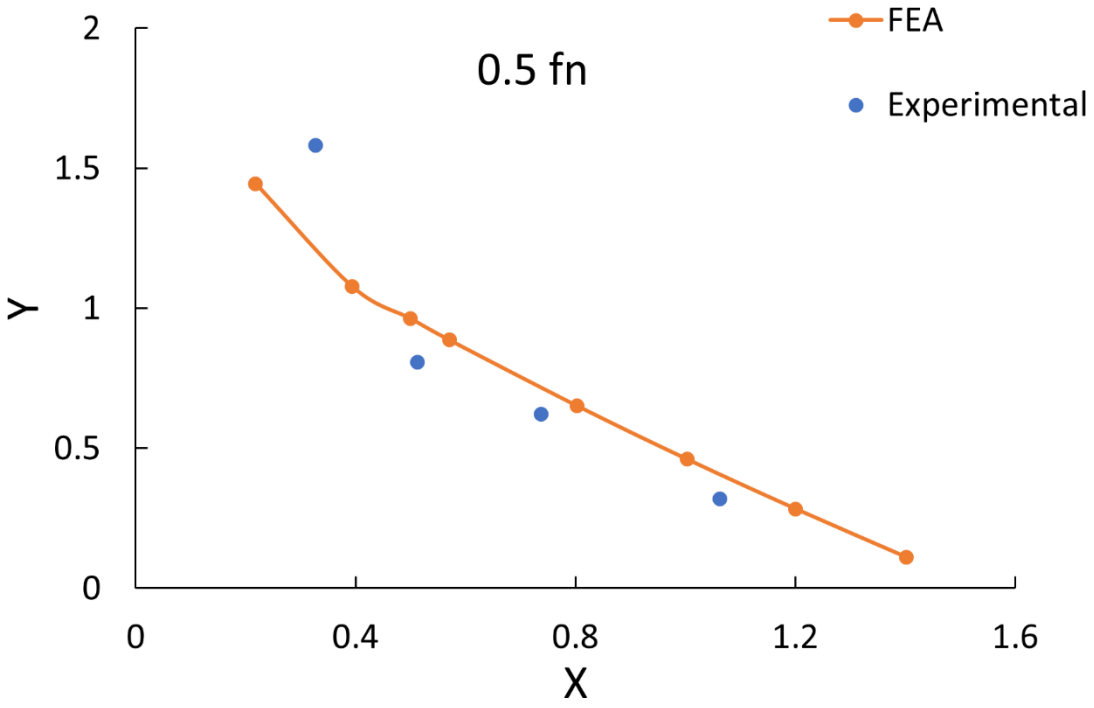

Figure 2-27 Experiment and numerical results under SIN acceleration waves at 0.5 fn

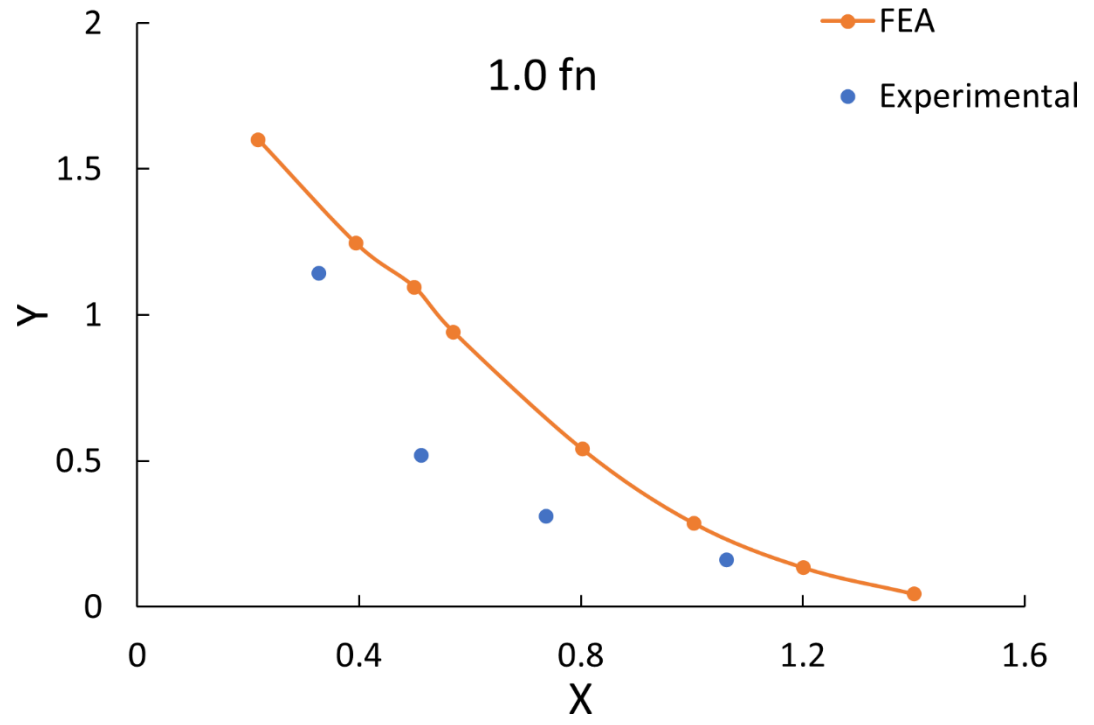

Figure 2-28 Experiment and numerical results under SIN acceleration waves at 1.0 fn

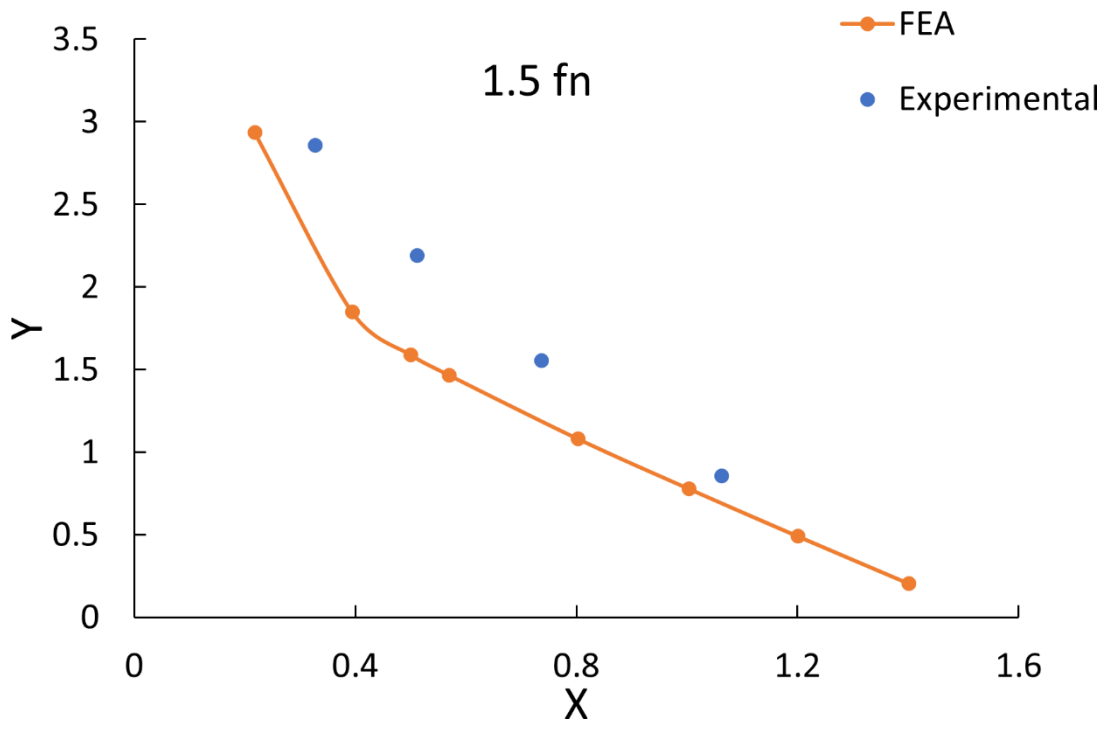

Figure 2-29 Experiment and numerical results under SIN acceleration waves at 1.5 fn

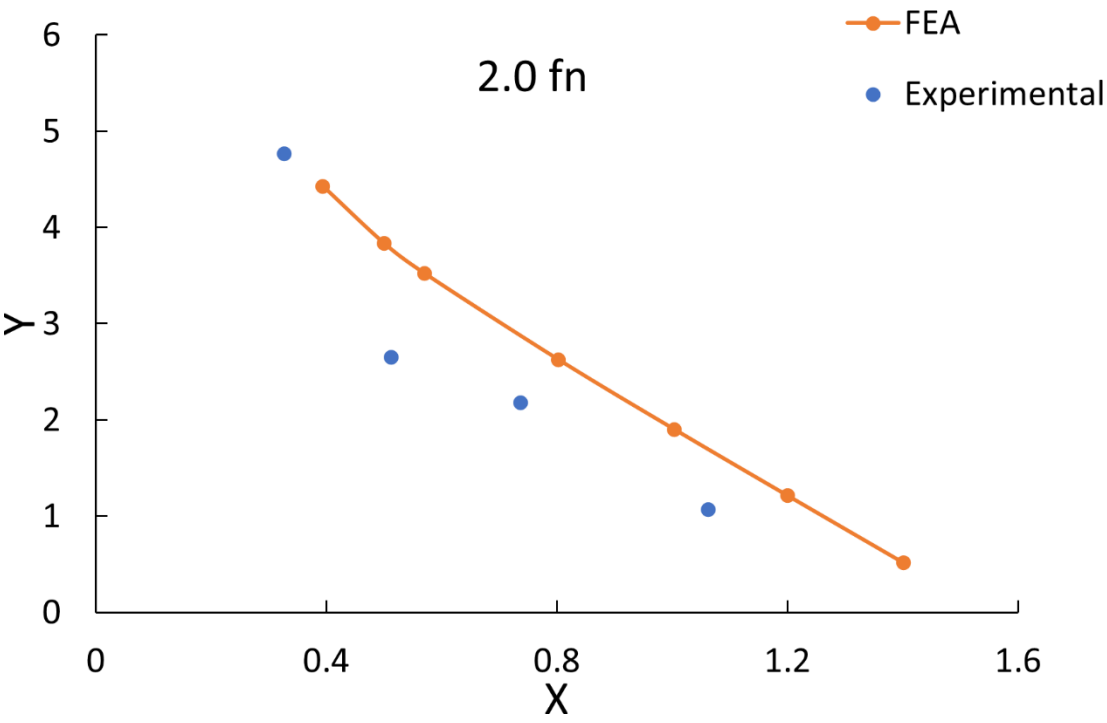

Figure 2-30 Experiment and numerical results under SIN acceleration waves at 2.0 fn

2.3 Beam models under SIN+SIN loads

The experimental and numerical conditions for the beam models under SIN+SIN loads are shown in Table 2-5 and Table 2-6, respectively.

Table 2-5 Experimental analysis conditions for ratcheting of beam models under SIN+SIN loads

Case #	Steady bending stress		Natural frequency (Hz)	Input functions (frequency ratio)
	Top additional mass (kg)	X		
1	0.245	0.400	Around 14.1	0.5 + 0.75
2				0.5 + 1.0
3				0.5 + 2.0
4				1.0 + 2.0
5	0.490	0.700	Around 9.6	0.5 + 0.75
6				0.5 + 1.0
7				0.5 + 2.0
8				1.0 + 2.0

Table 2-6 Numerical analysis conditions for ratcheting of the beam model under SIN+SIN loads

Case No.	Steady bending stress		Natural frequency (Hz)	Input functions (frequency ratio)
	Top additional mass (kg)	X		
1	0.050	0.394	36.185	0.5
2				0.75
3				1.0
4				1.5
5				1.75
6				2.0
7				0.5 + 0.75
8				0.5 + 1.0
9				0.5 + 1.5
10				0.5 + 1.75
11				0.5 + 2.0
12				1.0 + 1.5

13				1.0 + 1.75
14				1.0 + 2.0
15				1.5 + 1.75
16				1.5 + 2.0
17				1.75 + 2.0
18	0.100	0.570	28.330	0.5
19				0.75
20				1.0
21				1.5
22				1.75
23				2.0
24				0.5 + 0.75
25				0.5 + 1.0
26				0.5 + 1.5
27				0.5 + 1.75
28				0.5 + 2.0
29				1.0 + 1.5
30				1.0 + 1.75
31				1.0 + 2.0
32				1.5 + 1.75
33				1.5 + 2.0
34				1.75 + 2.0
35	0.223	1.003	20.277	0.5
36				0.75
37				1.0
38				1.5
39				1.75
40				2.0
41				0.5 + 0.75
42				0.5 + 1.0
43				0.5 + 1.5
44				0.5 + 1.75
45				0.5 + 2.0
46				1.0 + 1.5
47				1.0 + 1.75
48				1.0 + 2.0
49				1.5 + 1.75
50				1.5 + 2.0
51				1.75 + 2.0
52				0.5

53				0.75
54				1.0

2.3.1 Compare experimental and numerical results for ratcheting of beam models under SIN+SIN loads

Figure 2-31, Figure 2-32, Figure 2-33, and Figure 2-34 display the experimental and FEA results for the ratcheting of beam models under different SIN+SIN loads. Both approaches had a similar trend with a relatively small difference.

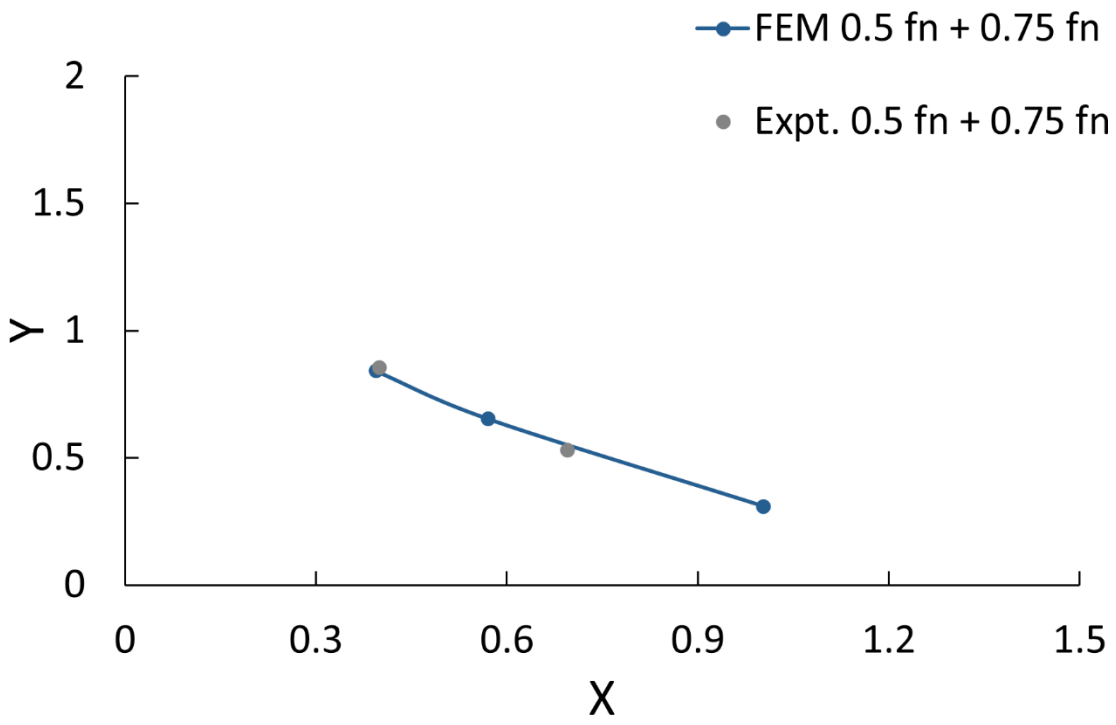

Figure 2-31 Comparison of experimental and numerical results (0.5 fn + 0.75 fn)

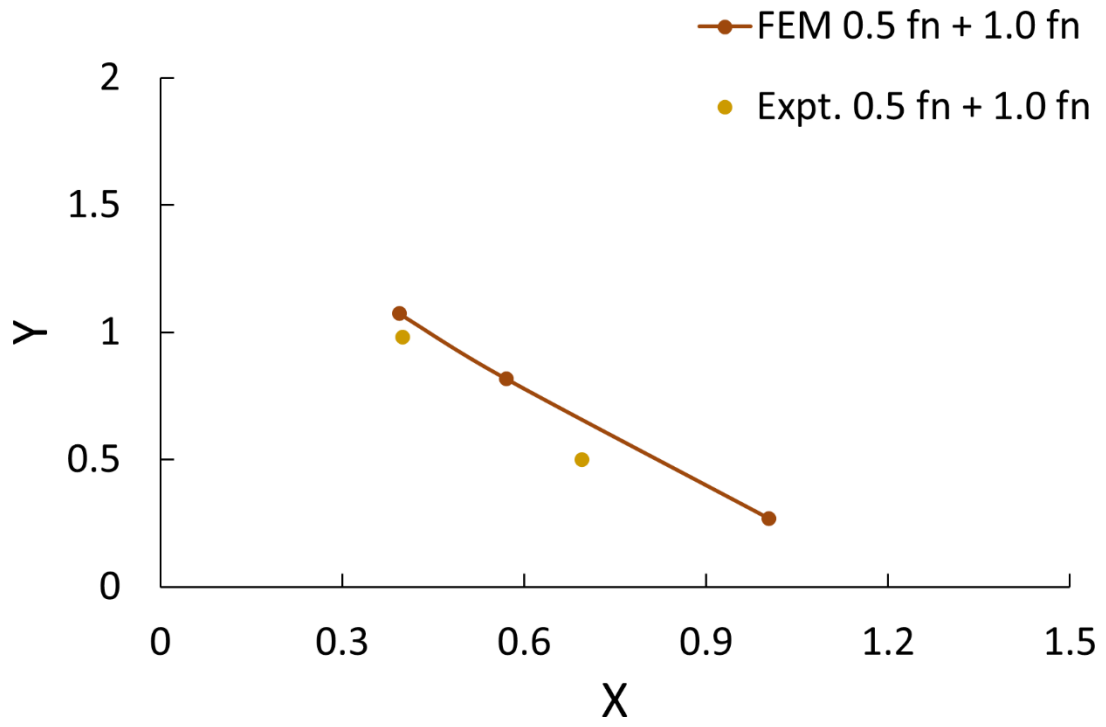

Figure 2-32 Comparison of experimental and numerical results (0.5 fn + 1.0 fn)

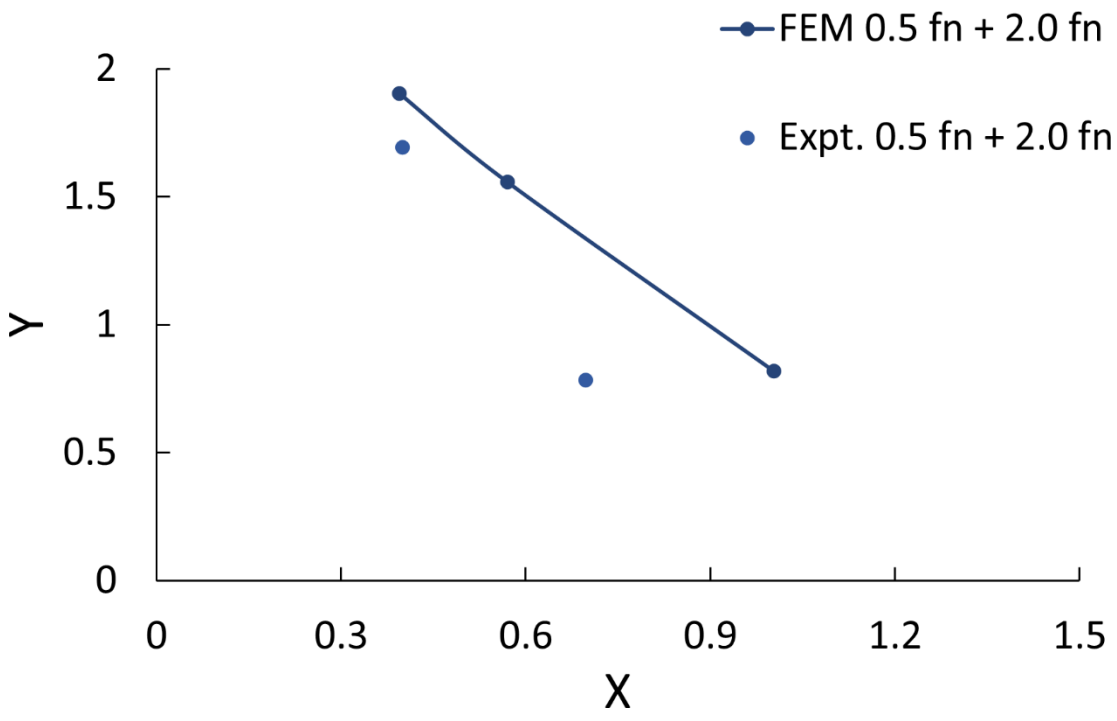

Figure 2-33 Comparison of experimental and numerical results (0.5 fn + 2.0 fn)

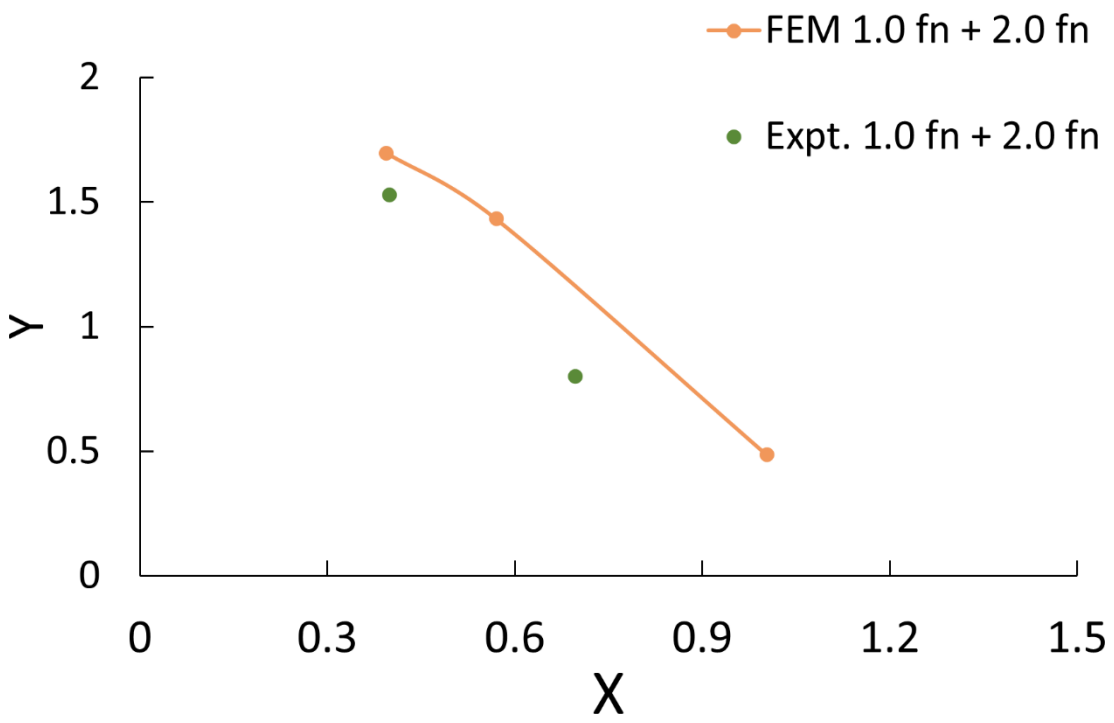

Figure 2-34 Comparison of experimental and numerical results (1.0 fn + 2.0 fn)

2.3.2 Numerical results and analyses for ratcheting of beam models under SIN+SIN loads

Figure 2-35, Figure 2-36, and Figure 2-37 show the numerical results of ratcheting occurrence conditions with SIN+SIN loads. In each figure, the frequency ratio of one component was set as a constant. The ratcheting line of the SIN load with that frequency ratio is added to each figure. The other frequency ratio varied from 0.5 to 2.0. In order to distinguish the characteristics of SIN+SIN loads, the collapse line and the Yamashita line are also referred. It is evident that if the frequency of one component increases from 0.5 fn to 2.0 fn, the ratcheting boundaries move upside. This phenomenon means that if one component is at a lower frequency, the load is close to the load-controlled load. In contrast, when one component is at a higher frequency, the vibration wave is close to a pure displacement-controlled load. Therefore, the composite accelerations of lower frequencies need smaller accelerations and play a dominant effect in terms of the occurrence of ratcheting.

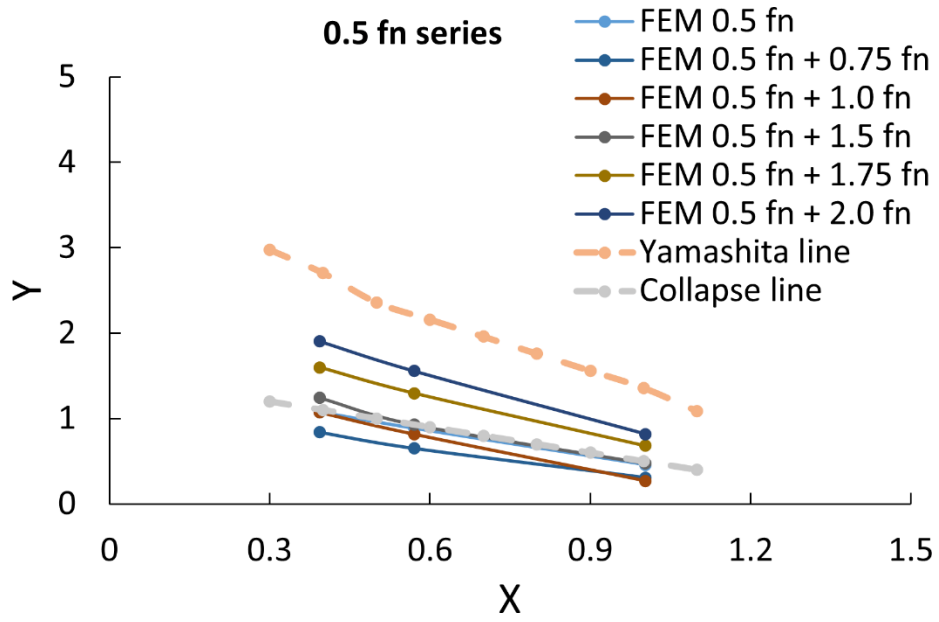

Figure 2-35 Ratcheting diagram of composite sinusoidal waves (0.5 fn series)

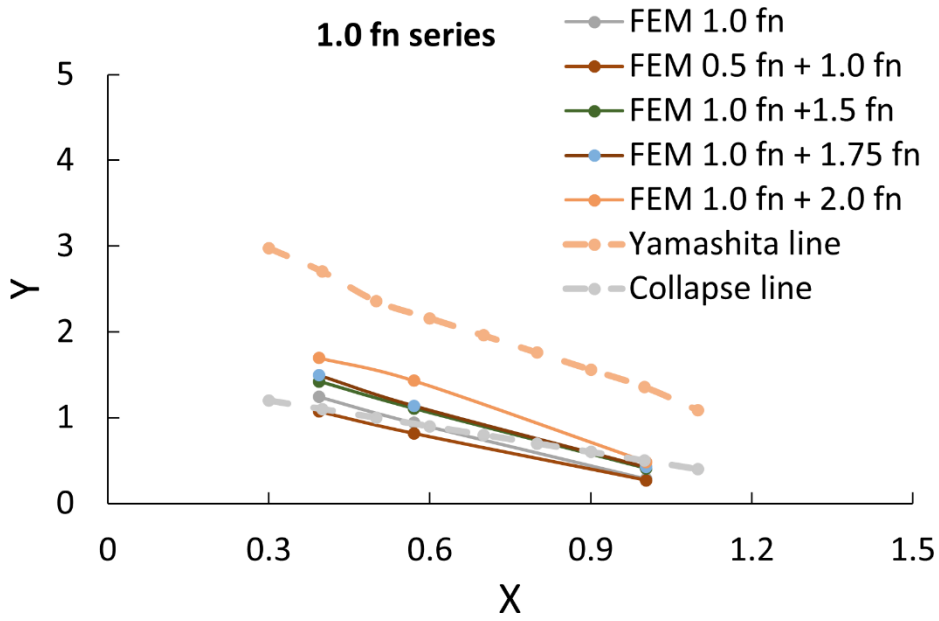

Figure 2-36 Ratcheting diagram of composite sinusoidal waves (1.0 fn series)

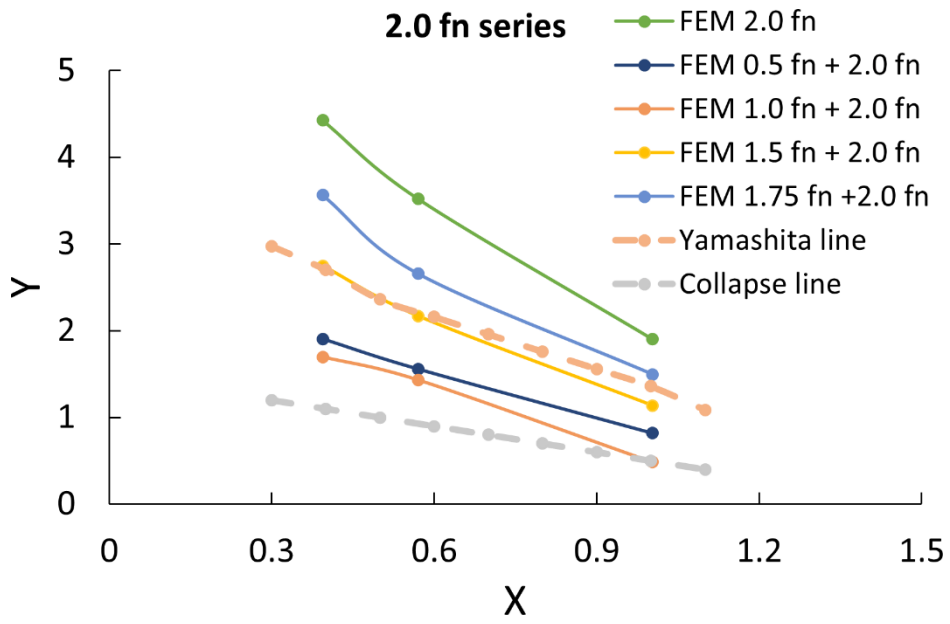

Figure 2-37 Ratcheting diagram of composite sinusoidal waves (2.0 fn series)

Figure 2-38 exhibits the deformation on the beam model after vibration—visible deformation distributed in the whole beam model. The displacement on the beam model's right vertex of the beam models under two different SIN+SIN waves is shown in Figure 2-39. The frequency combinations of the upper curve are 0.5 fn and 1.0 fn (Case 1); similarly, the frequency combinations of the lower curve are 0.5 fn and 2.0 fn (Case 2). After vibrations, the accumulated displacement of Case 1 was relatively larger compared to that of Case 2. This phenomenon can also verify that the composite acceleration of lower frequency contributes more to the occurrence of ratcheting.

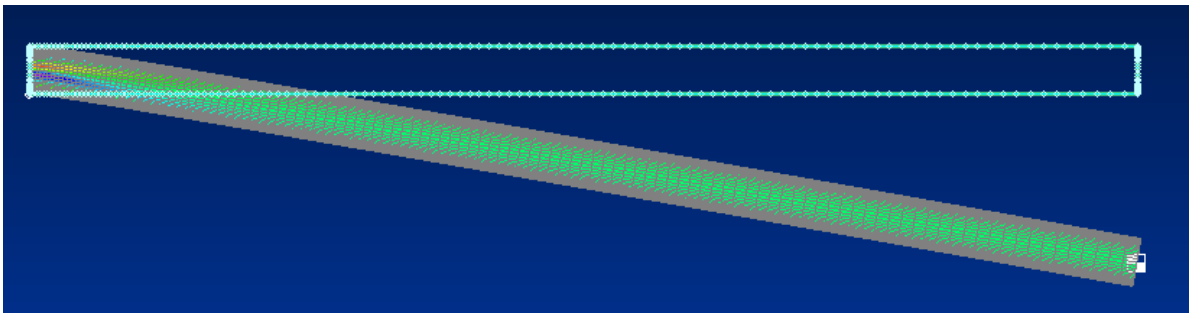

Figure 2-38 Deformation after vibrations

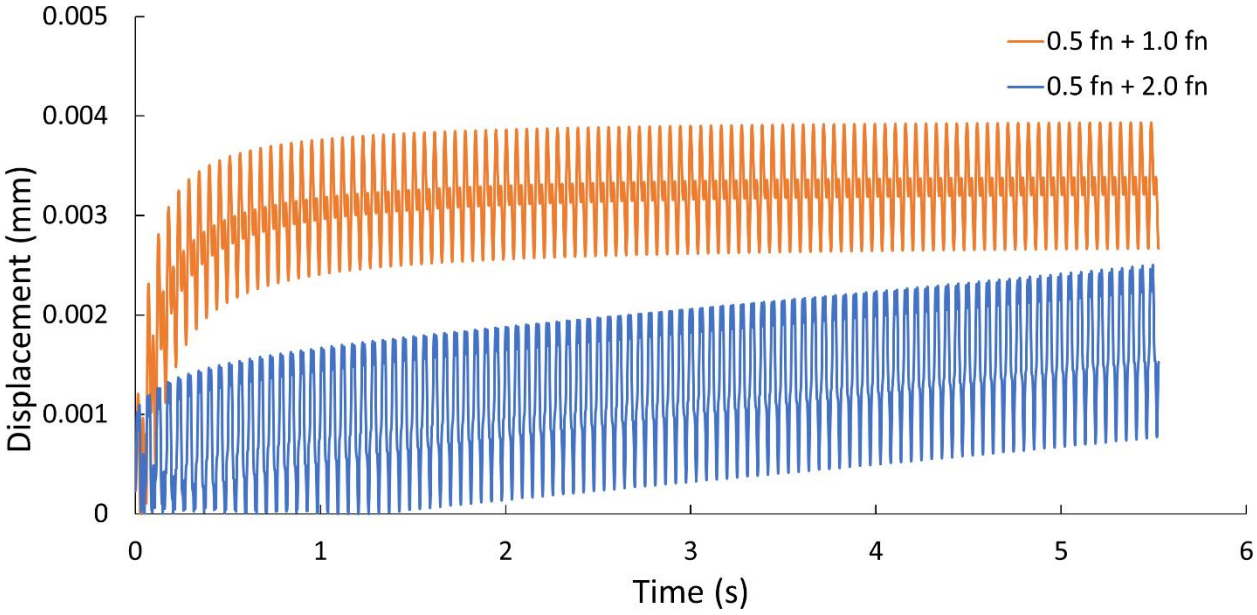

Figure 2-39 Displacement on the beam model's right vertex of the beam models in the two cases

The energy transferred from loading vibrations to beam models was calculated by the integration of the product of the external force and response velocity, as shown in Equation 2-13 (Figure 2-40). Figure 2-41 compares the transferred energy between SIN and SIN+SIN (0.5 fn series) vibrations. The forcing frequency of SIN loads varied from 0.5 fn to 2.0 fn. For SIN+SIN loads, the frequency of one component was fixed to be 0.5 fn. The second frequency varied from 0.75 fn to 2.0 fn. It is evident that if one more component of lower frequency (0.5 fn) was added to the loading vibrations, more energy would be transferred to the beam model.

$$\text{Work rate} = -m\ddot{x}_e \times \dot{x} \qquad \text{Equation 2-13}$$

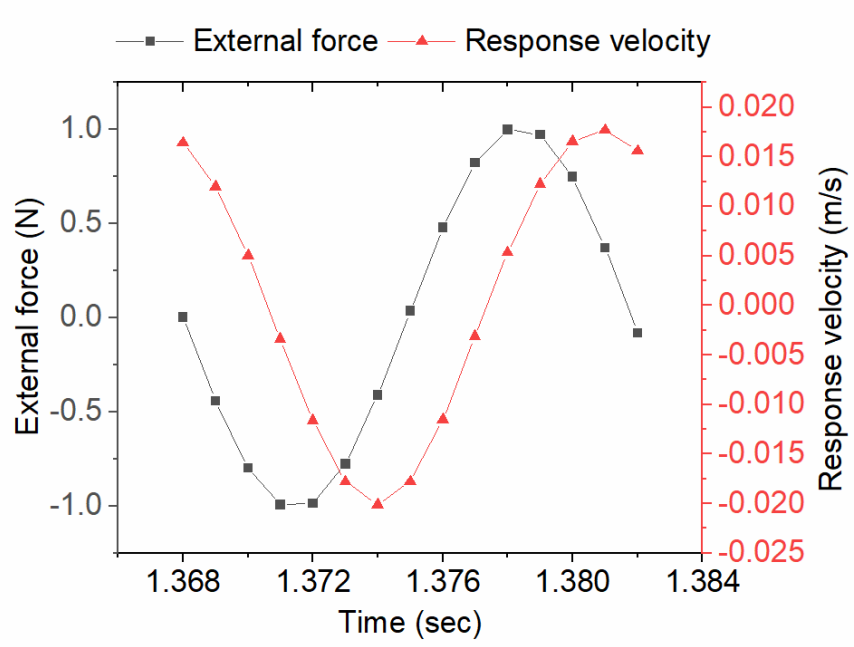

Figure 2-40 Energy transferred from loading vibrations to beam models (2.0 fn)

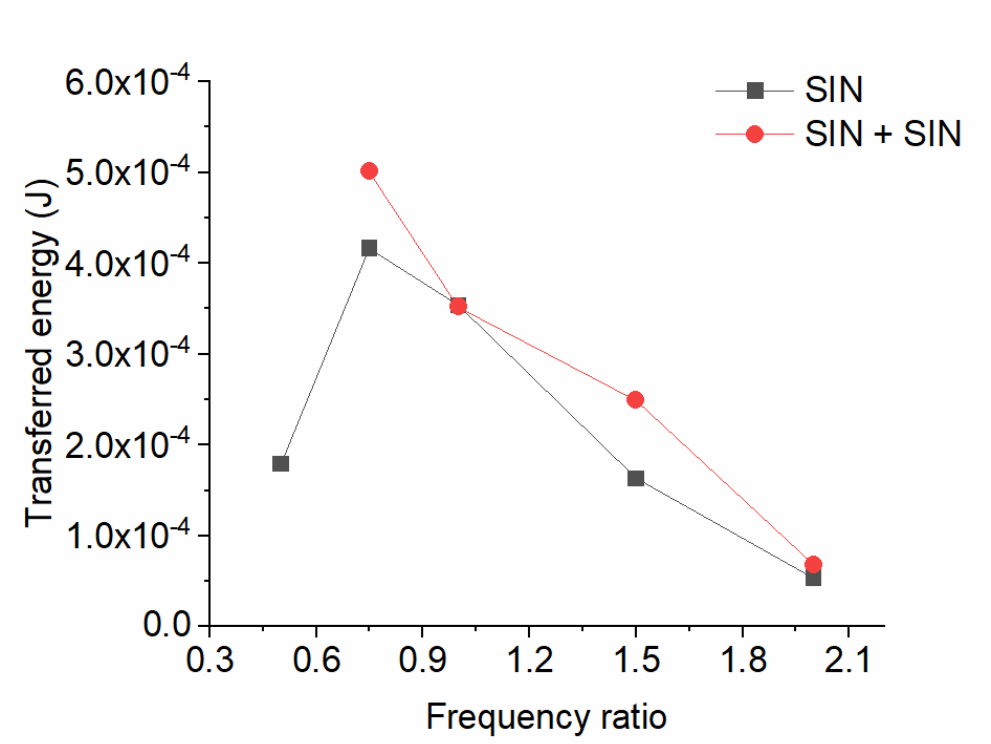

Figure 2-41 Comparison of the transferred energy between SIN and SIN+SIN (0.5 fn series) vibrations

2.4 Results and analyses for ratcheting of beam models under seismic loads

The experimental and numerical analysis conditions for ratcheting of beam models under seismic loads are shown in Table 2-7 and Table 2-8, respectively.

Table 2-7 Experimental analysis conditions for ratcheting of beam models under seismic loads

Case #	Steady bending stress		Natural frequency (Hz)	Input functions (frequency ratio)
	Top additional mass (gram)	X		
1	245	0.400	Around 14.1	0.5
2				1.0
3	490	0.700	Around 9.6	0.5
4				1.0

Table 2-8 Numerical analysis conditions for ratcheting of the beam model under seismic loads

Case No.	Steady bending stress		Natural frequency (Hz)	Input functions (frequency ratio)
	Top additional mass (kg)	X		
1	0.05	0.39	36.2	0.5
2				1.0
3				1.5
4	0.10	0.57	28.4	0.5
5				1.0
6				1.5
7	0.20	0.92	21.4	0.5
8				1.0
9				1.5
10	0.3	1.27	17.8	0.5
11				1.0
12				1.5

2.4.1 Compare experimental and numerical results for ratcheting of beam models under seismic loads

Figure 2-42 and Figure 2-43 compare the experimental and numerical results under seismic accelerations waves at 0.5 fn and 1.0 fn. The trend of experimental and FEA results is similar to each other, with a relatively smaller difference. It means that the experiments can validate the FEA results.

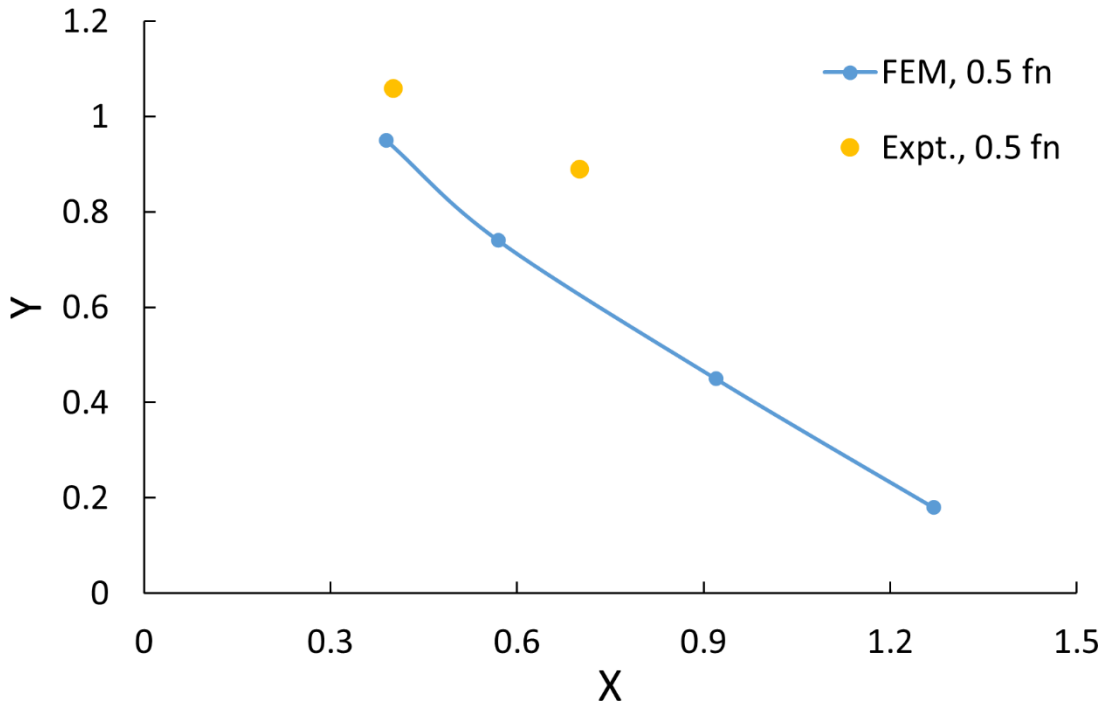

Figure 2-42 Experimental and numerical results under seismic accelerations at 0.5 fn

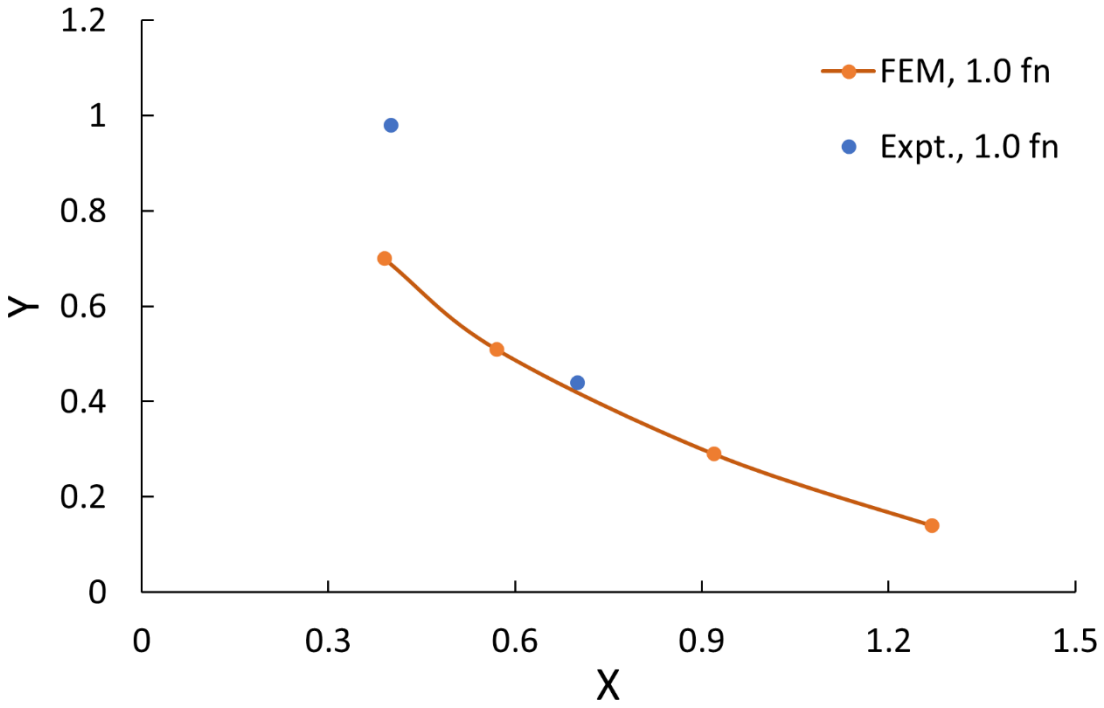

Figure 2-43 Experimental and numerical results under seismic accelerations at 1.5 fn

2.4.2 Numerical results and analyses for ratcheting of beam models under seismic loads

In the ratcheting diagram for seismic loads, the Yamashita line and the collapse line are also referred to in the ratcheting diagram to recognize the characteristics of the seismic excitations (Figure 2-44). The analytical results of seismic excitations have a reasonable correlation with that of SIN excitations (Figure 2-23) due to the relatively narrow sensitive region of the seismic wave. It means that it is reasonable to use simple SIN waves instead of the complicated seismic wave to judge the occurrence of ratcheting if the major frequency of the seismic wave is the same as the SIN wave.

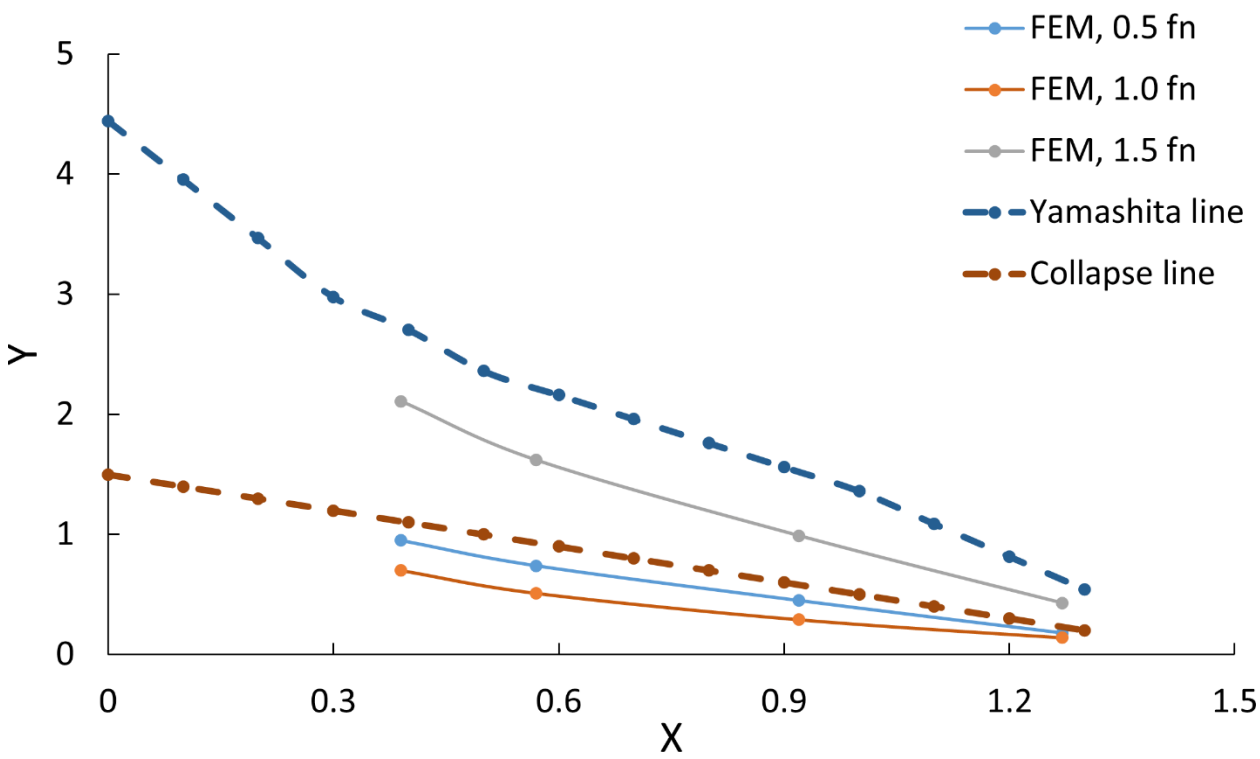

Figure 2-44 Ratcheting diagram for seismic loads

2.5 Conclusions of ratcheting research of beam models

This chapter focused on the ratcheting research of beam models under different loading waves. The lower frequency load has a relatively lower Y value, which means ratcheting was highly possible to occur in such a case. With lower frequency input, the load acts like a load-controlled load. With higher frequency input, the load acts like a displacement-controlled load. The whole region is divided into two parts: the pseudo load-controlled region and the pseudo displacement-controlled region according to the frequency ratio. The resonance effect is not evident in the beam model since the plastic deformation occurred in most parts of the beam model. In addition, it is meaningful to use simple SIN waves instead of the complicated seismic wave to judge the occurrence of ratcheting if the major frequency of the seismic wave is the same as the SIN wave.

Chapter 3. Ratcheting of Piping Models

Excessive vibrations are frequently encountered in piping, which is one of the most basic structures in nuclear power plants. Excessive vibrations can lead to ratcheting until the plastic collapse of the structure occurs. Collapse is usually considered as the failure mode under severe seismic loads in the seismic probabilistic risk assessment. However, this assumption is not appropriate when considering the best estimation for countermeasures against beyond design basis accidents. In this chapter, seismic ratcheting occurred due to the combined effect of constant external compressive force and dynamic cyclic vibrations. Experimental and numerical analyses were performed on round bent solid bars, which represented piping. Differences between round bent solid bars and pipes had small influences on conclusions because the interest of the current research was the relative strength. The solid bent bar was simple compared to a real complex piping system, but it also contained two elbow parts and three straight parts. Therefore, the solid bent bar was enough to present a real piping system in this research. Characteristics of seismic loads between load-controlled and displacement-controlled properties were studied from the viewpoint of the frequency ratio of the forcing frequency to the natural frequency of the piping model. The effect of supports on the occurrence of ratcheting was also considered.

3.1 Methods for ratcheting analyses of piping models

Experimental and numerical investigations on ratcheting of piping were conducted with round bent solid bars made of lead alloy to clarify the occurrence conditions of ratcheting under the beyond design level seismic loads.

3.1.1 The experimental method of the piping model

The purposes of the shaking table tests (experiments) were to observe the failure behavior of piping under excessive dynamic inputs and to validate the numerical analyses.

Similar to the beam model analyses, due to the limitation of the shaking table at the authors' laboratory and safety concerns, the material of the piping specimens was also lead alloy (Table 3-1). The experiment set is shown in Figure 3-1 with geometrical parameters shown in Figure 3-2. There was one mass (10 kg) attached to one end of the piping model and moved with the model. This mass did not provide the force of gravity since the shaking table supported it. The other end was fixed with the shaking table.

Table 3-1 Material parameters of piping models

Pb 99%- Sb 1%	Symbol	Unit	Value
Young's Modulus	E	MPa	19150 (23℃)
Poisson's ratio	ν	-	0.36
Yield stress	σ_y	MPa	8.5 (23℃)
Mass density	ρ	kg/m^3	11,340

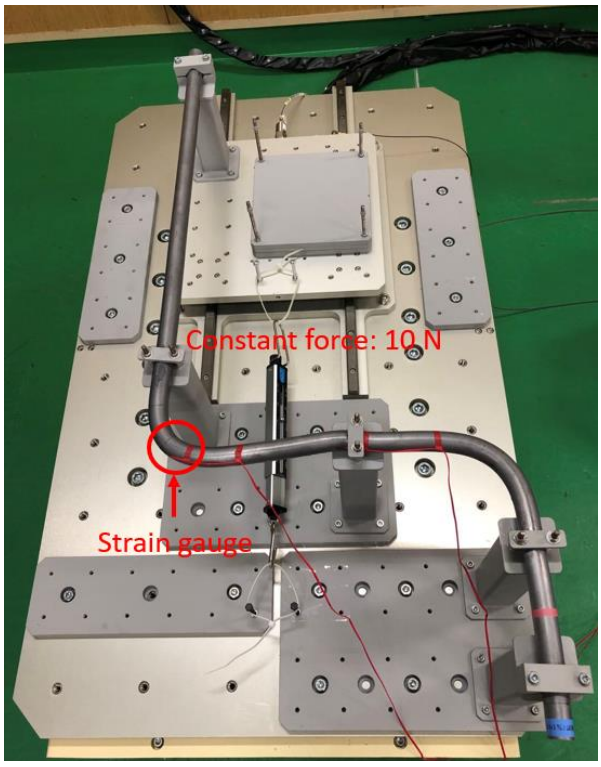

Figure 3-1 Piping model (10-S) after vibrations. One strain gauge was attached to the elbow part

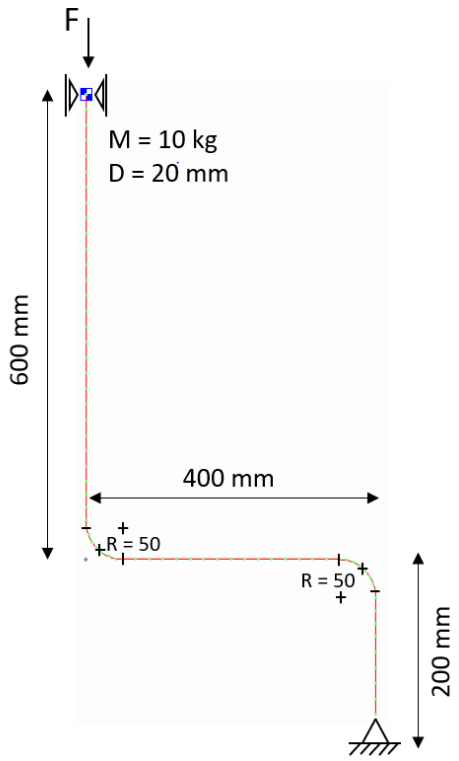

Figure 3-2 Geometrical parameters of the piping model (Piping-N)

There were two types of loads applied to the piping model. The first one was the external compressive force at the ends of the piping model, which acted as the load-controlled force and caused primary bending stress. The second load was cyclic accelerations from the shaking table, acting as the source of alternating dynamic loads. The alternating dynamic load exhibited either load-controlled or displacement-controlled characteristics according to the frequency ratio, as discussed in the next sections. The amplitude and frequency of input vibrations were adjusted to determine the onset of ratcheting at various load conditions.

Figure 3-3 shows four models in experiments. The piping models were divided into two categories. The first type was the piping model without additional supports such as a and c in Figure 3-3; this type was called “Piping-N” in this research. The other type was the piping model with three additional supports in the medium part, such as b and d in Figure 3-3, and this type was called “Piping-S” in this research.

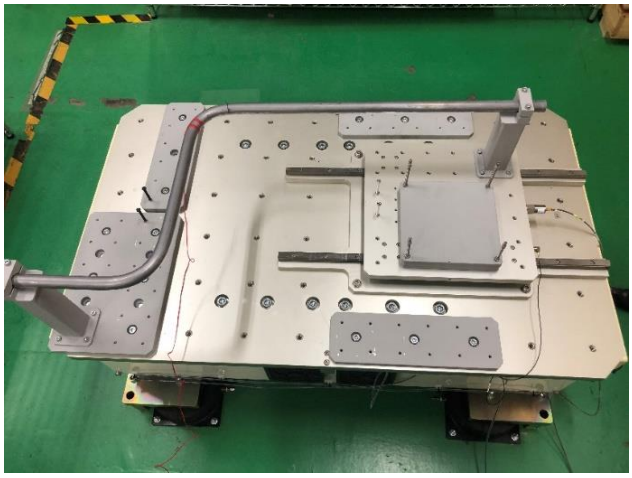

a. 0-N

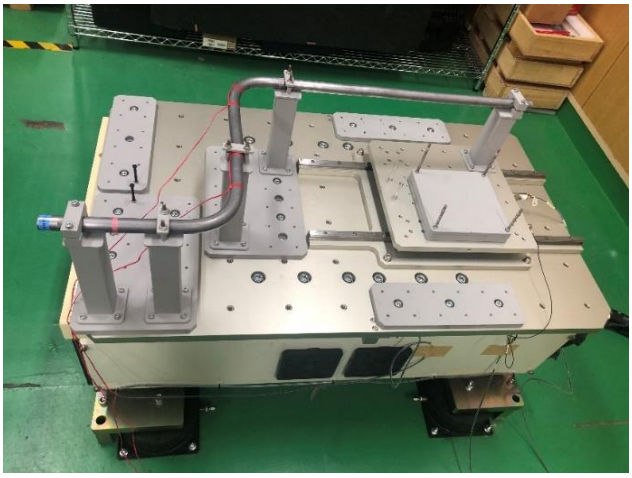

b. 0-S

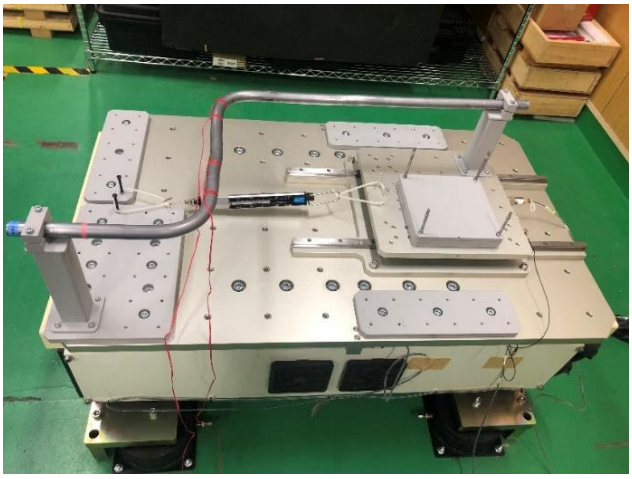

c. 10-N

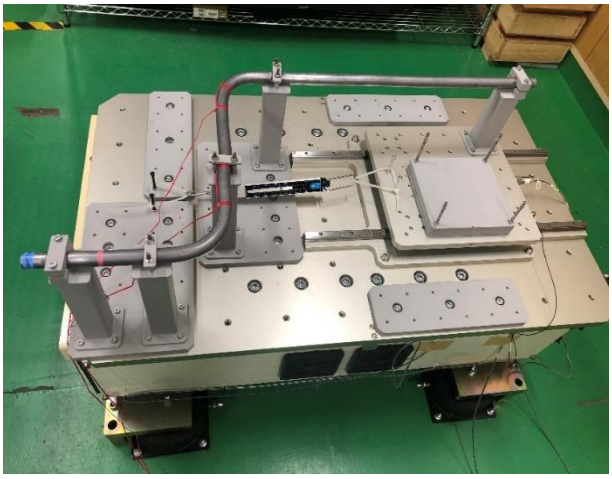

d. 10-S

Figure 3-3 Four models in experiments. Piping-N (a and c) did not contain three additional supports in the medium part. In contrast, there were three additional supports in the medium part of Piping-S (b and d).

The naming method was according to the external force and the supports (Table 3-2). For example, if one model had three additional supports with the external force equal to 10 N, it was named as “10-S”. Similarly, the model “10-N” meant that the external force was 10 N, and this model contained three more supports.

Table 3-2 Naming method of models

Model Name	External force	# of additional supports
Unit	**N**	-
0-N	0	None
0-S	0	3
10-N	10	None
10-S	10	3
15-N	15	None
15-S	15	3

Occurrence conditions of ratcheting were observed for loads with different frequencies. “fn” used in this study meant the first natural frequency of the piping model. “2.0 fn” meant that the frequency of the input load was twice the natural frequency of the piping model, and the frequency ratio was “2.0”.

3.1.2 The numerical method for the piping model

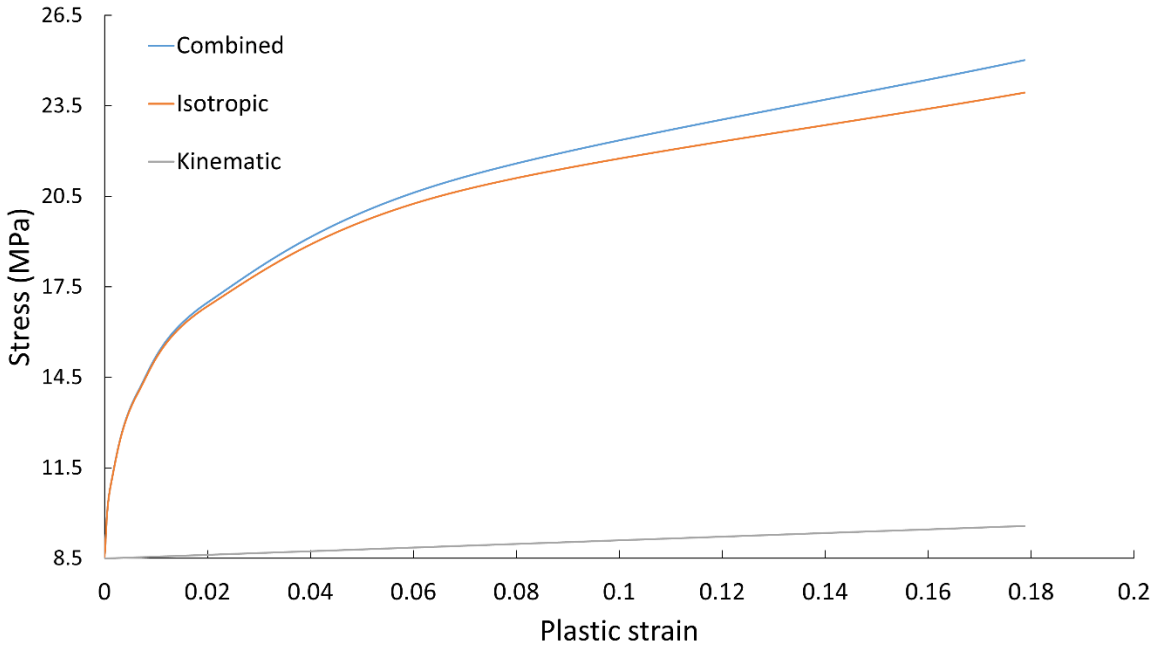

Figure 3-4 The nonlinear stress-strain curve used in the FEA of the piping model. Both kinematic and isotropic hardening rules were included.

In numerical analyses, similar to the studies in the beam model, FINAS/STAR [54] did the finite element analyses with the aid of the mesh generation by FEMAP [55]. The nonlinear stress-strain curve of the Pb99%-Sb1% alloy (Figure 3-4), which was from the tensile test at room temperature at the authors' laboratory, was applied in numerical analyses. The combined line is the material stress-strain relationship from tensile tests. Both kinematic and isotropic hardening rules were included in this study.

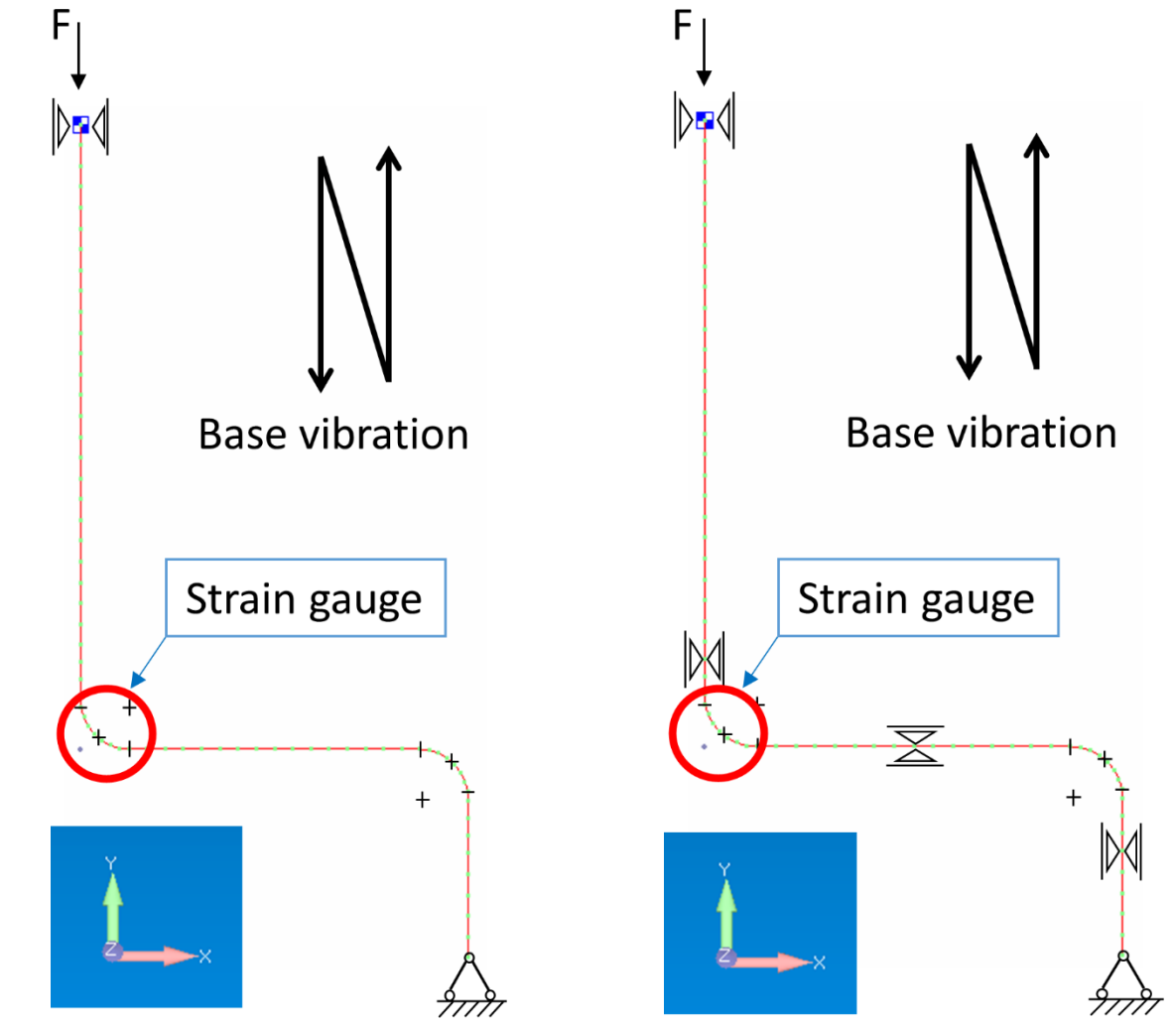

a. The piping model without three external supports (Piping-N).

b. The piping model with three external supports (Piping-S).

Figure 3-5 Two types of piping models in FEM

Same as the experimental method, the piping models in FEM were also divided into two categories, as shown in Figure 3-5: the piping model without additional supports (Piping-N) and the piping model with three supports in the medium part (Piping-S). The naming rule is the same as that in the experimental method.

3.1.3 Verification of the constitutive equation

The finite element analysis of the loading test of one element (0.167 mm × 0.167mm), shown in Figure 3-6, was conducted using the stress-strain data from the material tensile tests at the authors' laboratory (Figure 3-4) to verify the constitutive equation. One sinusoidal cycle load was applied to the element (Figure 3-7 and Figure 3-8).

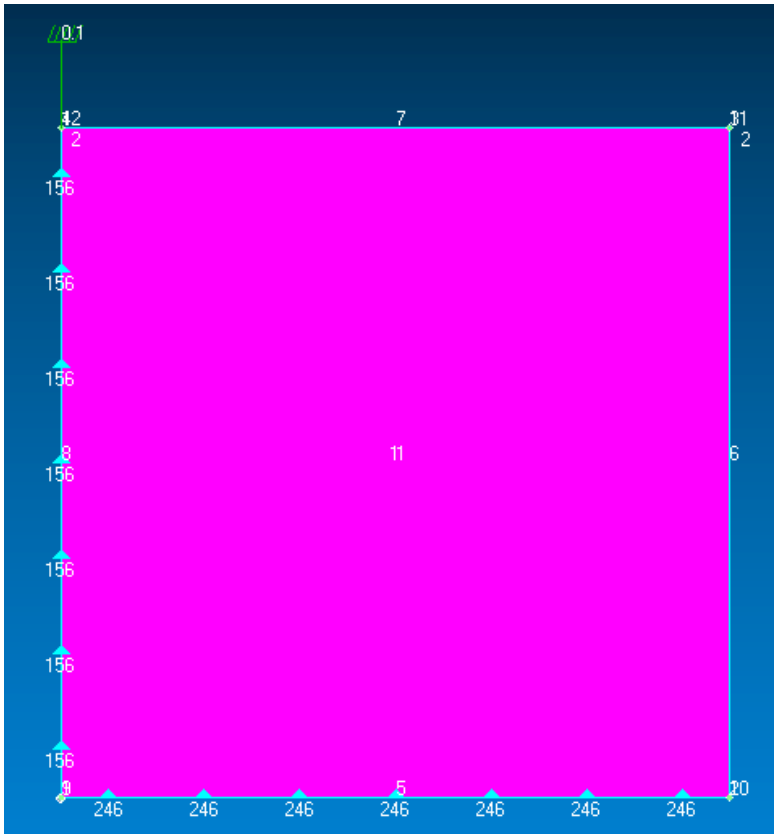

Figure 3-6 Loading test of one element in FEMAP

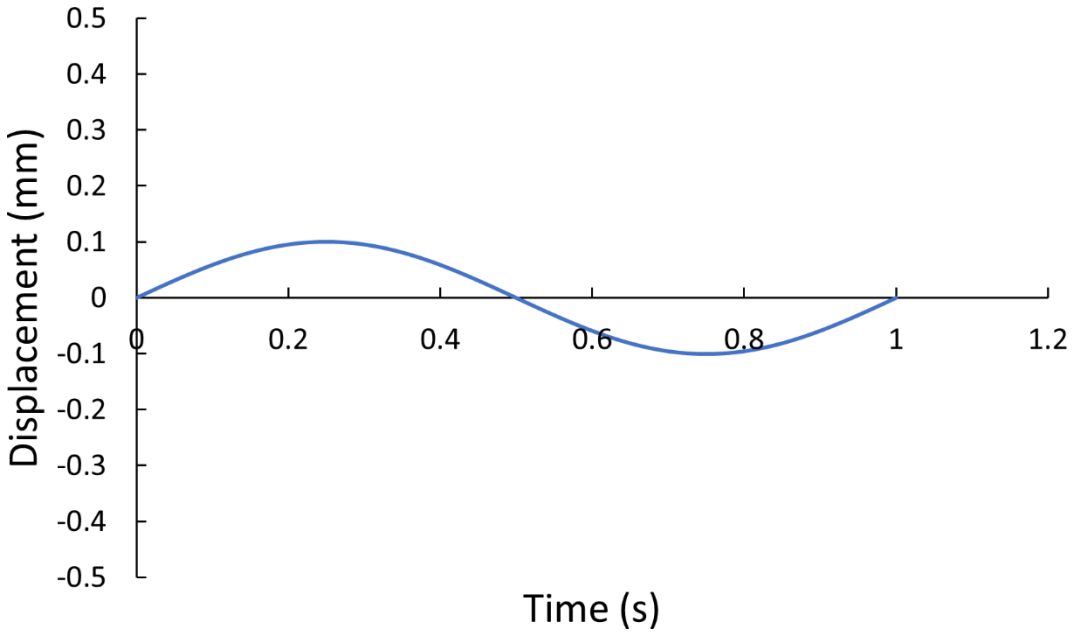

Figure 3-7 One sinusoidal cycle load (0.1 mm)

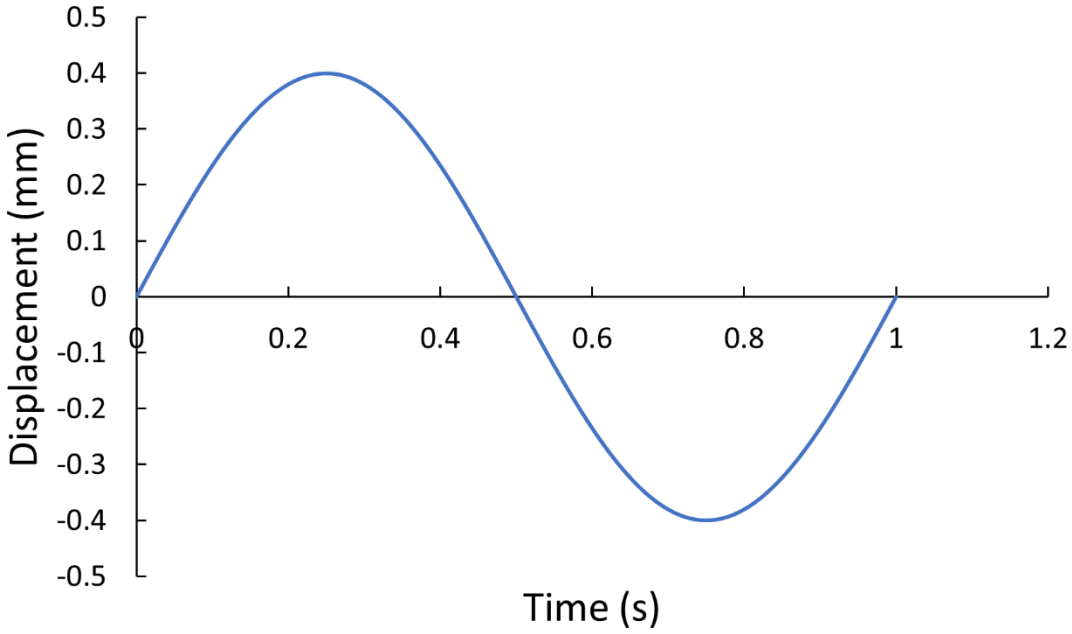

Figure 3-8 One sinusoidal cycle load (0.4 mm)

The responses of the one-element model under loads with two different amplitudes were shown in Figure 3-9 and Figure 3-10. The results indicated that the stress-strain performance in FEM had a good correlation with the material test results.

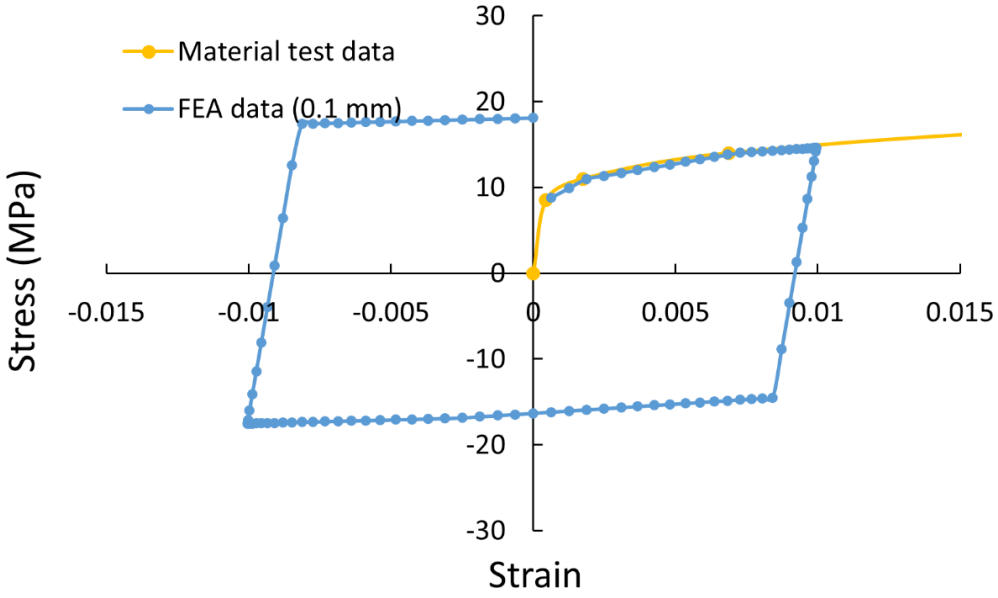

Figure 3-9 Loading results (0.1 mm)

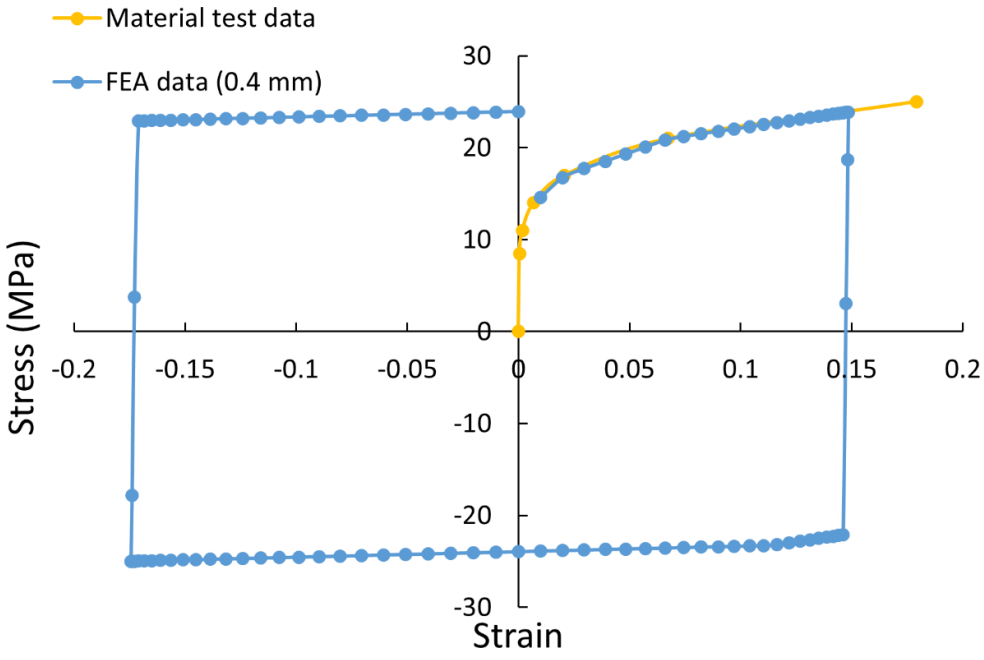

Figure 3-10 Loading results (0.4 mm)

3.1.4 Input waves

Understanding the response of structures to sinusoidal excitations provides insight into how the system responds to seismic loads. Figure 3-11 shows one example of input sinusoidal accelerations. There were 50 sinusoidal waves with external five gradual increasing cycles at the beginning and five gradual decreasing cycles in the end.

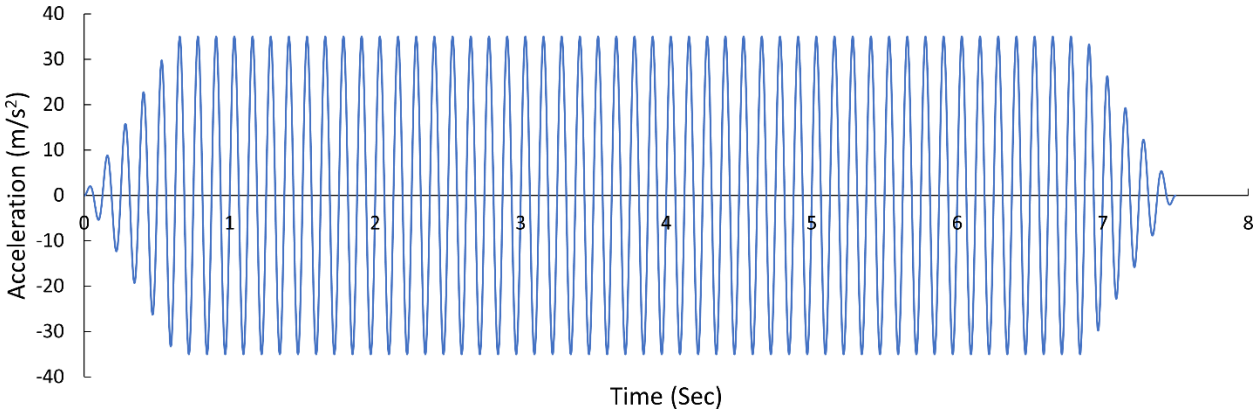

Figure 3-11 One example of input sinusoidal accelerations

3.1.5 Criteria for ratcheting

To draw the ratcheting diagram, a criterion was needed to judge the occurrence condition of ratcheting. For the piping model, it was determined to be a 0.5% plastic strain at the extrados of the elbow accumulated during 50 sinusoidal cycles.

3.1.6 Natural frequencies and sweep tests

Piping supports are usually applied to stop vibrations at the supports. It is well known that whenever the frequency of excitation coincides with one of the natural frequencies of the system, resonance occurs and can lead to the failure of the system. Thus, in any system, resonance conditions must be avoided. Therefore, it is necessary to check the natural frequencies of the piping to prevent resonance. Table 3-3 shows the first three natural frequencies of the two types of piping models in this research, which had similar results as the sweep excitation test in experiments. From the table, it is clear that the three external supports increased the natural

frequencies of piping. In the current research, only the first natural frequency was considered. The participation factor of the rest frequencies was negligible since they were much larger than the first natural frequency.

Table 3-3 Natural frequencies of the piping model in numerical analysis

Parameters	Unit	Piping-N	Piping-S
Natural frequencies (FINAS/STAR)	Hz	4.6	12.8
		36.2	78.0
		55.7	140.8

Sweep excitation tests were conducted to measure the natural frequency in experiments. Figure 3-12 shows the sweep excitation test of 0-N, and the primary natural frequency was 4.9 Hz, which had a good correlation with that in FEM (4.6 Hz).

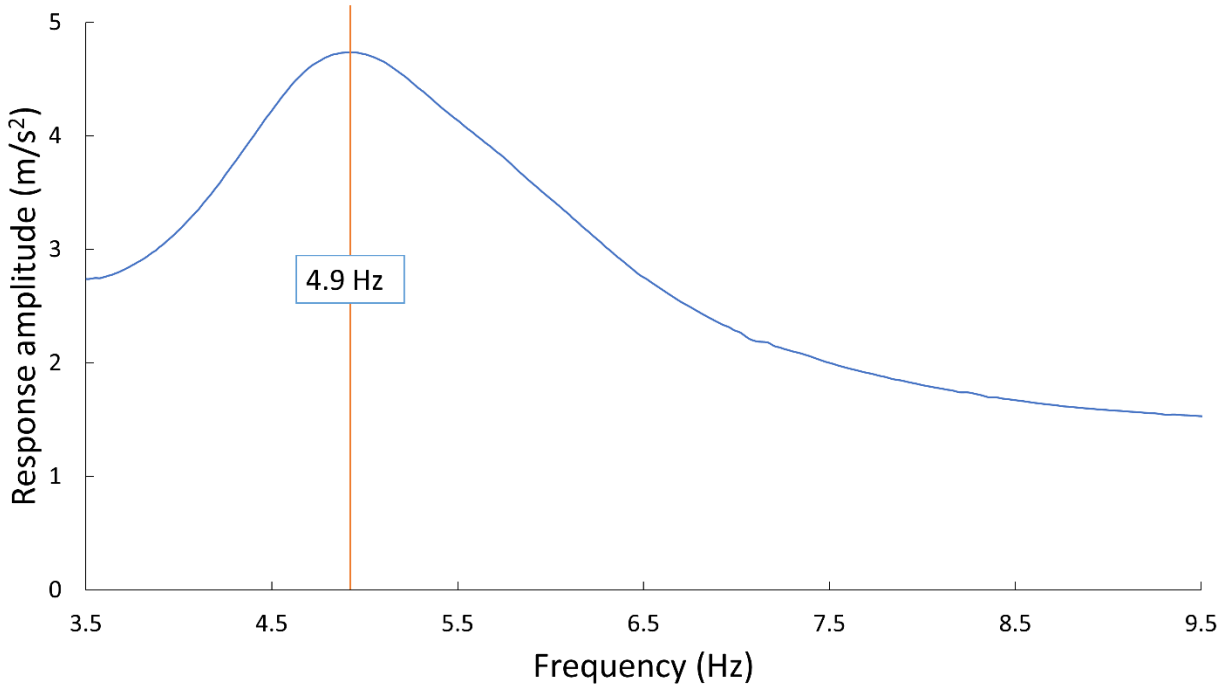

Figure 3-12 Sweep test of 0-N. The input acceleration amplitude is 2 m/s^2

Table 3-4 compares natural frequencies in FEM and experiments. The natural frequencies measured before experiments matched well the that in FEM. However, after experiments, natural frequencies decreased a little, especially in Piping-S. This phenomenon was due to the large plastic deformation around supports (Figure 3-13).

Table 3-4 Comparison of natural frequencies in FEM and experiments

Natural frequencies	Unit	Piping-N	Piping-S
FINAS/STAR	Hz	4.6	12.8
Before the experiment	Hz	4.9	11.5
After the experiments	Hz	4.4	8.5

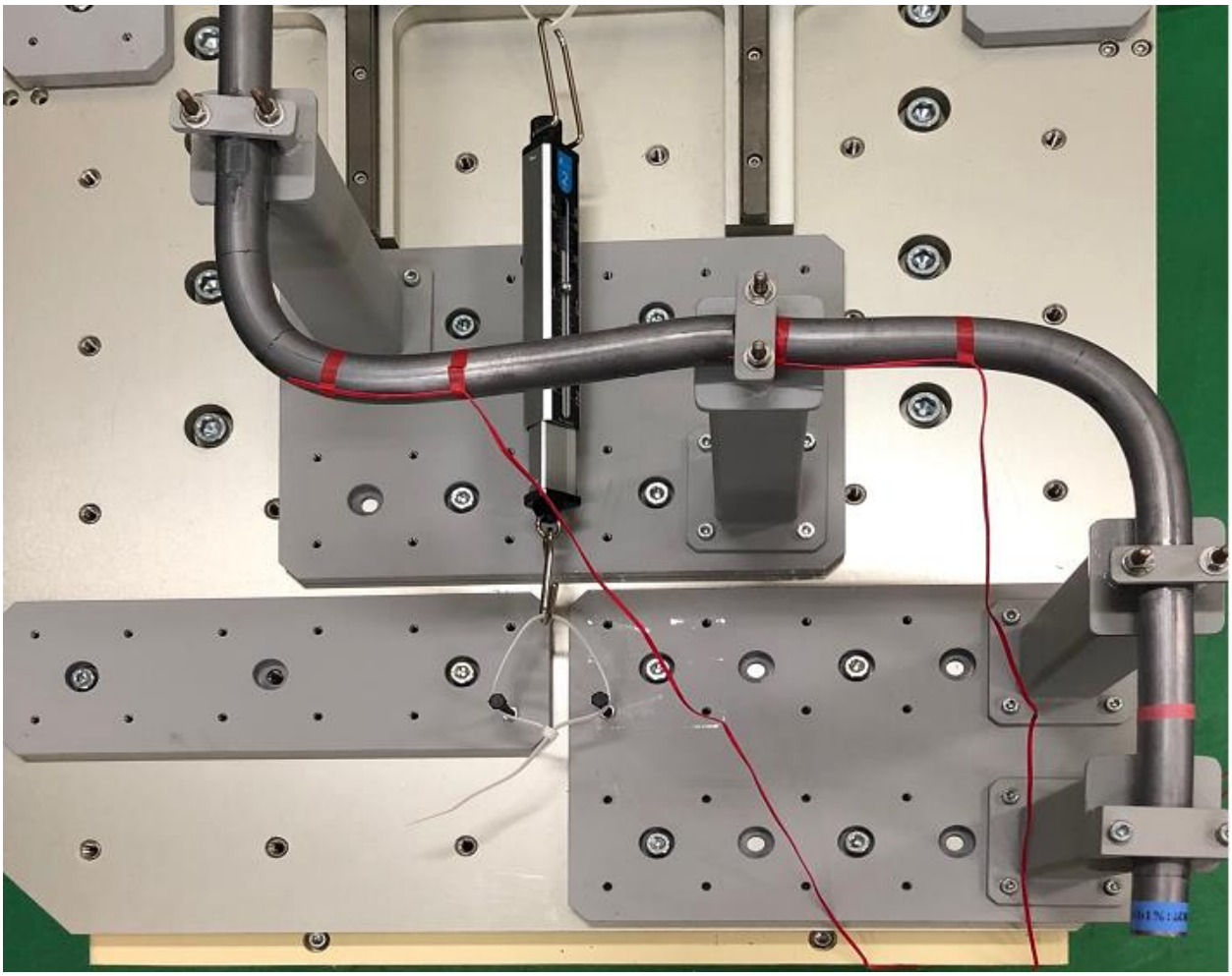

Figure 3-13 Sizeable plastic deformation around supports after vibrations

3.1.7 Influences of supports to piping models

Piping supports are designed to transfer the load from the piping to the supporting structures. Piping supports can provide functions such as anchoring, guiding, absorbing shock, supporting loading, and so on. Usually, the supports increase the natural frequencies of piping and prevent easy-to-vibrate modes forming in the piping. If a section of piping is not restrictively supported, there may be vibration modes with low natural frequencies associated with it. Therefore, this section of piping is susceptible to vibrate. The vibration control standard [45] requires that piping supports should have enough stiffness to stop vibration at the support and warn about the use of hangers, guides, etc.

On the other hand, piping and the attached supports should be designed in a way to make them flexible enough for thermal movements. However, such a flexibility and support scheme should not strongly reduce natural frequencies and make the piping vulnerable to vibrations. Electric Power Research Institute (EPRI) initiated a testing program to determine how piping and associated components should be analyzed for safe construction. The testing program showed that piping and components would withstand seismic events better if the design of the support permits adequate flexibility [59]. ASME Section III Code rules also suggested allowing plants to be designed without the use of an excessive number of snubbers and heavy restraints for significant cost savings and safer plant inspection.

The results in Chapter 2 showed that the component subjected to lower forcing frequency loads had higher probabilities in terms of the ratcheting occurrence. Therefore, the effect of supports on the reliability of piping, especially the occurrence of ratcheting, should also be considered.

3.2 Comparison between experimental and numerical results of piping models under sinusoidal loads

In this part, the comparison was conducted between experimental and numerical results under sinusoidal loads, with the forcing frequency equal to 8.0 Hz. The analysis conditions for ratcheting of piping models under sinusoidal vibration waves are shown in Table 3-5.

Table 3-5 Analysis conditions for ratcheting of the beam model under sinusoidal vibration waves

Case #	Model name	External force (N)	Natural frequency (Hz)	Forcing frequency (Hz)	Input sine waves
1	0-N	0	4.9	8	5 + 50 + 5
2	0-S	0	11.5		
3	10-N	10	4.9		
4	10-S	10	11.5		
5	15-N	15	4.9		
6	15-S	15	11.5		

3.2.1 Experimental results of piping models

In experiments, the frequency of input sinusoidal wave was 8.0 Hz, which intermediated between the natural frequency of Piping-N (around 4.9 Hz) and Piping-S (around 11.5 Hz) measured by sweep tests. Results show that the external force increased the accumulated strain in the extrados (Figure 3-14 and Figure 3-15). Besides, adding three supports increased the strain in most cases (Figure 3-16, Figure 3-17, and Figure 3-18). Therefore, when the forcing frequency was 8.0 Hz, ratcheting was possible to occur in Piping-S.

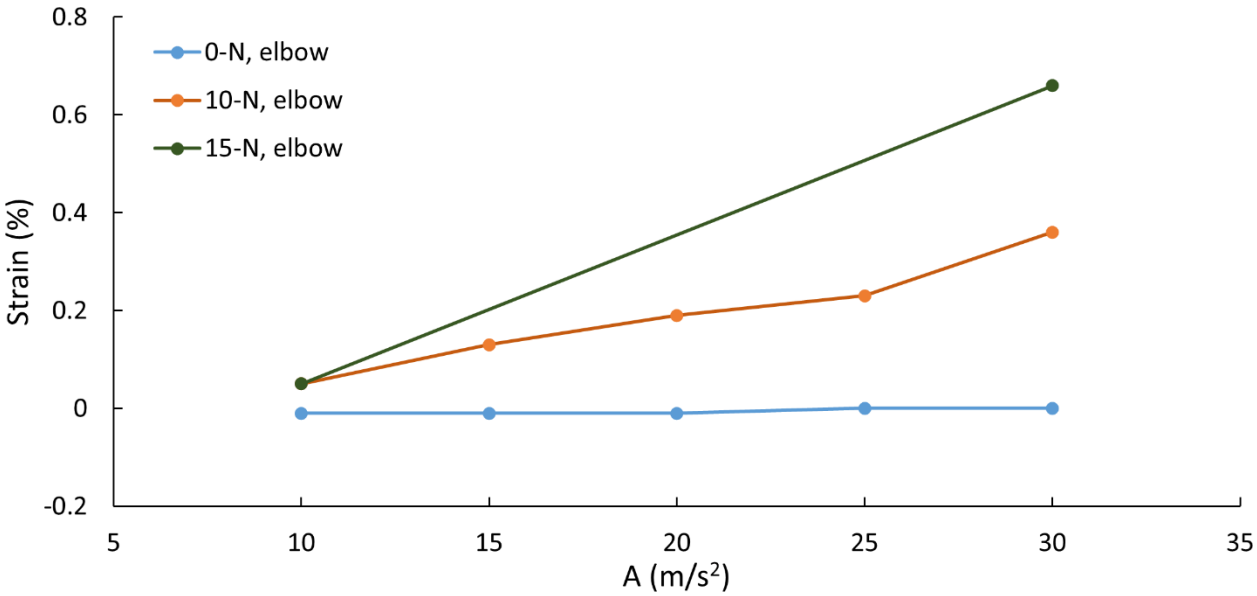

Figure 3-14 Strain increment in experiments (Piping-N)

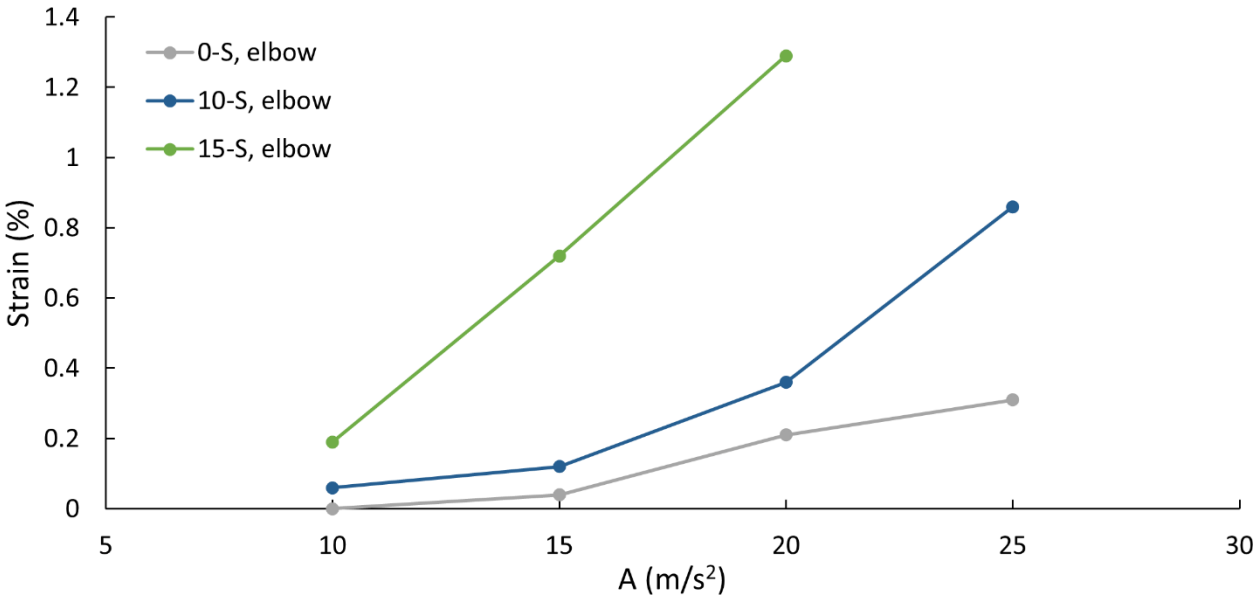

Figure 3-15 Strain increment in experiments (Piping-S)

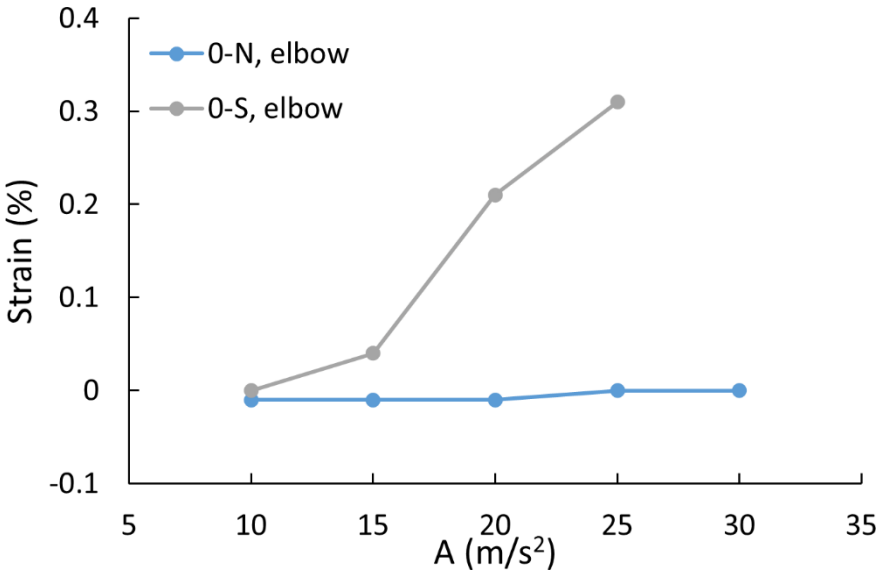

Figure 3-16 Strain increment in experiments (0 N)

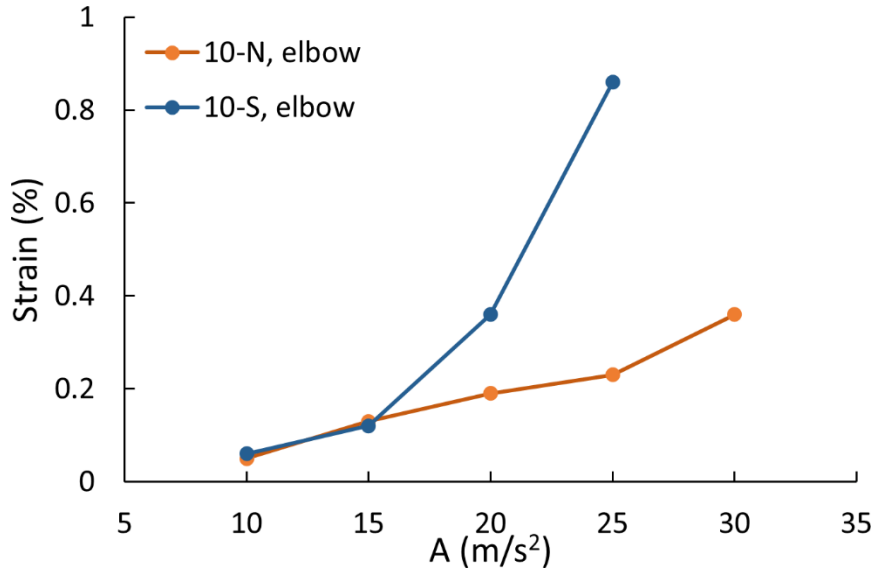

Figure 3-17 Strain increment in experiments (10 N)

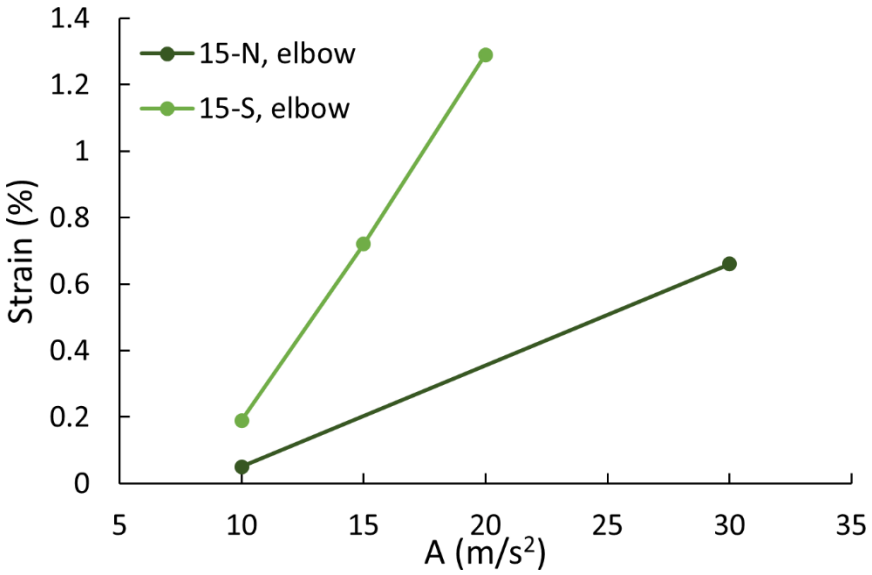

Figure 3-18 Strain increment in experiments (15 N)

Figure 3-19 compares the specimens before and after vibrations. Evident deformation concentrated on the support regions or the elbow part, and the plastic region did not extend in the straight parts.

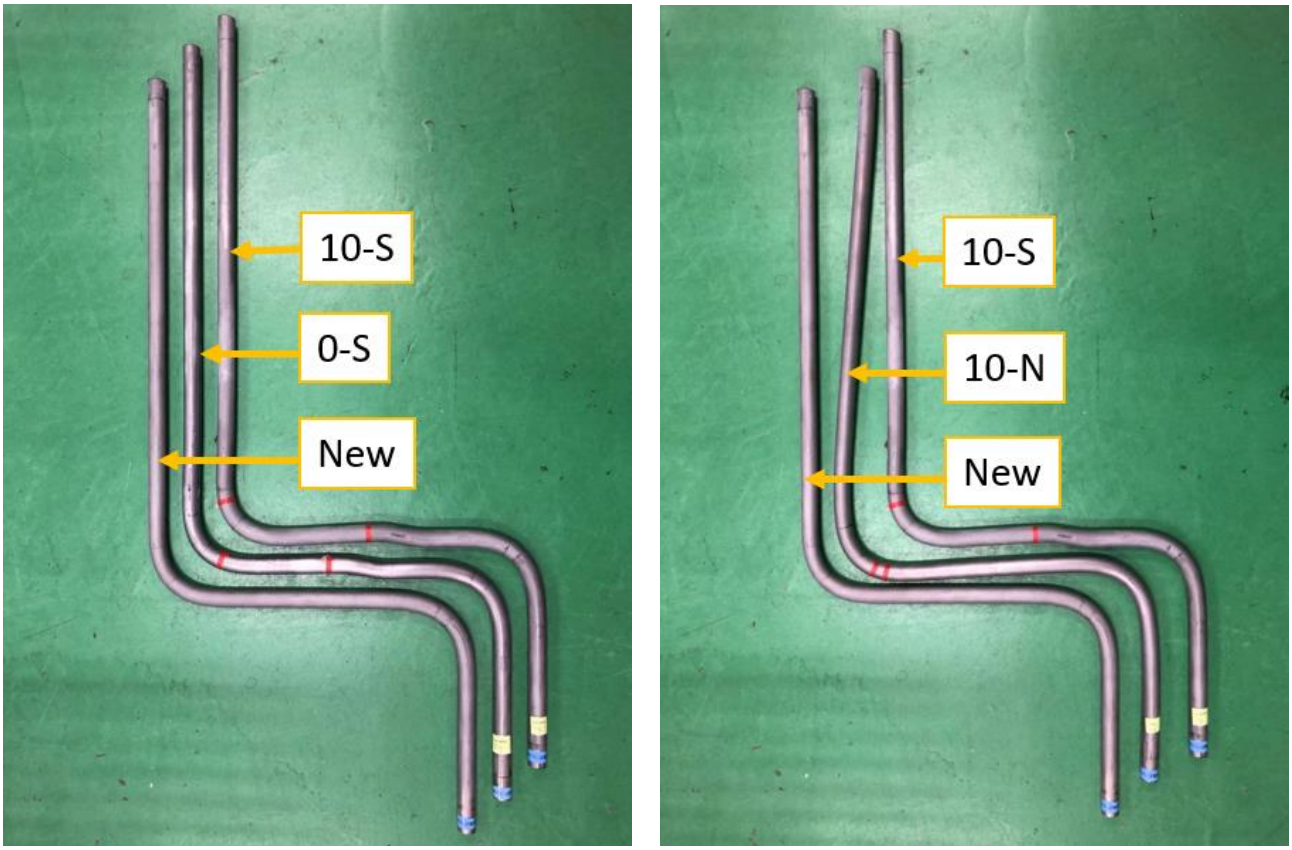

Figure 3-19 Comparison of specimens before and after vibrations

It is interesting to notice that the overall deformation of Piping-N (10-N) was larger than Piping-S (10-S). Since the lead was soft, the gravity of the bar itself played an important role in the deformation. Piping-N did contain three supports in the medium part; therefore, the overall deformation was larger than Piping-S. However, this study focused on the accumulated strain, which was proportional to the curvature. The curvature of Piping-S was larger than Piping-N (Figure 3-20).

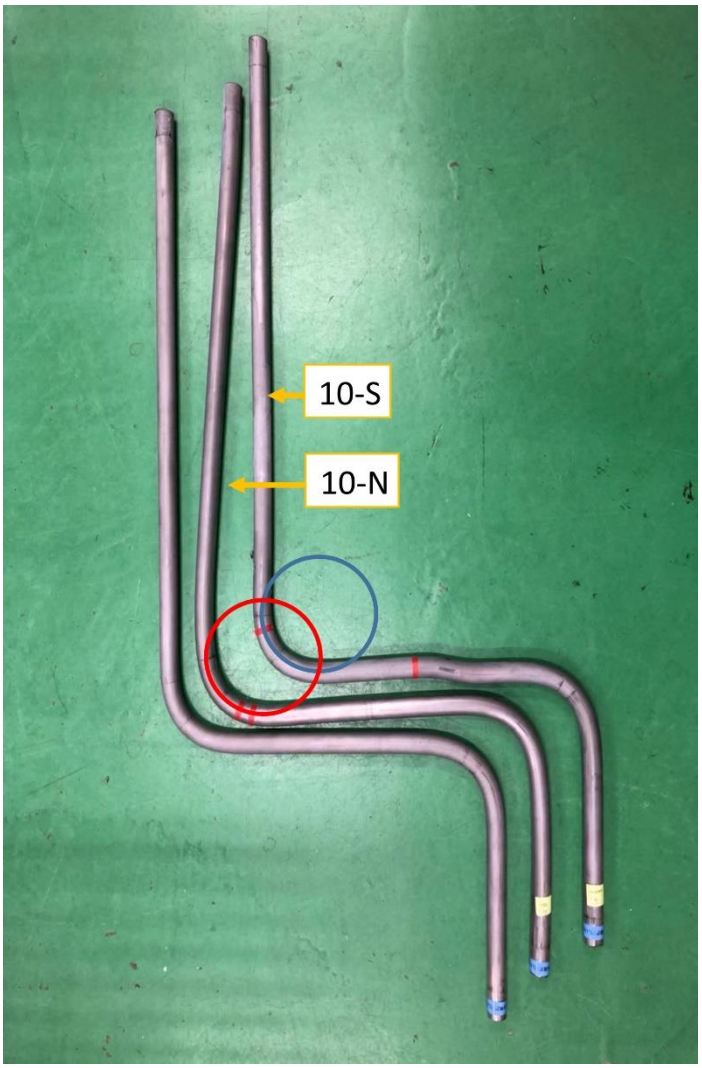

Figure 3-20 The curvature of the elbow part

3.2.2 Numerical results of piping models

The same loading conditions were also applied to numerical analyses. The frequency of the input sinusoidal wave was also 8.0 Hz. The numerical method was discussed in Section 3.1.2. Though the strain increment was not the same in the two methods, the conclusions were the same as the experiments: the external force increased the accumulated strain in the elbow part (Figure 3-21 and Figure 3-22); the existence of the external supports increased the strain in most cases (Figure 3-23, Figure 3-24, and Figure 3-25). Therefore, when the forcing frequency was 8.0 Hz, ratcheting was easier to occur in Piping-S.

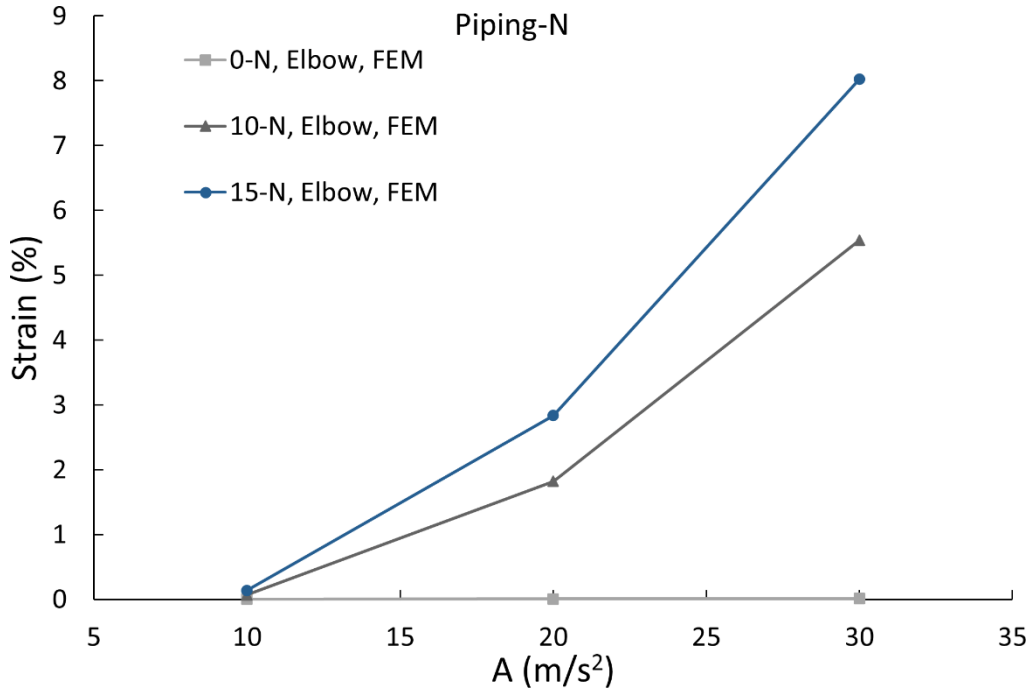

Figure 3-21 Strain increment in numerical analyses(Piping-N)

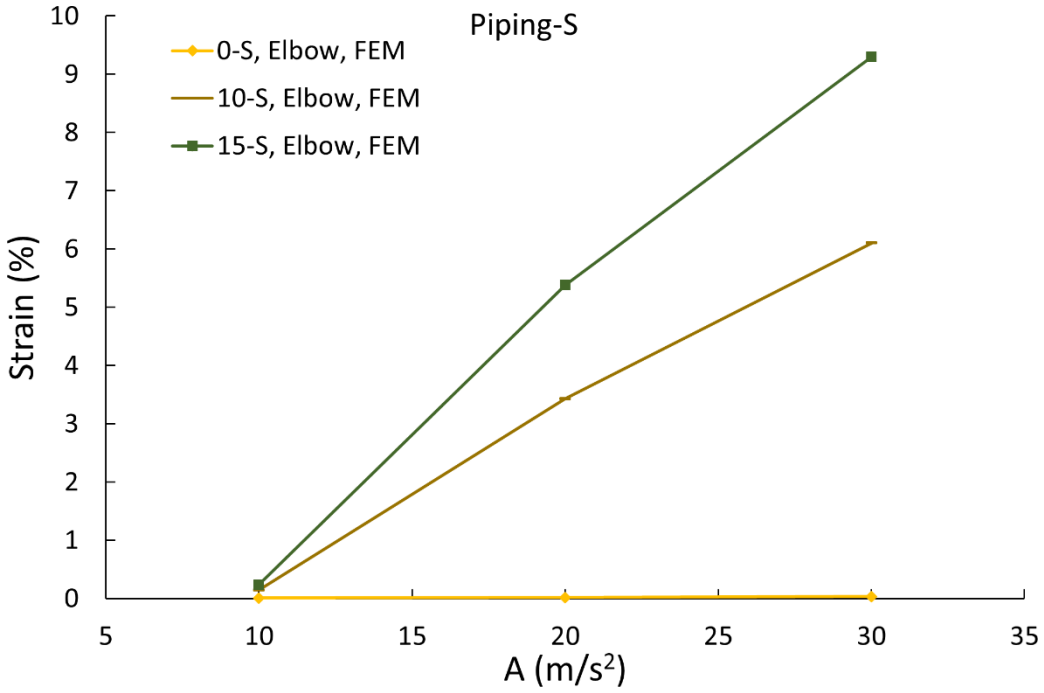

Figure 3-22 Strain increment in numerical analyses (Piping-S)

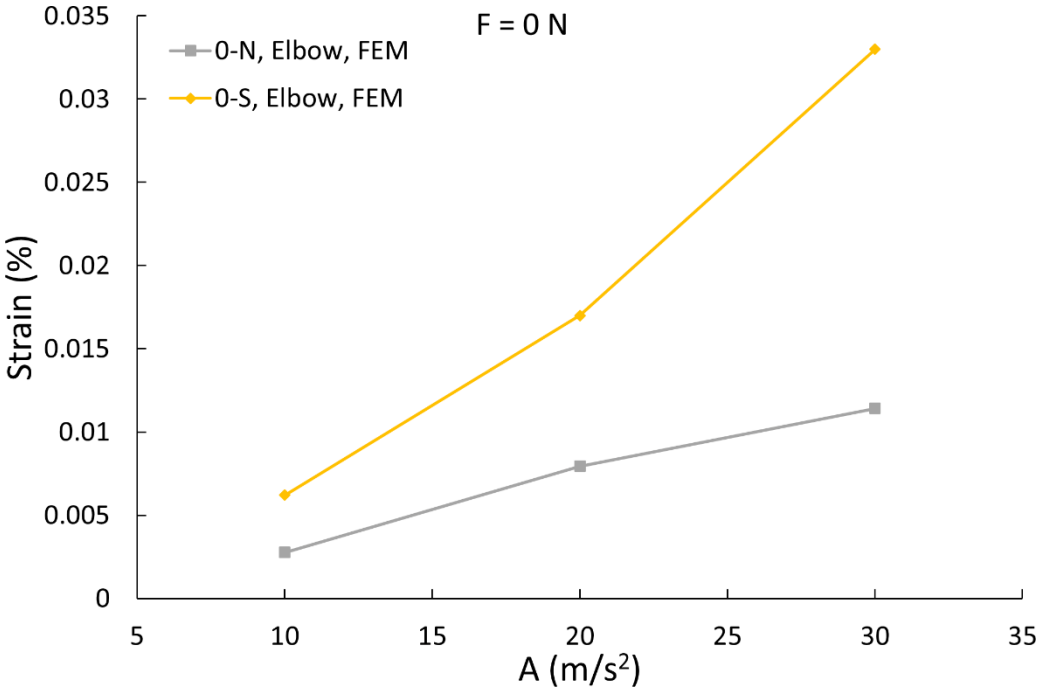

Figure 3-23 Strain increment in numerical analyses (0 N)

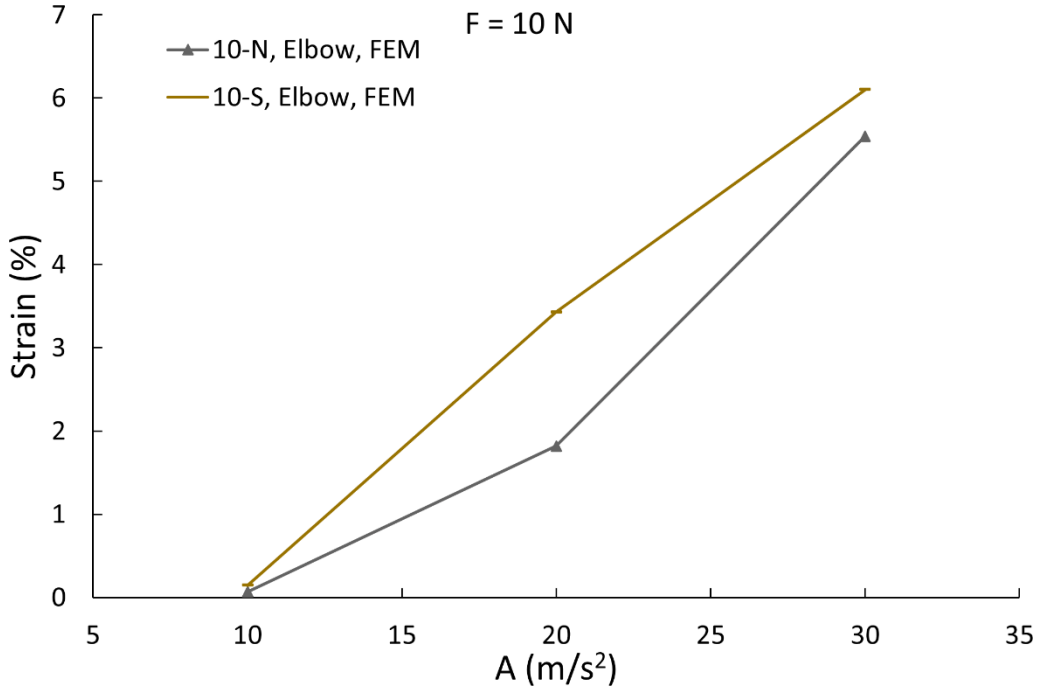

Figure 3-24 Strain increment in numerical analyses (10 N)

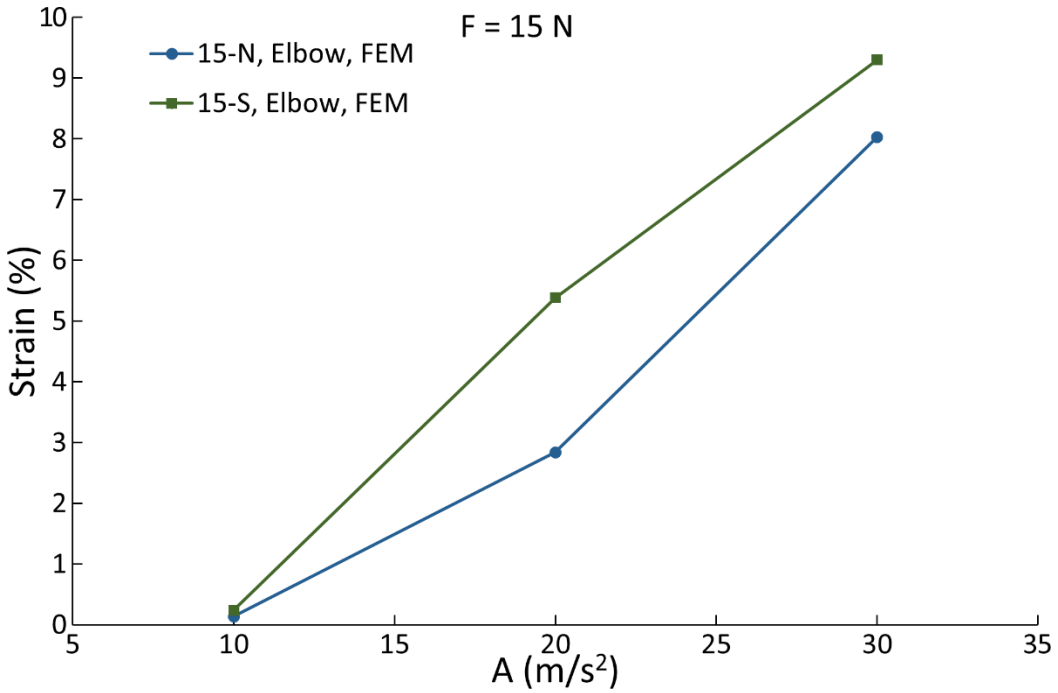

Figure 3-25 Strain increment in numerical analyses (15 N)

3.3 Numerical results and analyses for ratcheting of piping models under sinusoidal loads

The numerical conditions analyses for ratcheting of piping models under sinusoidal vibration waves are shown in Table 3-6 and Table 3-7, respectively.

Table 3-6 Numerical analysis conditions for ratcheting of the Piping-N under sinusoidal vibration waves

Case #	Model name	External force (N)	Natural frequency (Hz)	Frequency ratio
1	5-N	5	4.6	0.5
2				0.75
3				0.99
4				1.0
5				1.25
6				1.5
7				1.74
8				2.0

9				2.5
10	10-N	10	4.6	0.1
11				0.5
12				0.75
13				0.99
14				1.0
15				1.25
16				1.5
17				1.74
18				2.0
19				2.5
20	15-N	15	4.6	0.1
21				0.5
22				0.75
23				0.99
24				1.0
25				1.25
26				1.5
27				1.74
28				2.0
29				2.5
30	20-N	20	4.6	0.5
31				0.75
32				0.99
33				1.0
34				1.25
35				1.5
36				1.74
37				2.0
38				2.5
39	60-N	60	4.6	0.5
40				0.75
41				0.99
42				1.0
43				1.25
44				1.5
45				1.74
46				2.0
47				2.5

Table 3-7 Numerical analysis conditions for ratcheting of the Piping-S under seismic loads

Case #	Model name	External force (N)	Natural frequency (Hz)	Frequency ratio
	10-S	10	12.8	0.1
				0.5
				0.625
				0.75
				0.95
				1.0
				1.25
				1.5
				1.75
				2.0
	15-S	15	12.8	0.1
				0.5
				0.625
				0.75
				0.95
				1.0
				1.25
				1.5
				1.75
				2.0
	20-S	20	12.8	0.5
				0.625
				0.75
				0.95
				1.0
				1.25
				1.5
				1.75
				2.0
	40-S	40	12.8	0.5
				0.625
				0.75
				0.95
				1.0
				1.25
				1.5
				1.75

				2.0
	150-S	150	12.8	0.5
				0.625
				0.75
				0.95
				1.0
				1.25
				1.5
				1.75
				2.0

3.3.1 Ratcheting occurrence conditions in the frequency ratio

Figure 3-26 and Figure 3-27 show the ratcheting boundaries for the two types of models, respectively. The abscissa is the frequency ratio, which is the ratio of the frequency of the input vibration to the natural frequency of the piping model. The ordinate is the amplitude of input sinusoidal loads. The lines are the ratcheting boundaries, and ratcheting occurs in the areas above the lines. It is evident that the existence of the external force made the occurrence of ratcheting more easily. The lowest cases, which mean the highest possibility of the occurrence of ratcheting, are a little smaller than 1.0 fn: 0.99 fn for Piping-N and 0.95 fn for Piping-S. Some models (10-N,15-N, 10-S, and 15-S) contain the results at 0.1 fn, and the ratcheting boundary before 0.5 fn is relatively flat.

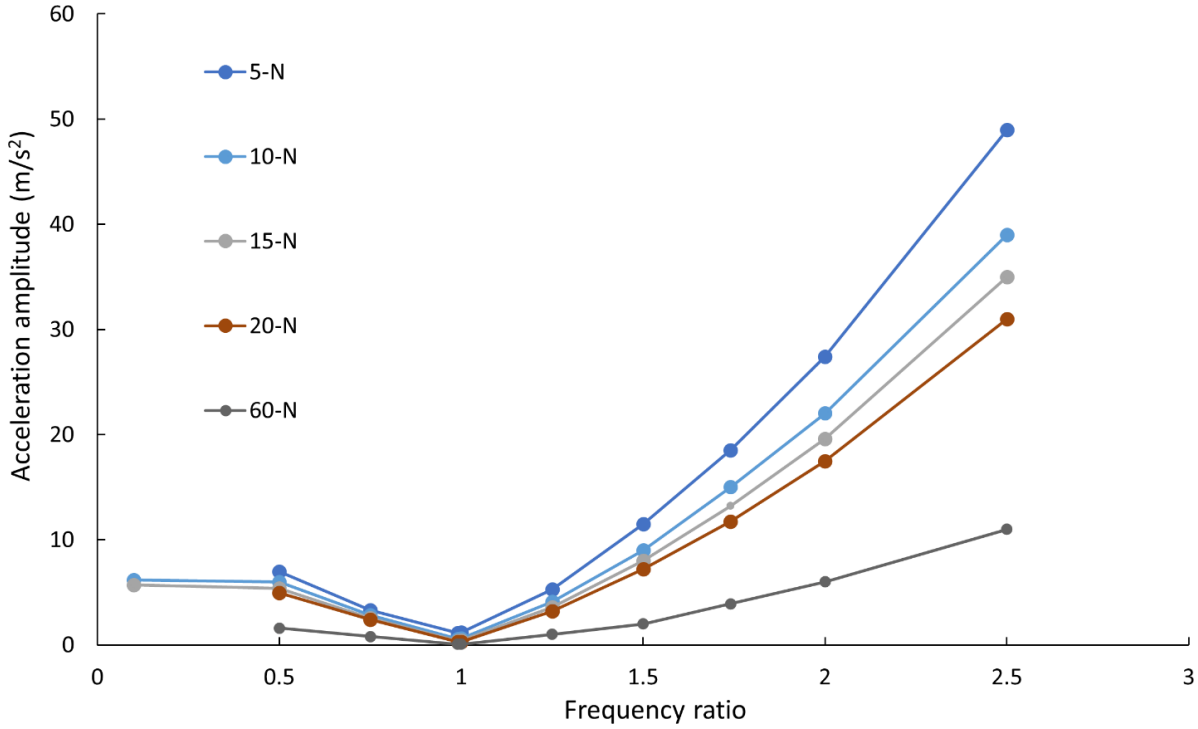

Figure 3-26 Ratcheting boundaries in frequency ratio (Piping-N)

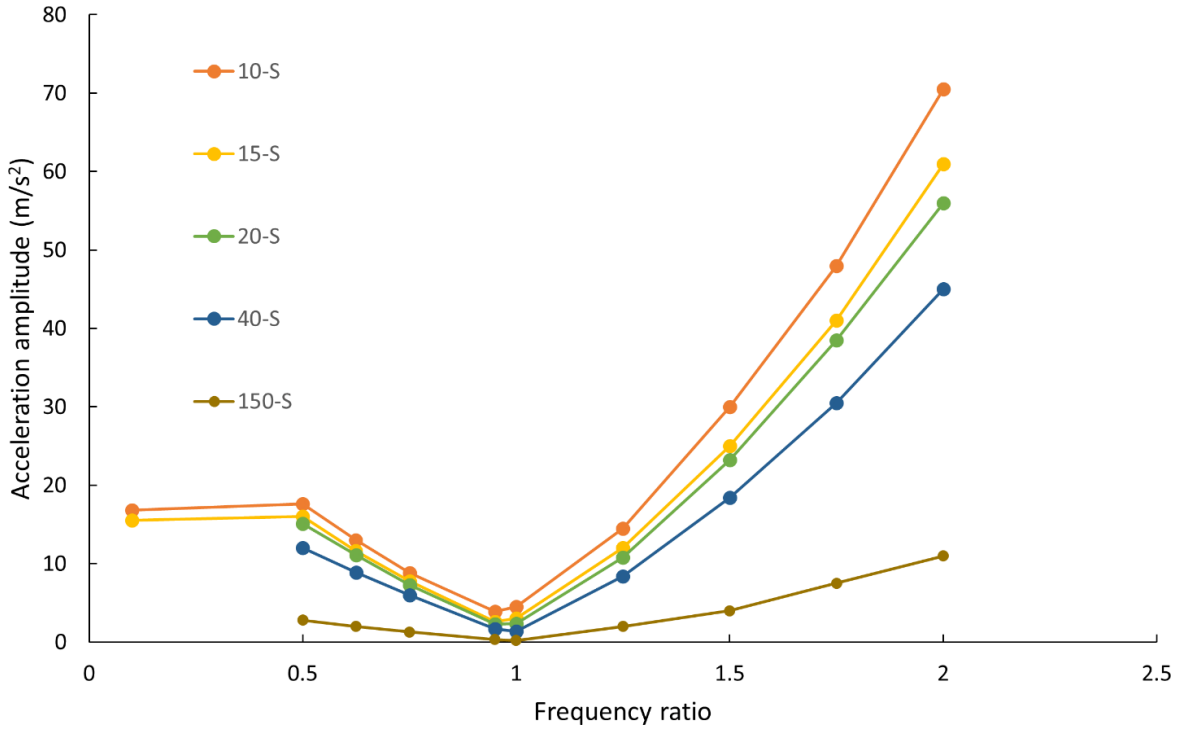

Figure 3-27 Ratcheting boundaries in frequency ratio (Piping-S)

Figure 3-26 and Figure 3-27 show evident frequency-dependent characteristics in the occurrence of ratcheting. Chapter 2 has shown that seismic loads have both load-controlled and displacement-controlled characteristics. To prevent catastrophic accidents, it is necessary to clarify the characteristics of seismic loads for the piping model. In the previous chapter on the ratcheting occurrence conditions of beam models, authors divided the sinusoidal excitations into the pseudo load-controlled load and the pseudo displacement-controlled load according to the frequency ratio. In this chapter, the whole region was divided into three parts: the pseudo load-controlled region, pseudo resonance region, and pseudo displacement-controlled region (Figure 3-28). The region "pseudo load-controlled region" means that the seismic load in this region has more load-controlled characteristics. However, it is not purely a load-controlled load. Similar to Figure 2-25 for the beam model, the boundary was also decided according to the slope of those curves. The resonance effect was not evident in the beam model; however, it was evident in the piping model. The main reason is that the plastic deformation occurred continuously in most parts of the beam. However, in the piping model, due to the horizontal arrangement of system structure, large strain concentrated on the elbow parts and the regions around supports; the plastic region did not extend in the straight parts, as shown in Figure 3-19.

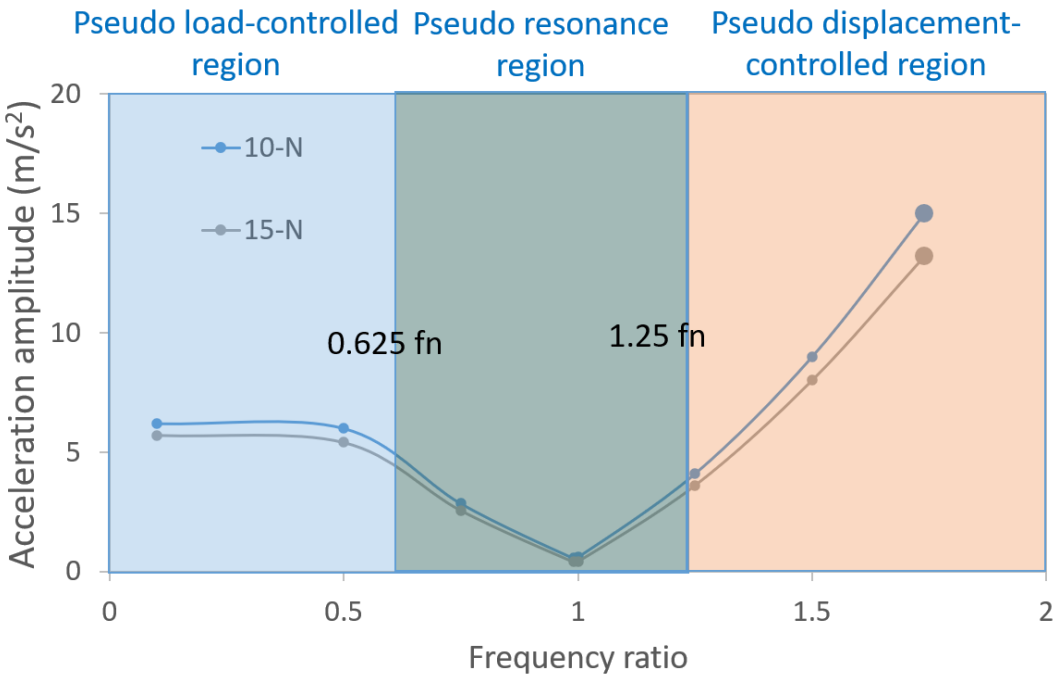

Figure 3-28 Three parts according to the frequency ratio

Figure 3-29 shows the deformation by the end of vibrations in Model 15-N and 15-S, respectively. It is evident that considerable deformation concentrated on the regions around supports. In terms of strain, as shown in Figure 3-30, in Piping-N, plastic strain focused on the elbow part. In Piping-S, plastic strain concentrated on the elbow part and the region around supports. Therefore, the damping effect was not dominant in the piping model.

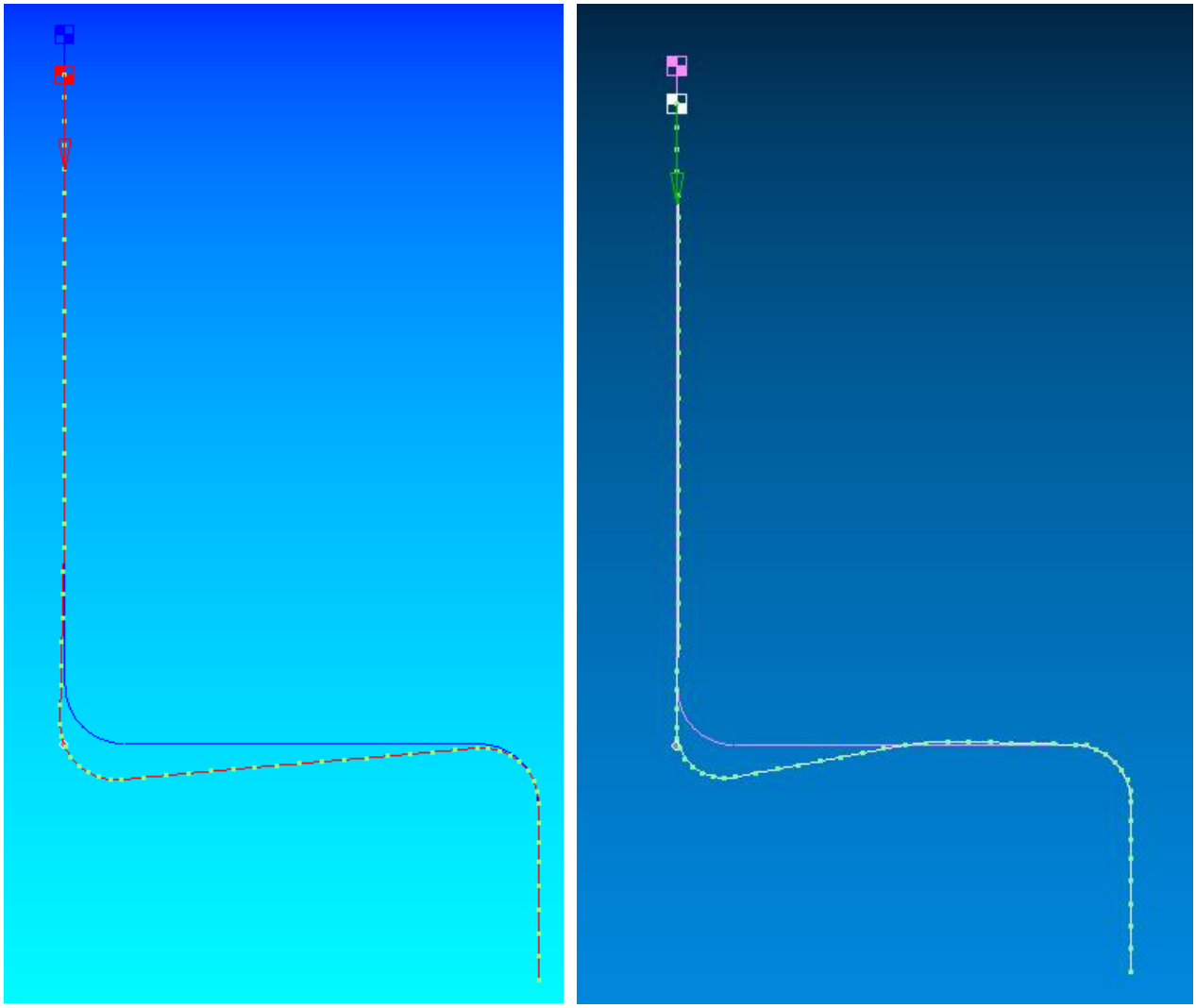

15-N, 1.0 fn, 0.41 m/s^2 15-S, 1.0 fn, 3 m/s^2

Figure 3-29 Deformation after vibrations

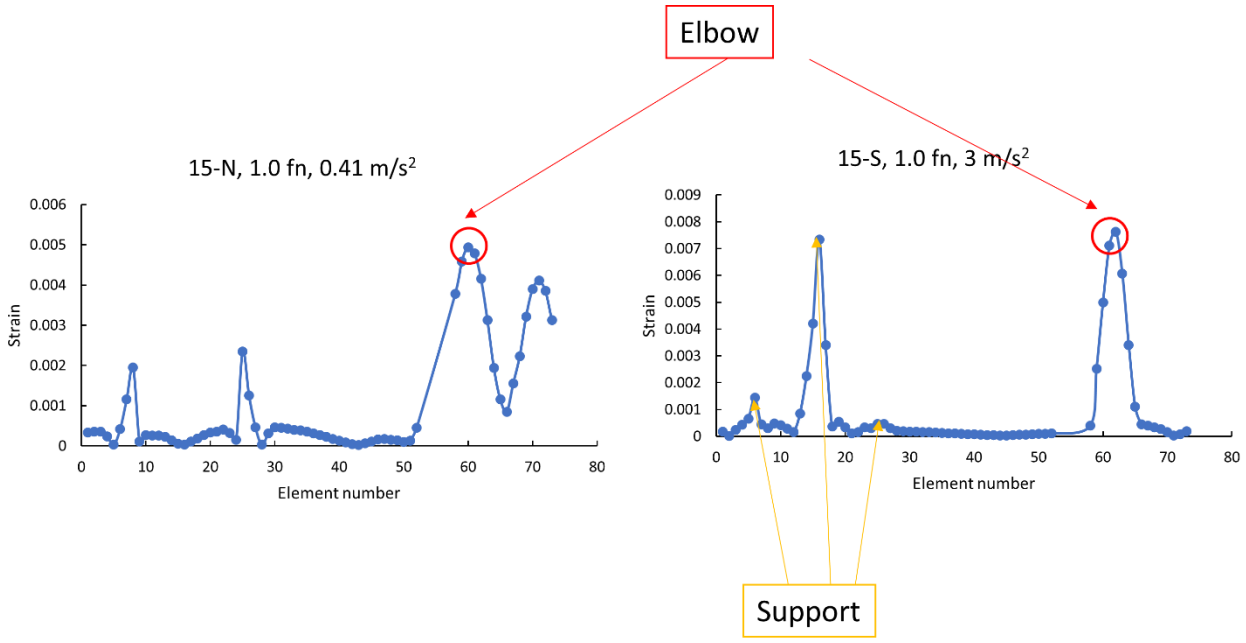

Figure 3-30 Strain distribution after vibrations

3.3.2 Ratcheting occurrence conditions in the frequency

In order to check the influence of supports, numerical analysis results are shown in the forcing frequency (Figure 3-31 and Figure 3-32). The lines also mean ratcheting boundaries. At the lower frequency (smaller than 7.8 Hz), ratcheting was easier to occur in Piping-N. In contrast, at the higher frequency (larger than 7.8 Hz), ratcheting occurred easily in Piping-S. This phenomenon was due to the difference in frequency ratio. Supports increased the natural frequency of piping and decreased the frequency ratio. Therefore, the sinusoidal load had different characteristics between Piping-N and Piping-S. From the two figures, it is evident that, in terms of the occurrence of ratcheting, providing more supports does not increase the safety of piping in some cases. It is essential to point out that the results cannot be used to prove that the application of supports increases the possibility of failure of the piping. Supports may help to avoid other failure modes. However, those failure modes are beyond the scope of this thesis.

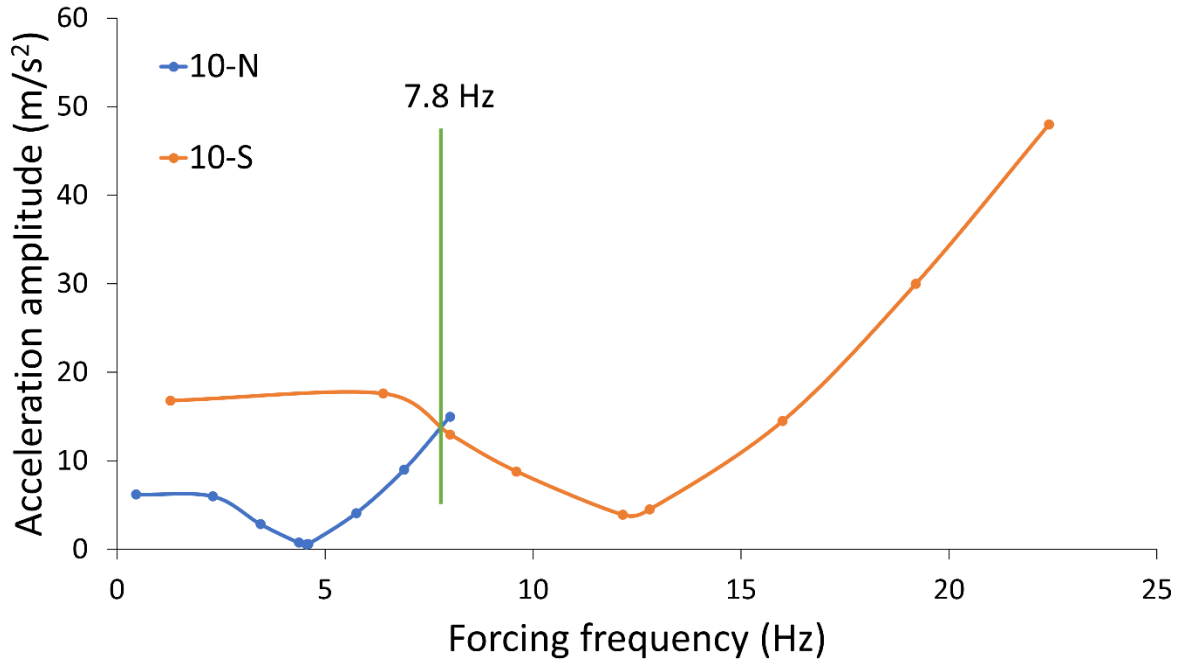

Figure 3-31 Ratcheting boundaries in frequency (F = 10 N)

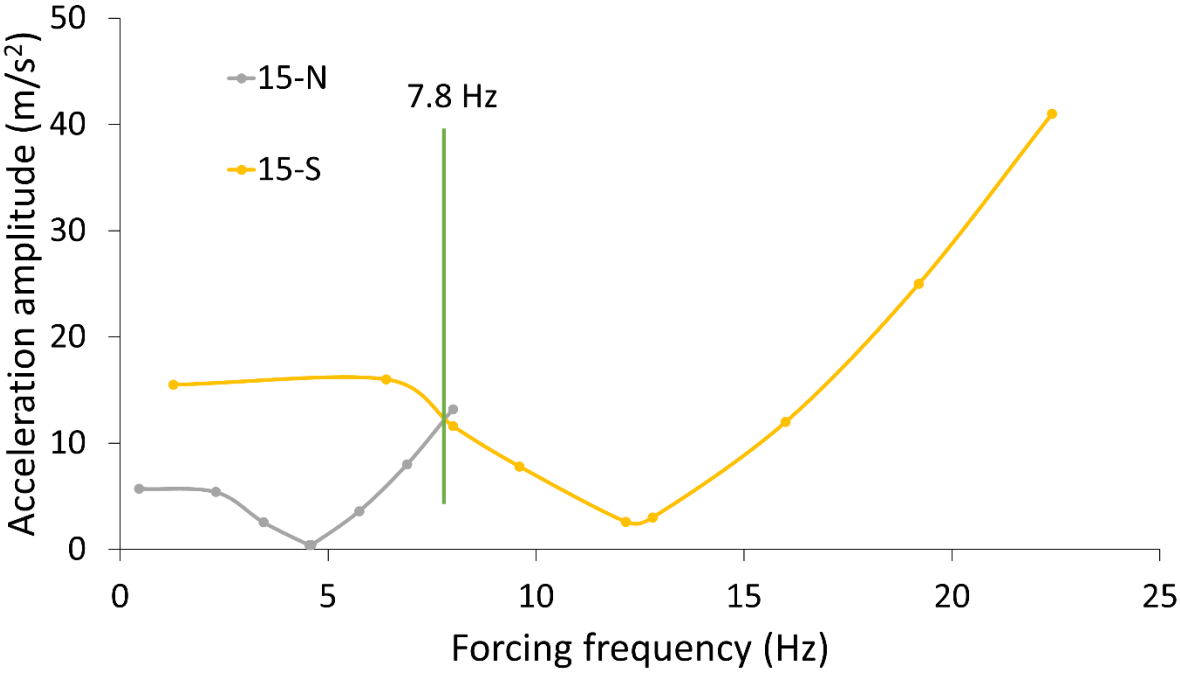

Figure 3-32 Ratcheting boundaries in frequency (F = 15 N)

3.3.3 Ratcheting occurrence conditions in the X-Y diagram

In Chapter 2, the ratcheting occurrence conditions of the beam model were shown in the non-dimensional X-Y diagrams. For the convenience of comparison, it is better to show the ratcheting occurrence conditions of the piping model in the X-Y diagram. Similar to the beam model, the X and Y in the piping model are also the ratios of the bending stress to the yield stress.

$$\mathrm{X} = \frac{\sigma_s}{\sigma_y} \qquad \text{Equation 3-1}$$

$$\mathrm{Y} = \frac{\sigma_a}{\sigma_y} \qquad \text{Equation 3-2}$$

where σ_s and σ_a are the bending stress due to the external force and vibration, respectively.

σ_s was calculated elastically at the elbow part with the neglection of vibrations. The relationship between X and external force is shown in Figure 3-33. X increased with force linearly due to the elastic calculation according to the definition.

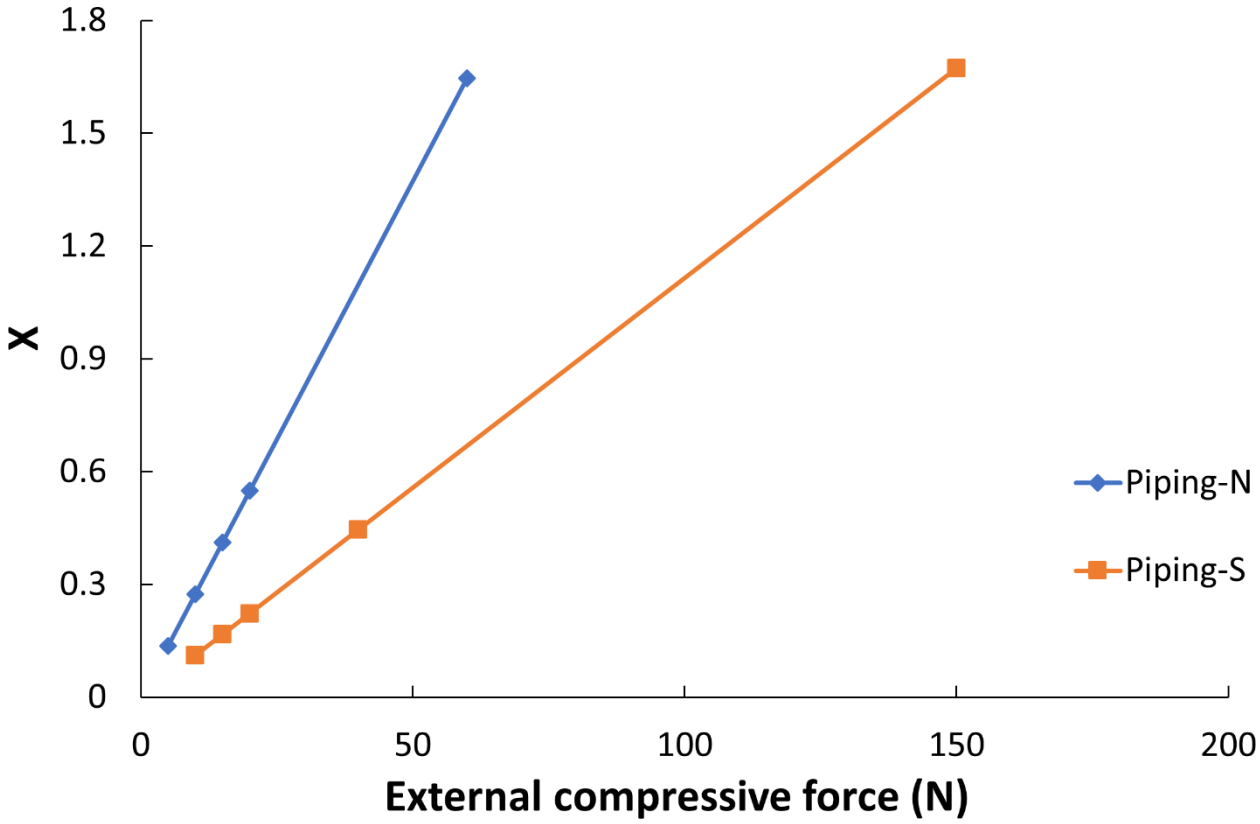

Figure 3-33 X with external compressive force

Similarly, σ_a was calculated elastically at the elbow part from the static equilibrium to maximum accelerations with the neglection of the external compressive force provided by the spring. The relationship between Y and constant vibration acceleration is shown in Figure 3-34. Y also increased with force linearly.

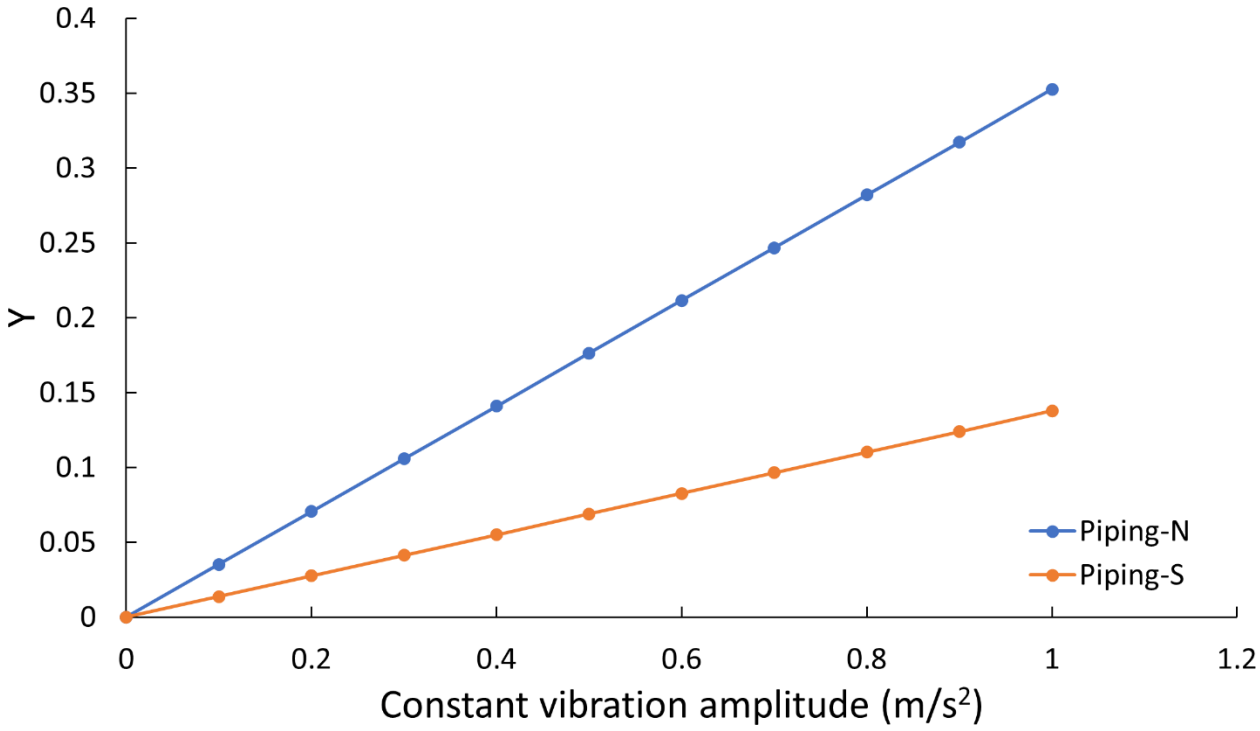

Figure 3-34 Y with constant vibration amplitudes

The X-Y diagrams of Piping-N and Piping-S are shown in Figure 3-35 and Figure 3-36, respectively. The elastic boundary and the collapse line are also added for reference. The collapse line means the occurrence of the theoretical plastic collapse of the rod with a circular cross section, which occurs when the elastically calculated stress at the surface point reaches 1.7 times of yield stress of the material for the circular section. It is worthwhile to notice that 1.0 fn line is below the elastic boundary. This phenomenon is due to the concentration of plastic deformation around elbow parts and supports in the piping model. The plastic region did not extend in the straight parts. Therefore, the damping effect due to plasticity was relatively smaller, and the resonance effect became evident.

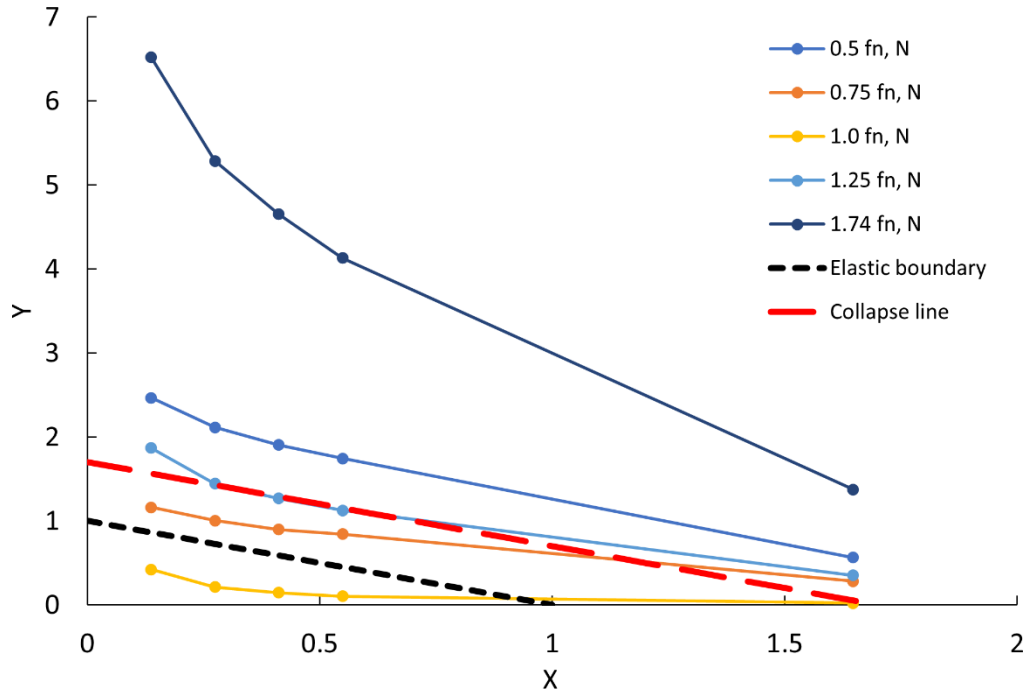

Figure 3-35 Ratcheting diagrams in X-Y for Piping-N

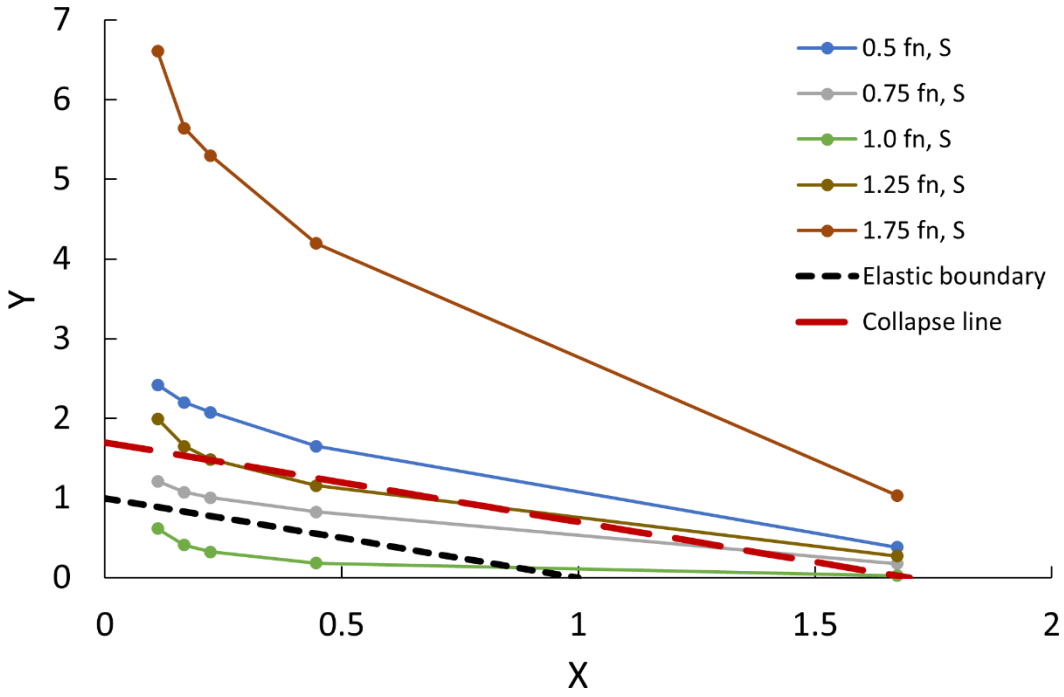

Figure 3-36 Ratcheting diagrams in X-Y for Piping-S

If comparing the ratcheting occurrence conditions of the Piping-N and Piping-S in one X-Y diagram, as shown in Figure 3-37, the difference between the two types of piping models is negligible. However, it is necessary to notice that the X-Y diagram cannot show the influence of the natural frequencies of the two types of models, which is discussed in Section 3.3.2.

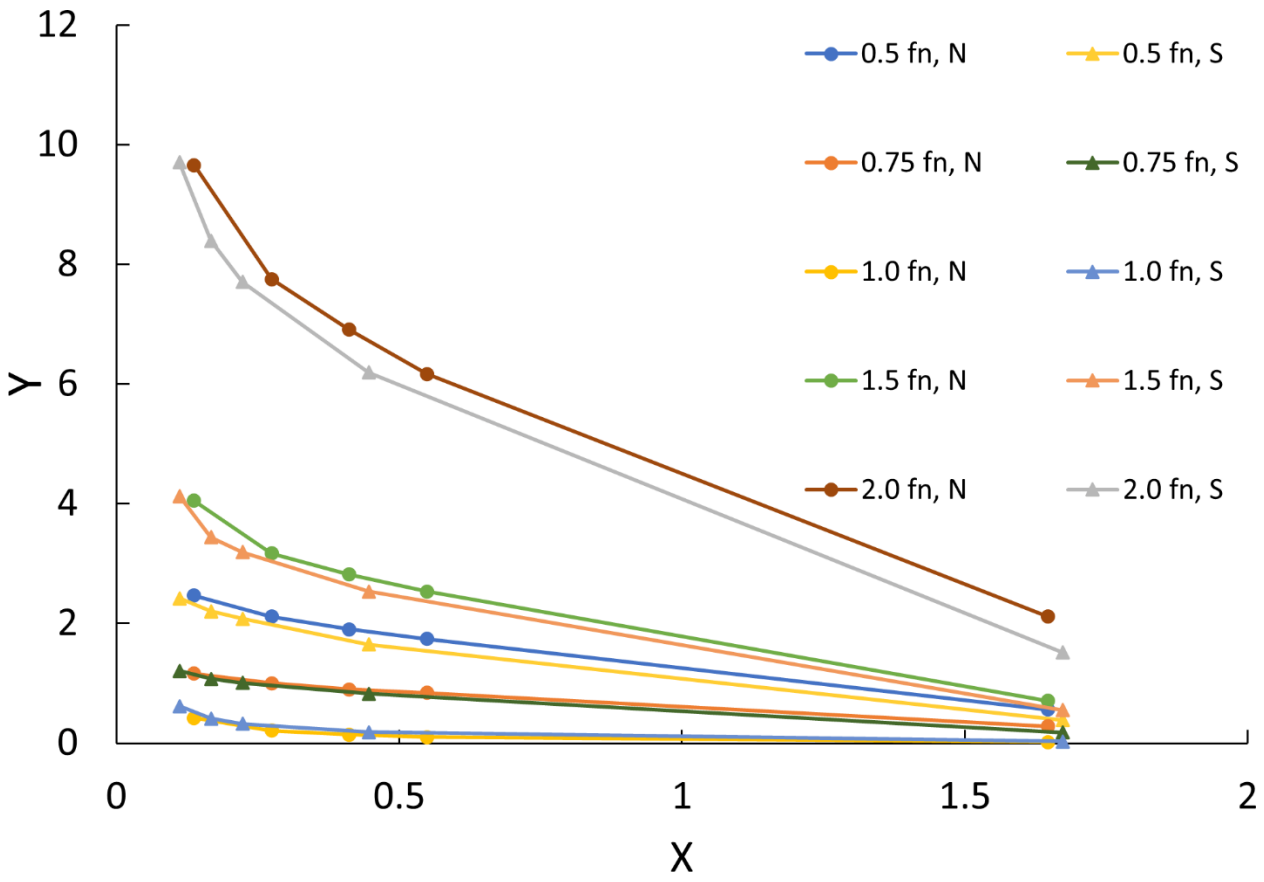

Figure 3-37 Comparison of ratcheting occurrence conditions between the two types of models in one X-Y diagram

3.3.4 Energy consumption and phase delay

The energy dissipated by damping is defined as the area enclosed by the inelastic stress-strain curve. Figure 3-38, Figure 3-39, and Figure 3-40 show the stress-strain curves of Model 15-S with the forcing frequency equal to 0.5 fn, 1.0 fn, and 1.5 fn, respectively. By calculating the area enclosed by the curves, the energy lost in the elbow part of the curved rod is shown in Figure 3-41. It is evident that more energy was consumed with lower forcing frequency. This

phenomenon was due to the phase delay, which is the time by which the response lags behind the force. The loading force and related response (strain) of the extrados of the elbow in Model 15-S with different loading frequencies are shown in Figure 3-42, Figure 3-43, and Figure 3-44. If the forcing frequency is 0.5 fn, the excitation slowly varied, and the displacement was generally in phase with the applied excitation. At 1.5 fn, the excitation quickly varied, and the displacement was almost of opposite phase relative to the applied excitation. The phase delay caused the difference in energy transferred to the piping, therefore with 0.5 fn, more energy was dissipated.

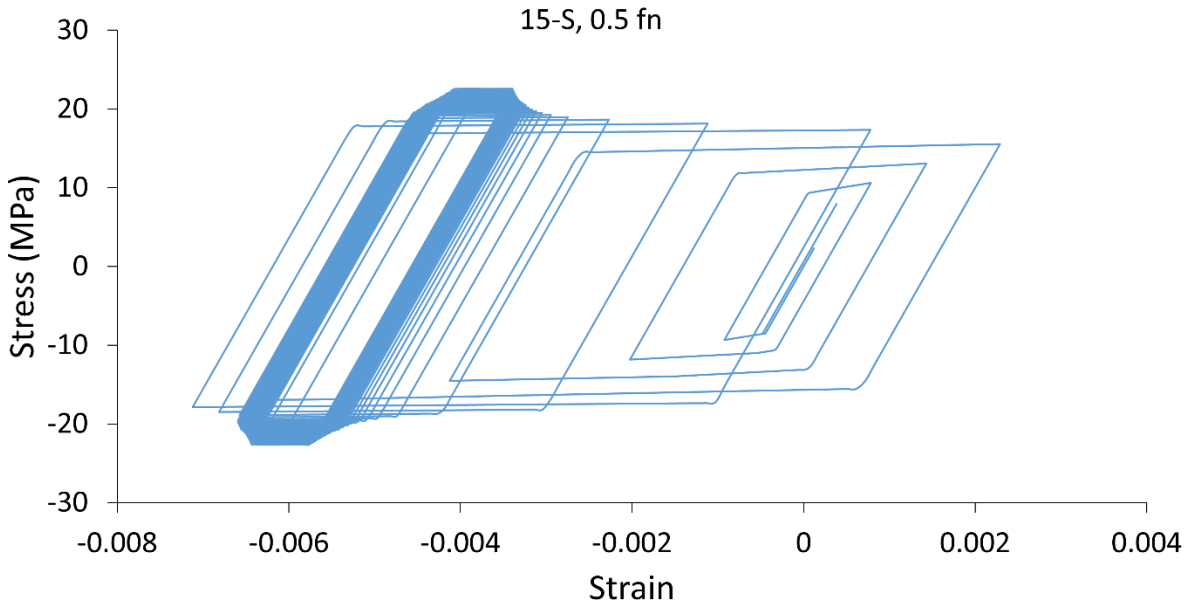

Figure 3-38 Inelastic stress-strain curve of 15-S with forcing frequency equal to 0.5 fn

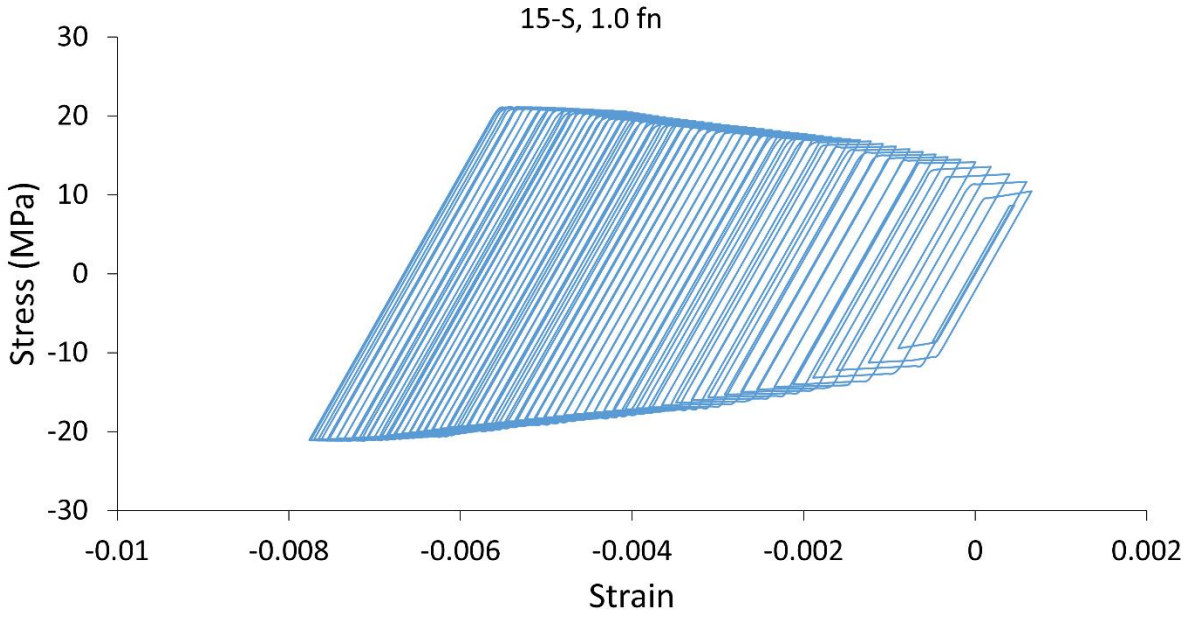

Figure 3-39 Inelastic stress-strain curve of 15-S with forcing frequency same as the natural frequency of the system

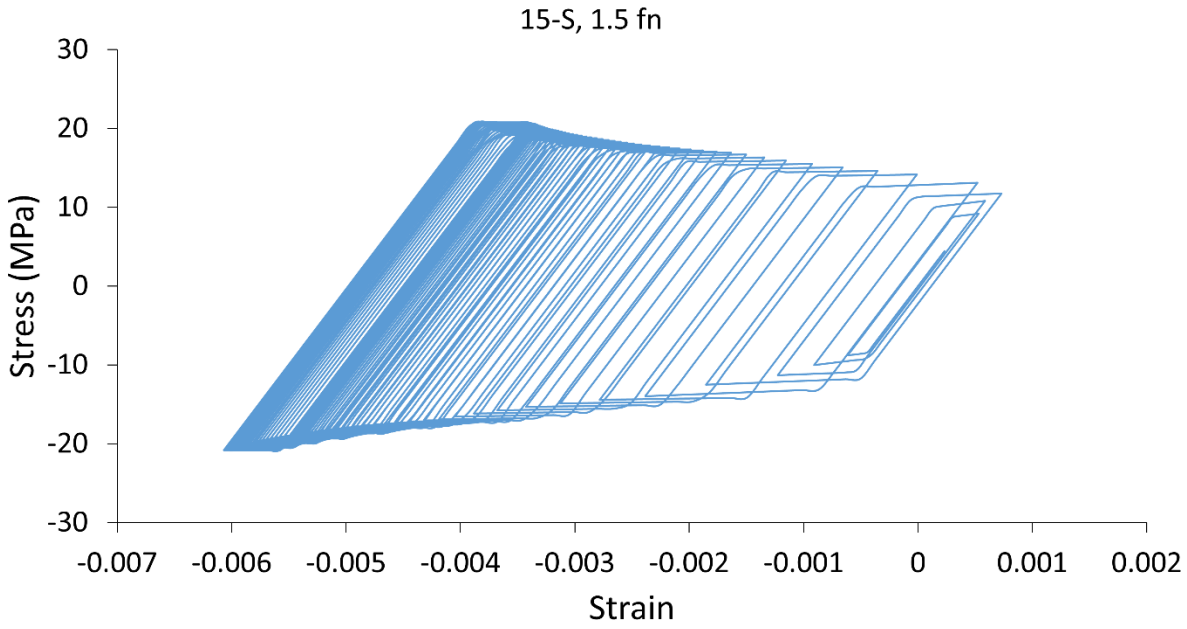

Figure 3-40 Inelastic stress-strain curve of 15-S with forcing frequency equal to 1.5 fn

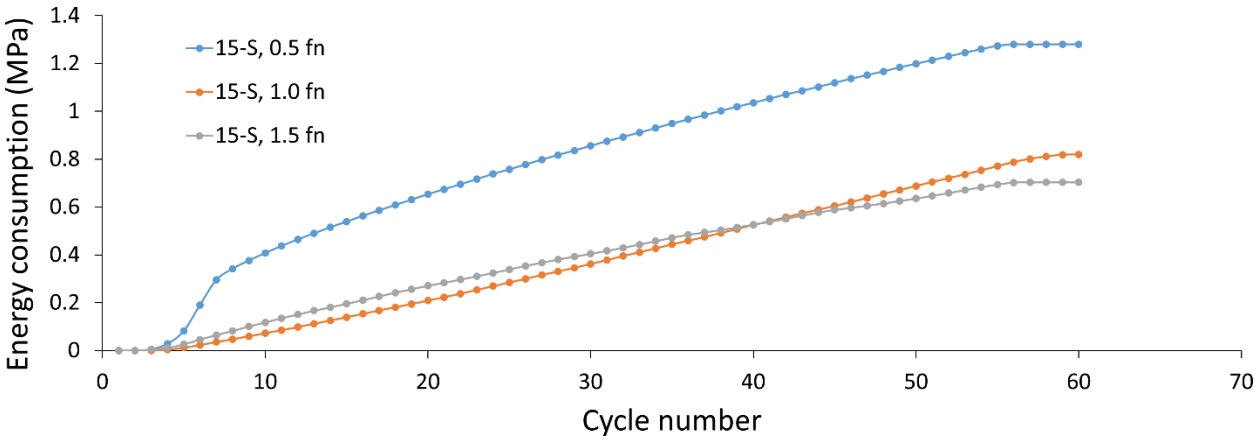

Figure 3-41 Accumulated energy in all 60 cycles of Model 15-S with 0.5 fn, 1.0 fn, and 1.5 fn

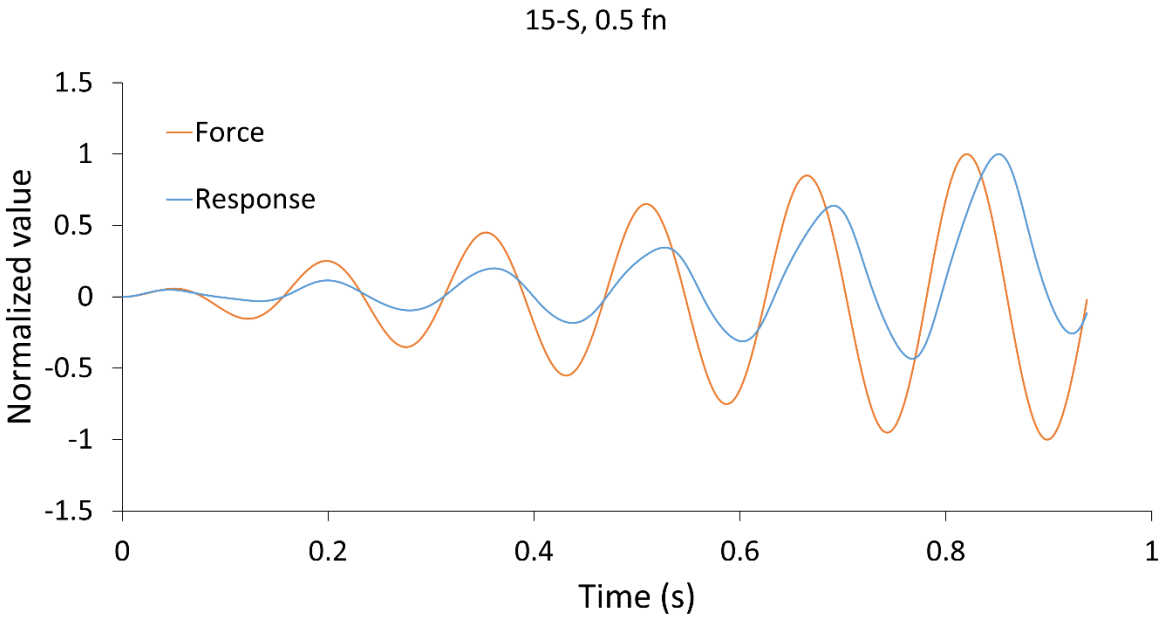

Figure 3-42 Force and the related response of the extrados of the elbow in Model 15-S with forcing frequency equal to 0.5 fn

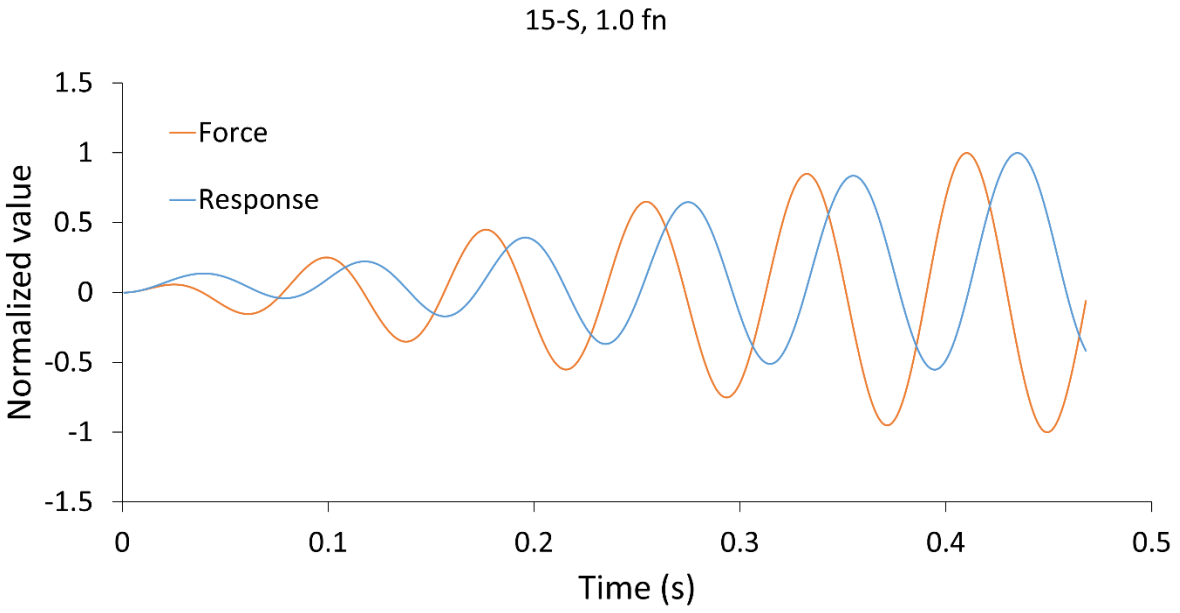

Figure 3-43 Force and the related response of the extrados of the elbow in Model 15-S with forcing frequency the same as the natural frequency of the system

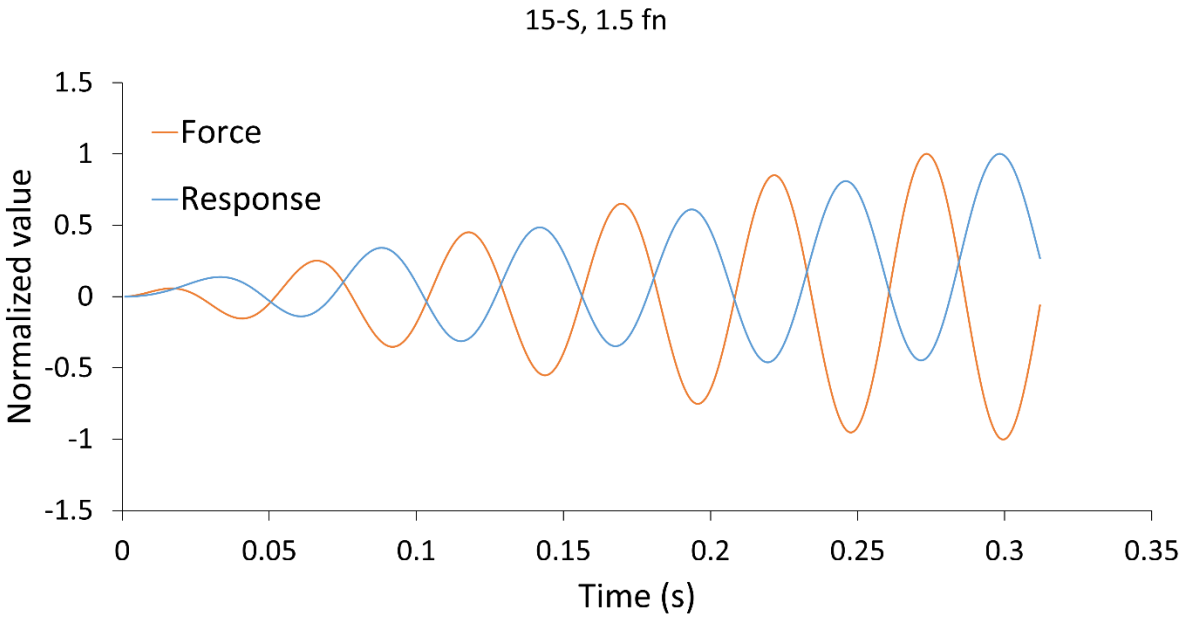

Figure 3-44 Force and the related response of the extrados of the elbow in Model 15-S with forcing frequency equal to 1.5 fn

3.4 Conclusions of ratcheting research of piping models

In this chapter, finite element analyses and experiments were conducted to obtain the ratcheting occurrence conditions of piping. At higher natural frequency, ratcheting was easier to occur in the piping with external supports because additional supports increased natural frequencies and decreased frequency ratio. The vibration with a lower frequency ratio showed load-controlled characteristics. In contrast, the vibration with a higher frequency ratio had displacement-controlled characteristics. The whole region was divided into three parts according to the frequency ratio: the pseudo load-controlled region, pseudo resonance region, and pseudo displacement-controlled region. The resonance effect was evident in the piping model compared with the beam model due to the limited plastic area in the piping model.

Chapter 4. Comparison among four models

Table 4-1 compares the primary and secondary stresses among the cylinder model in the Bree diagram [43], the beam model in the Yamashita diagram [44], the beam model in Chapter 2, and the piping model in Chapter 3. Since both the second and third models are beam models, to avoid confusion, the beam model in Yamashita et al.'s research would be called the Yamashita model, and the ratcheting boundary of the Yamashita model would be called the Yamashita line in this chapter.

Table 4-1 Comparison of stresses among four models

Model	Source of X	Property	Source of Y	Property
Cylinder model (the Bree diagram)	Pressure stress (Membrane stress)	load-controlled	Cyclic thermal stress	displacement-controlled
Beam model (the Yamashita diagram)	Bending stress due to distributed force	load-controlled	Bending stress due to lateral deflection	displacement-controlled
Beam model (in Chapter 2)	Bending stress due to gravity	load-controlled	Bending stress due to vibrations	Both
Piping model (in Chapter 3)	Bending stress due to spring force	load-controlled	Bending stress due to vibrations	Both

The four models are shown in Figure 4-1. Both the Bree diagram and the Yamashita diagram focused on the thermal ratcheting. The Bree diagram concentrated on the pressurized cylinder subjected to cyclic thermal stresses (Figure 4-1, a). Enhanced creep strains in the elastic region (E), shake-down regions (S), plastic cycling (P), and ratcheting (R) were estimated conservatively in that work (Figure 4-2, a). However, conventional ratcheting models of the pressurized cylinder cannot explain the ratcheting mechanism of bellows, which was the model in the Yamashita diagram. The ratcheting of bellows occurred under the interaction of bending moments between the root and the crown of the bellow. Yamashita et al. proposed a rational-analysis model by using a beam model (Figure 4-1, b). They applied the perfect elastic plasticity with a minimal work-hardening coefficient in the bilinear stress-strain relation and proposed a non-dimensional failure mode map, which had many similarities to the Bree diagram (Figure 4-2, b).

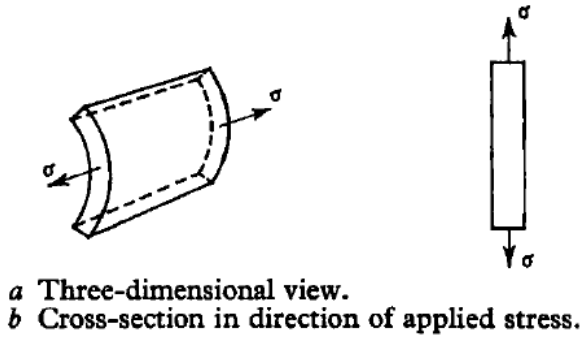

a Three-dimensional view.
b Cross-section in direction of applied stress.

a. Cylinder model in the Bree diagram

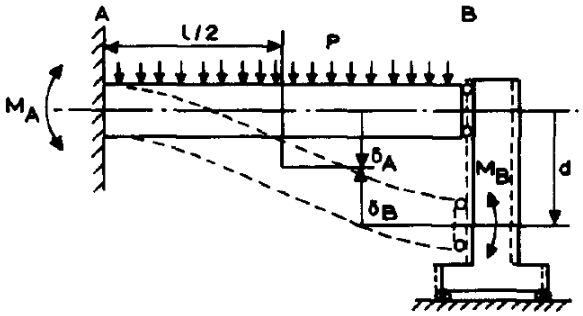

b. Beam model in the Yamashita diagram

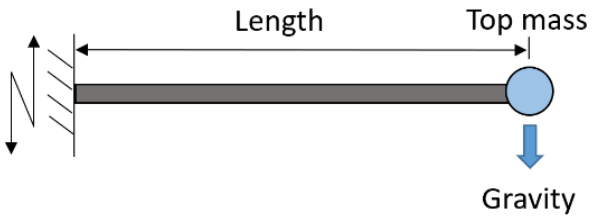

c. Beam model in Chapter 2

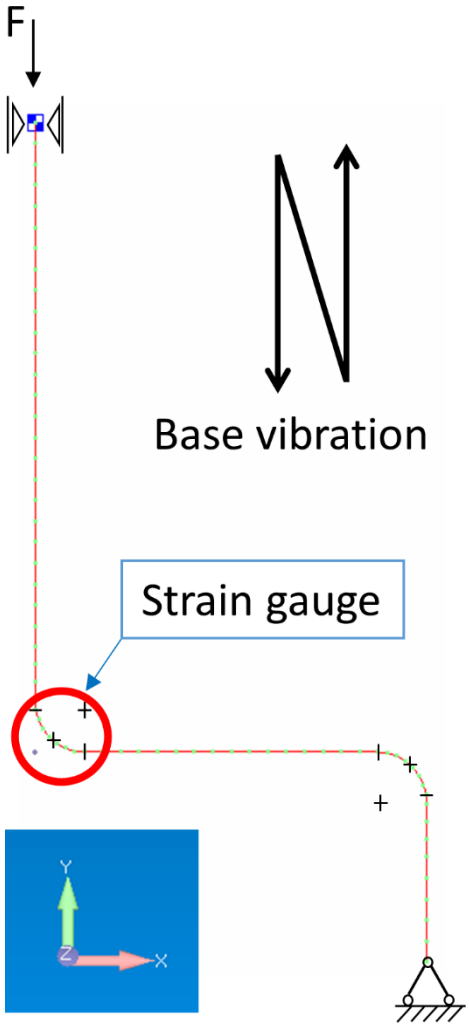

d. Piping model in Chapter 3

Figure 4-1 Comparison among four models

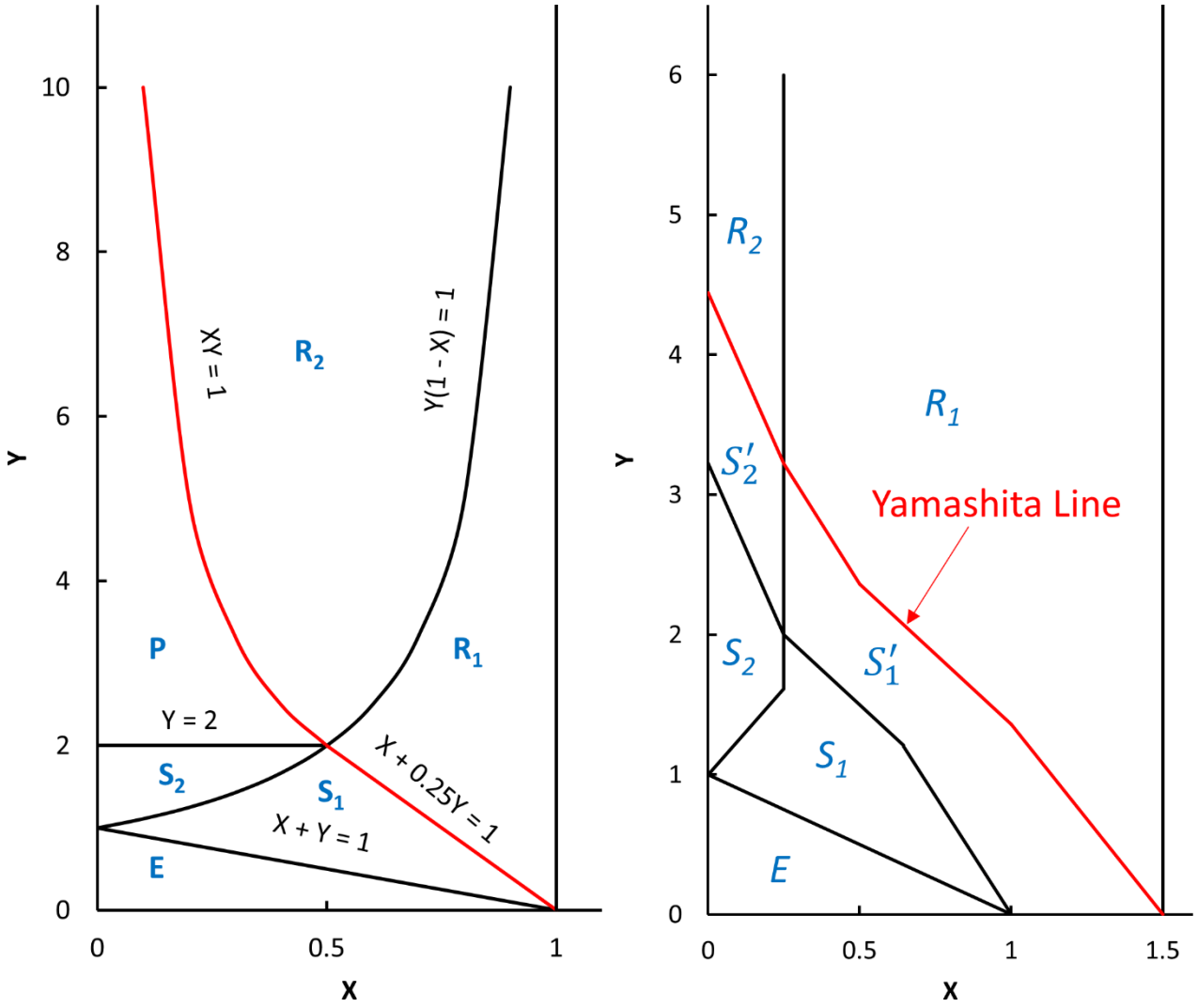

Stress regime	Cylinder behavior
R_1 and R_2	Ratcheting
S_1 and S_2	Shakedown after first half-cycle
P	Plastic cycling
E	Elastic

a. The Bree diagram in non-dimensional form

Stress regime	Beam behavior
R_1 and R_2	Ratcheting
S_1 and S_2 (S_1' and S_2')	Shakedown after first half-cycle
E	Elastic

b. The Yamashita diagram in non-dimensional form

Figure 4-2 Comparison between the Bree diagram and the Yamashita diagram

This research focused on vibration ratcheting. Two models were considered: the bean model (Figure 4-1, c) and the piping model (Figure 4-1, d). The ratcheting occurrence conditions were different between the two models. Seismic ratcheting occurred in the beam model due to the combined effect of load-controlled load (gravity) and alternative cyclic accelerations. In contrast, for the piping model, ratcheting occurred due to the combined effect of constant external compressive force and dynamic cyclic vibrations.

4.1 The Bree diagram and the Yamashita diagram

It is interesting to notice that in the Bree diagram, the ratcheting boundary intersects with the X-axis at 1.0, at which the static collapse occurs. However, in the Yamashita diagram, the Yamashita line intersects with the X-axis at 1.5. This phenomenon is due to the difference in model shapes. Therefore, it is meaningful to consider the shape factor, which is the ratio of the plastic moment to the yield moment. For the model with the rectangular cross section, the shape factor is 1.5. Then the Yamashita line matches well with the Bree diagram, as shown in Figure 4-3. In this figure, the definitions of X' and Y' are shown below:

$$X' = \frac{X}{Shape\ factor} \qquad \text{Equation 4-1}$$

$$Y' = \frac{Y}{Shape\ factor} \qquad \text{Equation 4-2}$$

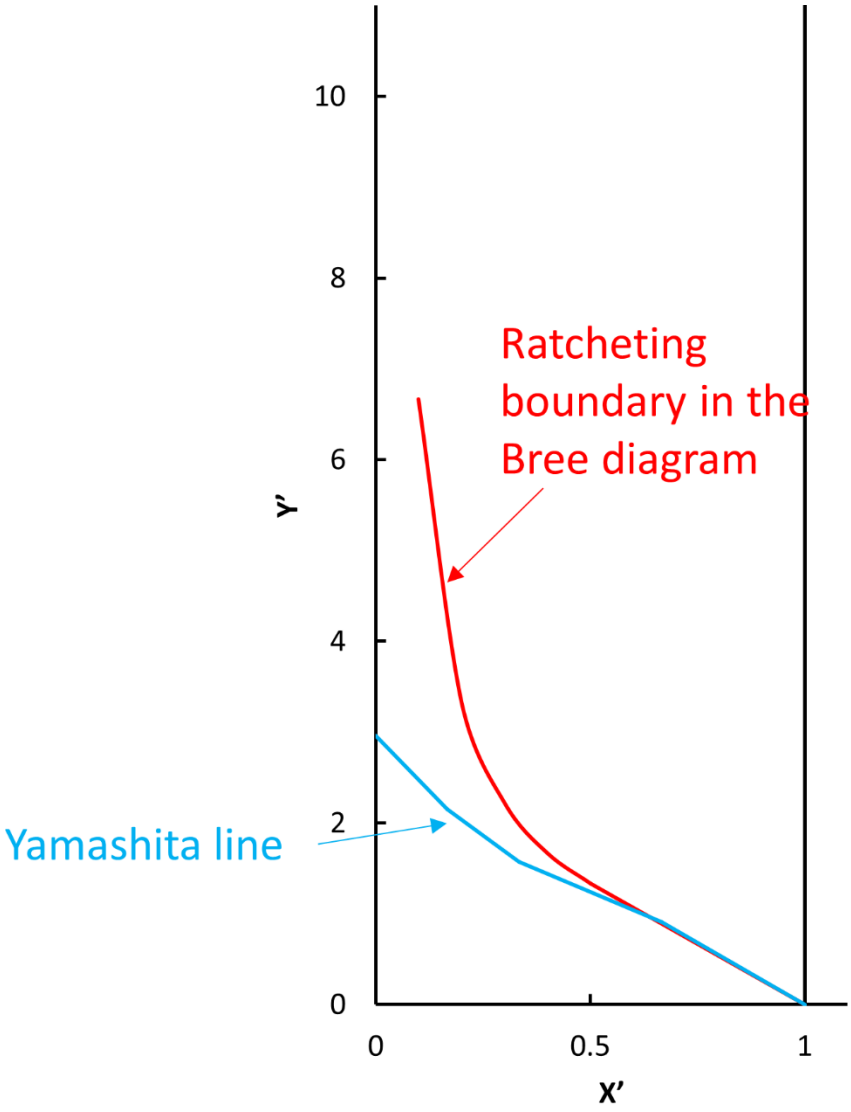

Figure 4-3 Ratcheting boundaries of the Bree diagram and the Yamashita diagram considering the shape factor

4.2 The Yamashita model and the beam model

Frequency-dependent characteristics were the main topic in this research. In addition, since seismic loads have both load-controlled and displacement-controlled characteristics, the recognition according to the frequency is also necessary to prevent related failure modes. The beam model is applied in both the Yamashita model and this research in Chapter 2; therefore, it is meaningful to refer to the Yamashita line to clarify the characteristics of seismic loads. The bending stress due to lateral deflection in the Yamashita model was the displacement-controlled

stress. Therefore, if the ratcheting boundary is close to the Yamashita line in the non-dimensional X-Y diagram, the seismic load is close to the displacement-controlled load. The analyses of the ratcheting occurrence condition of the beam model in Chapter 2 contains such comparison. For convenience, the ratcheting diagram of numerical results under the SIN accelerations (Figure 2-23) is repeated here. The analogy between the Yamashita line and the ratcheting boundary of 1.75 fn proves that the load at 1.75 fn had displacement-controlled characteristics.

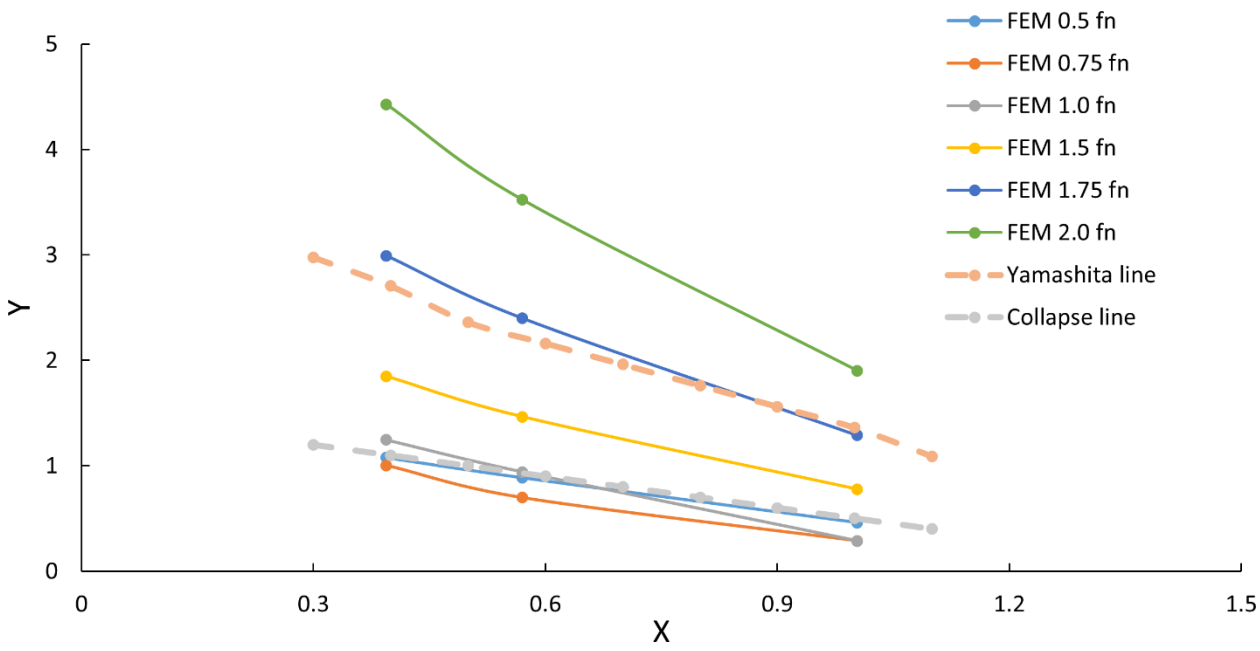

Figure 4-4 Ratcheting diagram of the beam model under the SIN accelerations

If considering the shape factor, it will be interesting to find that all ratcheting boundaries intersect with the X-axis at 1.0, as shown in Figure 4-5. The Yamashita line is also added neglecting the influence of shape and matches well with the 1.75 fn.

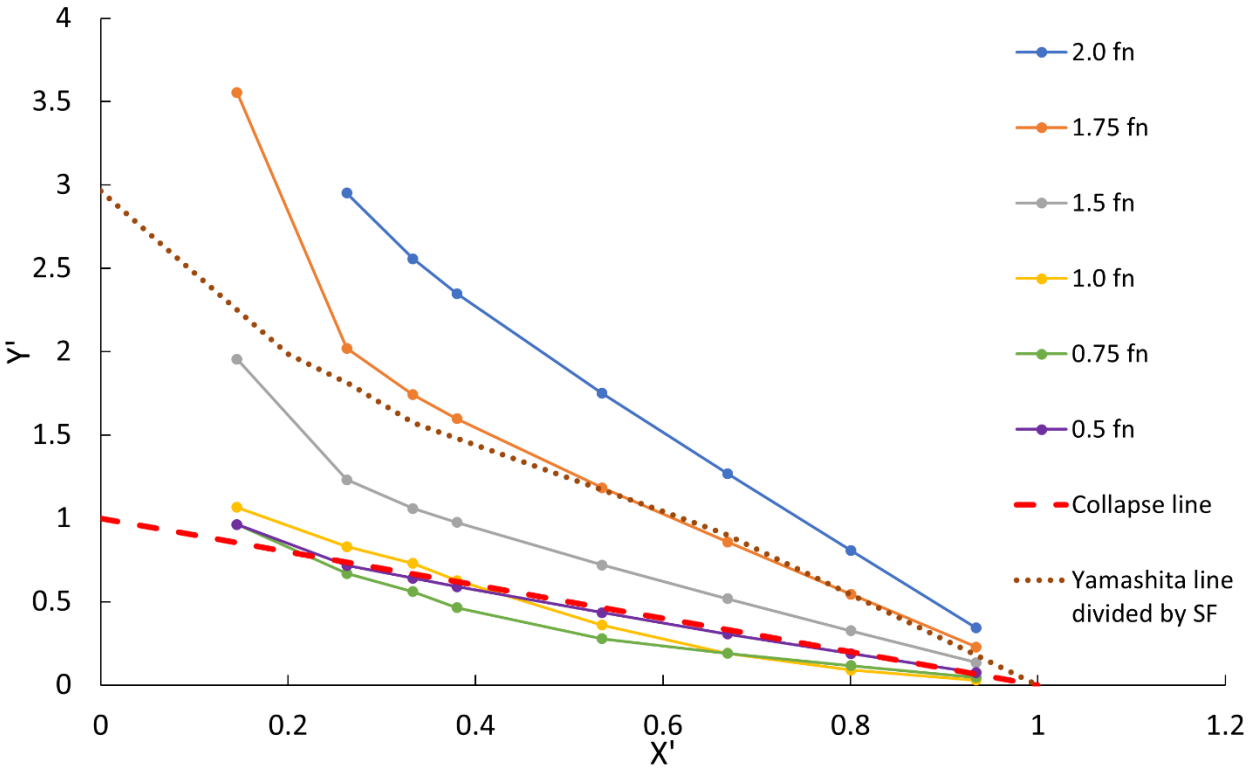

Figure 4-5 Revised ratcheting diagram of the beam with the neglection of shape effect

4.3 The piping model in X'-Y' diagram

The shape factor of the piping is not easy to calculate since the piping model is complex, and the work hardening should also be included. Instead, the collapse load was calculated to clarify the occurrence conditions of collapse. Figure 4-6 and Figure 4-7 show the load parameters against the deformation parameters of two different piping models. According to the ASME B&PV Code Section VIII Division 2 Appendix 4 [50] [60], the collapse load is defined by using the Twice Elastic Slope (TES) criterion for a characteristic load-deformation curve. As shown in the two pictures, TES lines are then drawn from the origin with the slope as twice the slope of the initial elastic response relative to the load axis. The collapse load is the load corresponding to the intersection of the TES line and the load-deformation curve.

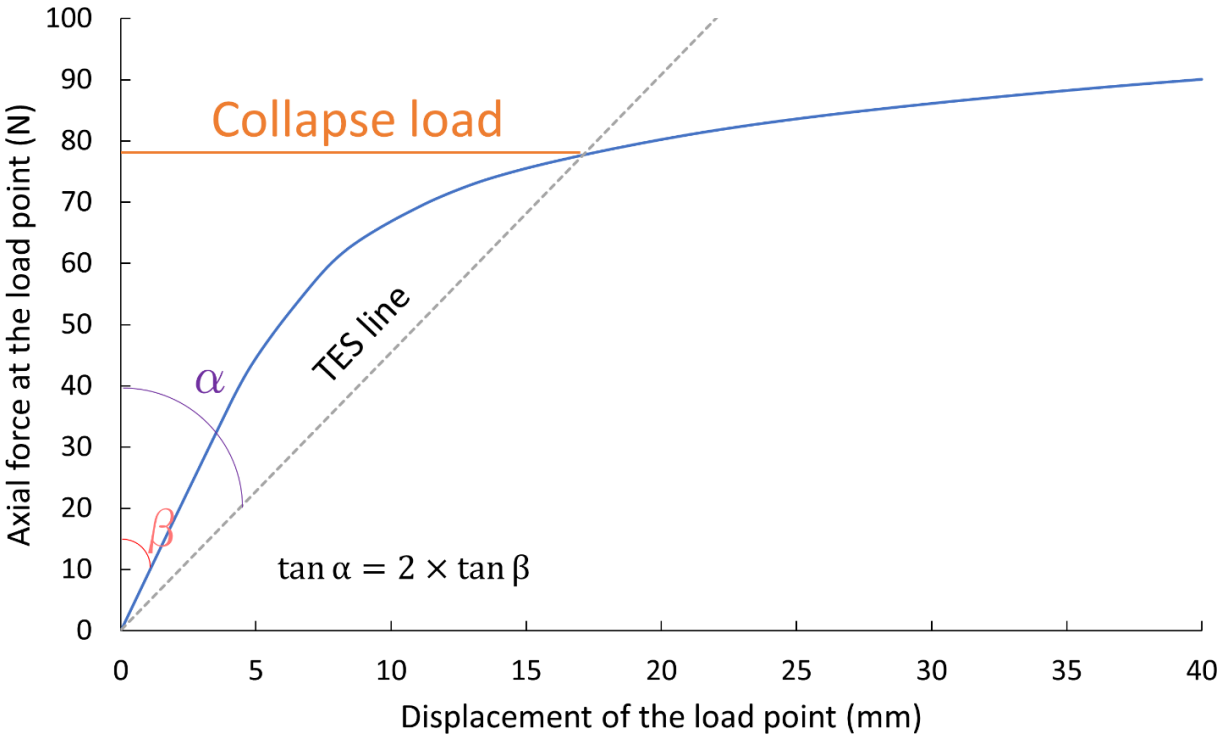

Figure 4-6 The load-deformation curve for Piping-N

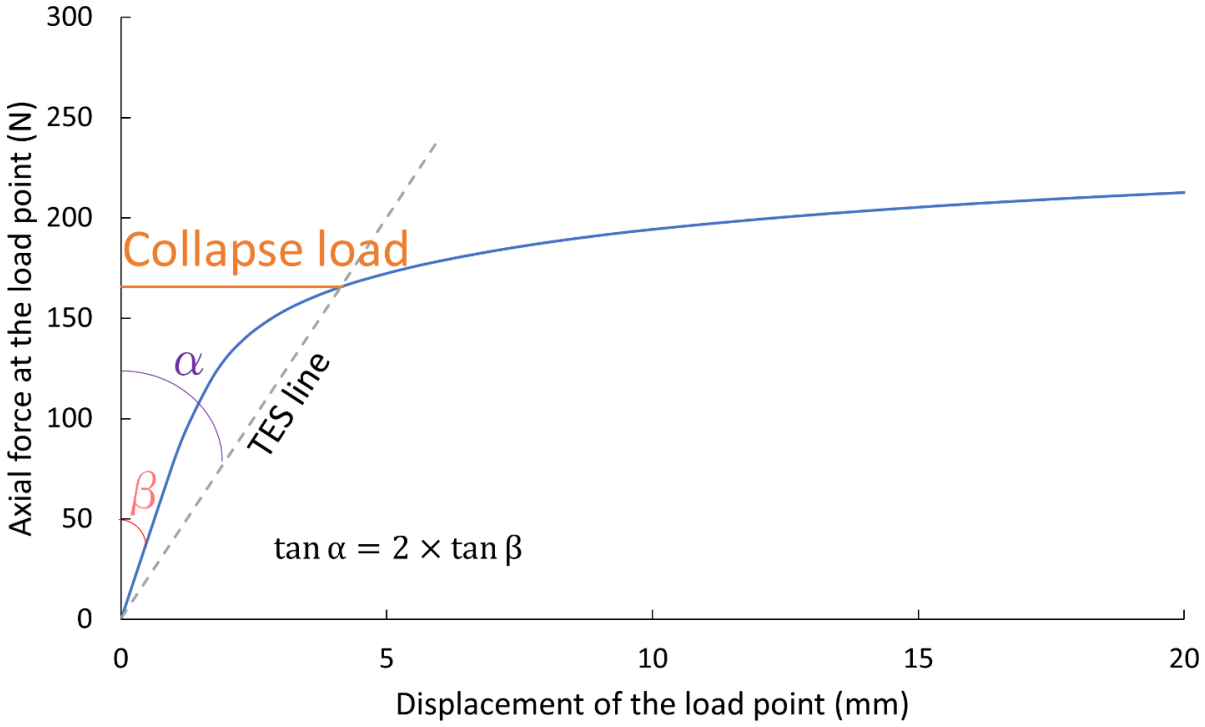

Figure 4-7 The load-deformation curve for Piping-S

Then the ratcheting diagrams of the piping model are shown in Figure 4-8 and Figure 4-9 with the consideration of shape factors, work hardening, etc. The parameter X' is defined as the ratio the spring load to the collapse load, and Y' is adjusted accordingly. Similar to the Beam model, the Yamashita line is still very close to the 1.75 fn line, especially for the piping without external supports. All ratcheting boundaries intersect with the X-axis at around 1.0.

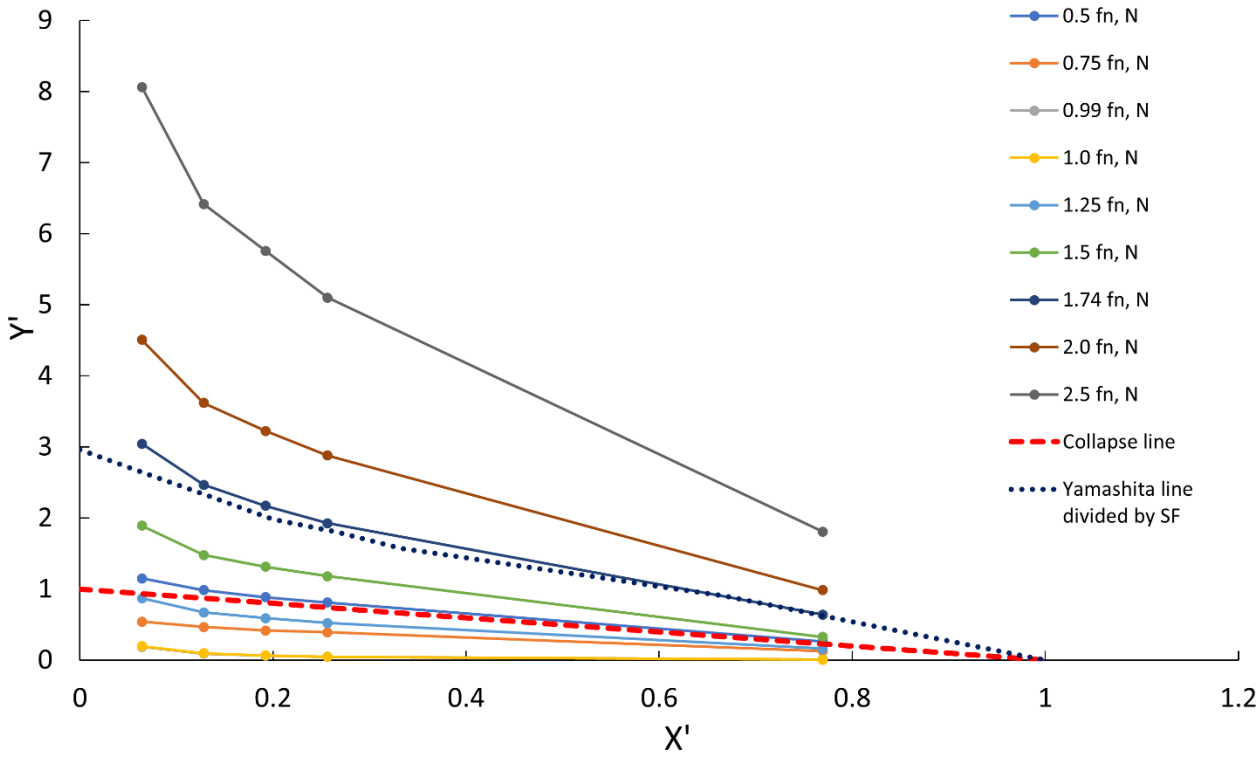

Figure 4-8 Revised ratcheting diagram of Piping-N

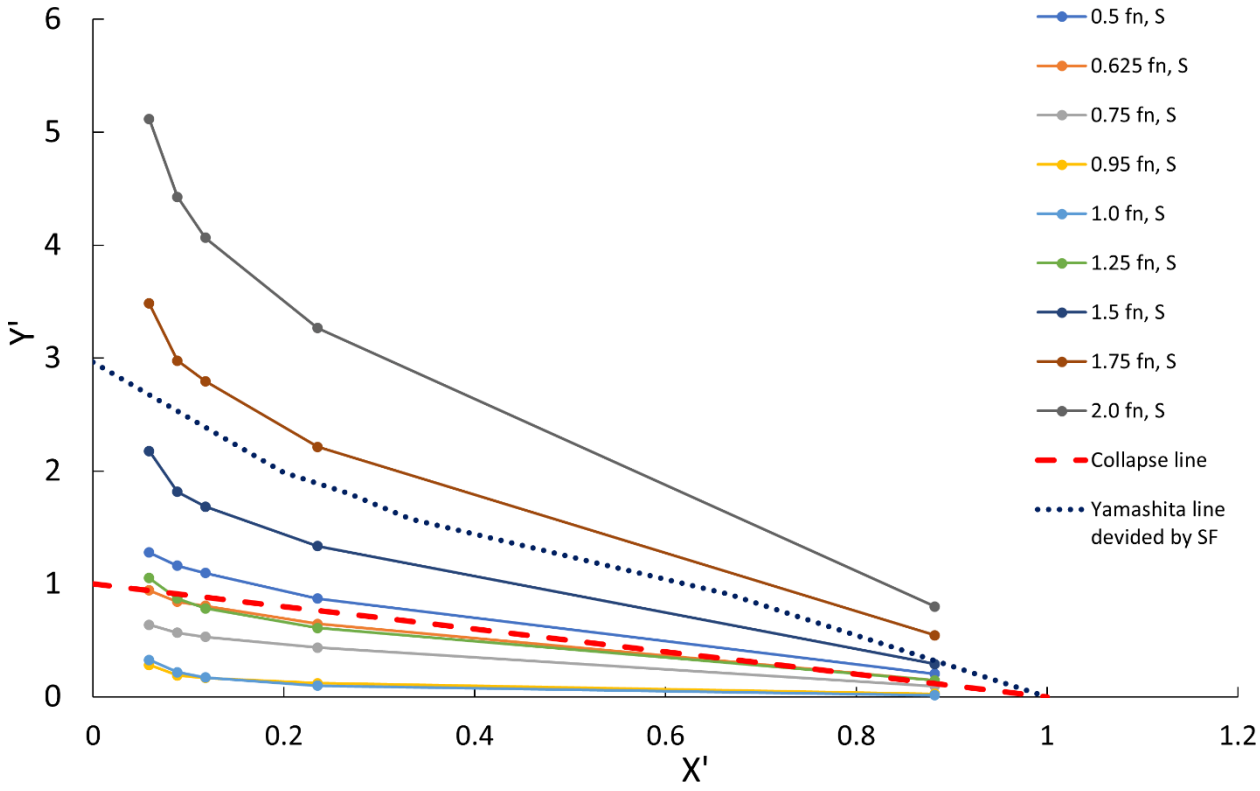

Figure 4-9 Revised ratcheting diagram of Piping-S

If we compare the two piping models in the X'-Y' diagram, the difference between the two types of piping models is also negligible as shown in Figure 4-10, which is similar to Figure 3-37 since X' and Y' are converted from X and Y with the same ratio.

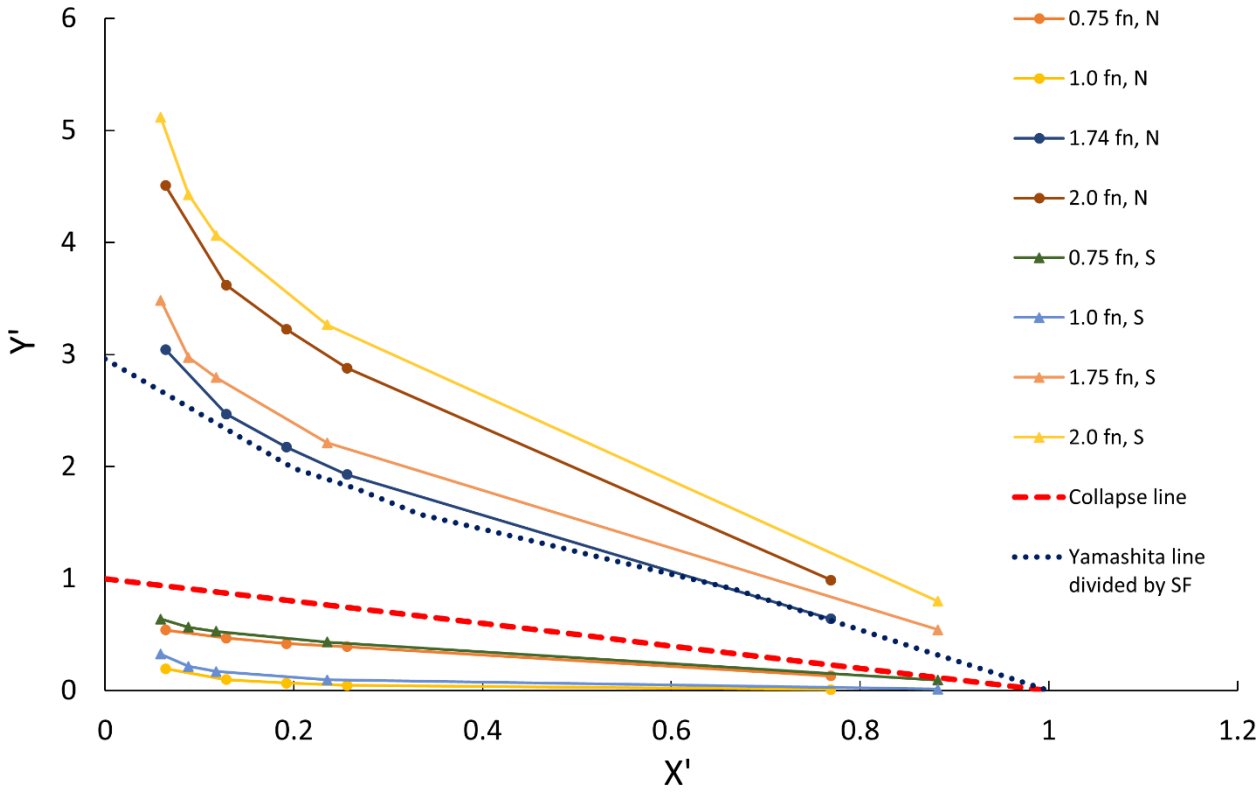

Figure 4-10 Comparison of ratcheting occurrence conditions between the two types of piping models in the X'-Y' diagram

4.4 Normalized vibration ratcheting diagram

In Chapter 3, the ratcheting analyses were to extend the realistic, intricate piping. The beam model and the piping model are closely connected; therefore, it is meaningful to compare the phenomenon between the two models. For example, the apparent frequency-dependent characteristic was found in both models. On the other hand, the resonance effect was not evident in the beam model; however, it was evident in the piping model (Figure 4-11). This difference was due to the distribution of plastic deformation, which caused the difference in the damping effect in the two models. In addition, the plastic deformation decreased the system's natural frequency, especially the beam model. Therefore, in the beam model, the lowest Y values were around 0.75 fn. In contrast, for the piping model, the lower Y values occurred around 1.0 fn due to smaller plastic deformation.

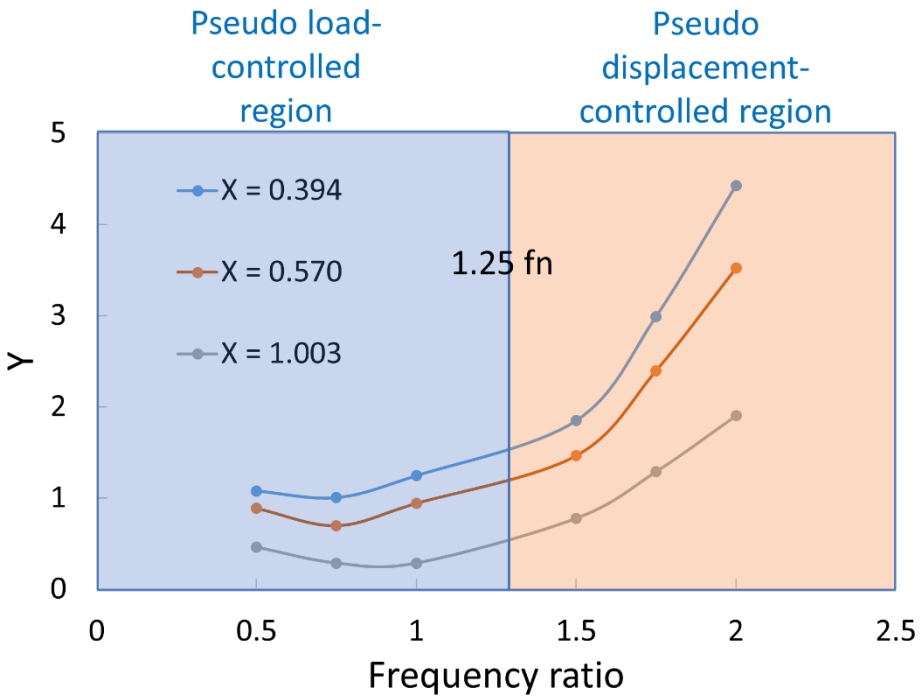

a. Two parts in the beam model, according to the frequency ratio.

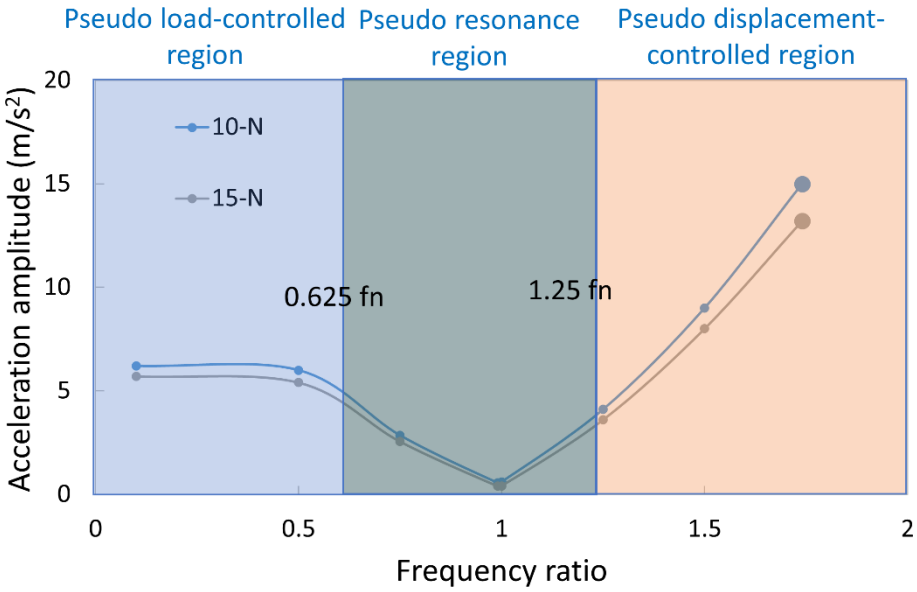

b. Three parts in the piping model, according to the frequency ratio.

Figure 4-11 The difference in the frequency-dependent characteristics among the beam and the piping models in this research

Figure 4-12 compares the ratcheting occurrence conditions of the Yamashita model, the beam model in Chapter 2, and the piping model in Chapter 3. This figure is called the “normalized vibration ratcheting diagram” since the ratcheting occurrence conditions with different materials and shapes can be displayed in one non-dimensional diagram. Since the ratcheting diagrams of Piping-N and Piping-S are similar to each other, for conciseness, Figure 4-12 only contains ratcheting boundaries of Piping-N. The Yamashita line agrees well with both the beam model and the piping model at higher forcing frequencies, which means that the two models have displacement-controlled characteristics with higher frequencies. All ratcheting boundaries intersect with the X’-axis at around 1.0 since this point means the occurrence of static collapse. At lower X’ values, the beam model and the piping model have some differences mainly due to the shape. In the complex piping model, plastic deformation concentrated on the parts of the elbow and around the supports. Therefore, even at lower X’ values, some ratcheting boundaries of the piping elbow part are below the collapse line. In contrast, plastic deformation distributed continuously in the whole beam; therefore, ratcheting boundaries of the beam root parts are higher than those of the piping elbow parts. Another important factor is the resonance effect. The plastic region of the piping model was smaller than the beam model. Therefore, the resonance effect was stronger in the piping model. With the increase of the plastic deformation, the resonance effect became weaker. Therefore, the ratcheting boundaries were close to the beam model at larger X’ values.

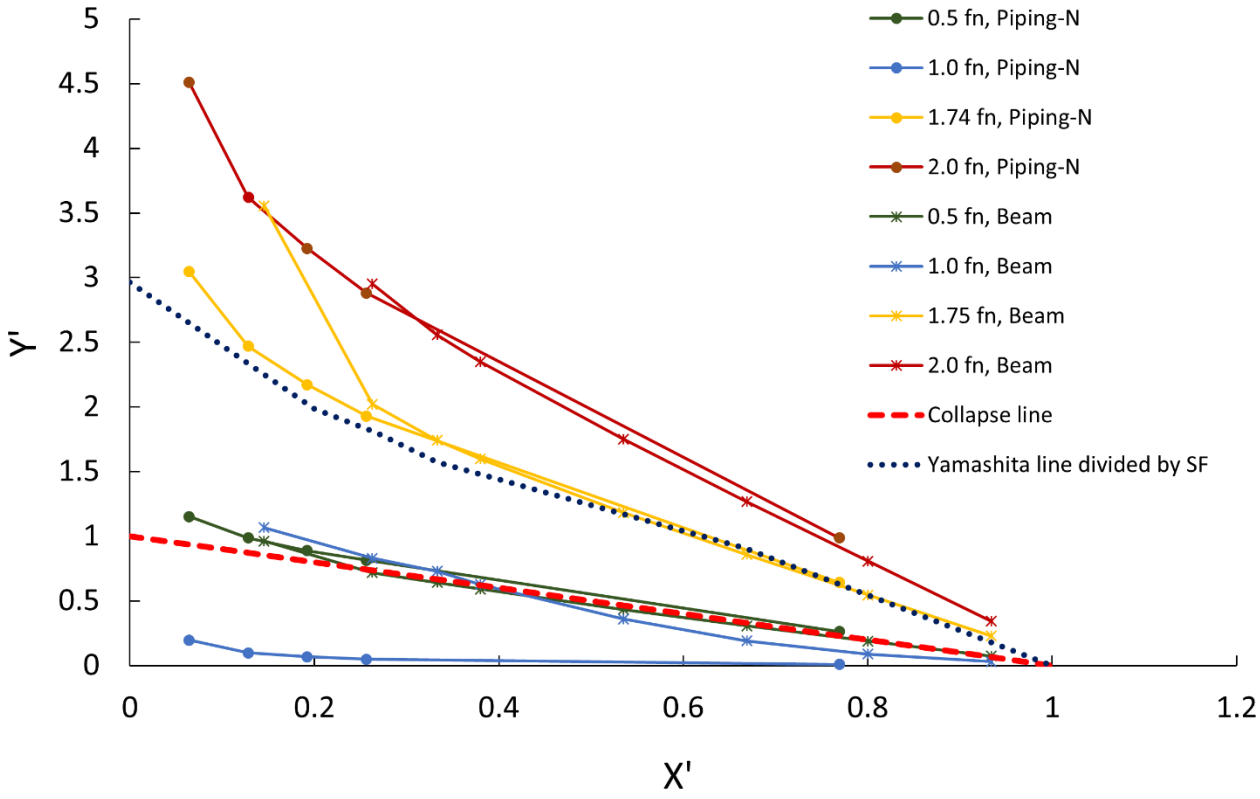

Figure 4-12 Normalized vibration ratcheting diagram

Chapter 5. Conclusions

This research focused on the vibration ratcheting of the beam and the piping model. The mechanism is clarified as follows:

Vibration ratcheting occurred under the combination of constant loads, such as gravity or external force, and cyclic vibration loads. There were evident frequency-dependent characteristics for the occurrence of vibration ratcheting. The seismic load had both natures of load-controlled and displacement-controlled types. It was close to the load-controlled type in the region lower than the natural frequency of the structure, and near the displacement-controlled type in the high-frequency region. This phenomenon could be identified using the frequency ratio, which was the ratio of the frequency of loading vibrations to the system's natural frequency. Besides, ratcheting occurred easily with a lower frequency ratio in both beam and piping models.

It was meaningful to use the simple SIN wave instead of the complicated seismic wave to judge the occurrence of ratcheting if the frequency of the SIN wave was close to the major frequency of the seismic wave.

In the piping model, supports increased the natural frequency of piping and decreased the frequency ratio. Therefore, in terms of the occurrence of ratcheting, providing more supports sometimes did not mean increasing the safety of piping.

Since there were many consistent mechanisms in the beam and piping models, it was meaningful to compare ratcheting occurrence conditions of the Yamashita model, the beam model in Chapter 2, and the piping model in Chapter 3 in one normalized diagram. This non-dimensional diagram was called the “normalized vibration ratcheting diagram” in this research, which accounted for the effect of material and shapes. Comparing to the Yamashita line, loading waves with lower frequency had load-controlled characteristics, and the waves with higher frequencies were close to the displacement-controlled loads. All ratcheting boundaries intersected with the X’-axis at 1.0 since this point meant the occurrence of static collapse. At lower X’ values, they had some

differences mainly due to the difference in plastic deformation, which caused differences in the resonance effect. If the damping due to the plastic deformation became larger, the resonance effect reduced. In this situation, the ratcheting behavior of the piping model was closer to the beam model.

Further study for countermeasures against ratcheting

In terms of the countermeasures against the occurrence of ratcheting, from the conclusions of this research, decreasing the system's natural frequency and increasing the forcing frequencies can help to increase the frequency ratio. Then the system under such vibrations would have displacement-controlled characteristics. Decreasing the load-controlled load (e.g., gravity or external force) helps to decrease the X value. Therefore, ratcheting would be more difficult to occur. In addition, controlling the natural frequencies of the system can also avoid resonance under external excitations. The stiffness of the system is one important factor in altering the natural frequencies. Introducing a damping or energy-dissipating mechanism can help to control vibrations. Vibration isolation can also be applied to reduce the undesirable effects of vibrations [61].

Nomenclature

FEA	Finite element analyses
FEM	Finite element method
BDBEs	Beyond design basis accidents
DBEs	Design basis events
DECs	Design extension conditions
DiD	Defence in depth
PRA	Probabilistic risk assessment
P	Probability
C	Consequent damage
fn	Natural frequency
fi	Forcing frequency
fr	Frequency ratio
SIN excitations	Sinusoidal excitations
SIN+SIN excitations	Superposition of two sinusoidal acceleration excitations
Pb-Sb	Lead-antimony
A	Amplitude of input acceleration
E	Young’s modulus
ν	Poisson's ratio
σ_p	Pressure stress
σ_t	Thermal stress
σ_y	Yield stress
σ_g	Bending stress caused by the gravity of the top mass
σ_i	Bending stress caused by the peak floor acceleration
M_g	Moment caused by gravity
M_i	Moment caused by inertia force

Z	Section modulus
l, d, h, l_{mass}, l_{rod}, l_1, l_2,	Geometrical parameters of the beam model
a	Acceleration amplitude
X	Non-dimensional primary stress parameter
Y	Non-dimensional secondary stress parameter
Piping-N	the piping model without additional supports
Piping-S	the piping model with three supports in the medium part
ρ	Mass density
TES	Twice Elastic Slope

Reference

[1] William D. Magwood IV, Niel Jean-Christophe, Fuketa Toyoshi, Brian Sheron, Michael Boyd, Ann McGarry, and Dussart-Desart Roland. Five Years after the Fukushima Daiichi Accident: Nuclear Safety Improvements and Lessons Learnt. Organisation for Economic Co-Operation and Development. 2016.

[2] Srinivasan TN, and Gopi Rethinaraj TS. Fukushima and thereafter: Reassessment of risks of nuclear power. Energy Policy. 2013;

[3] Wittneben Bettina BF. The impact of the Fukushima nuclear accident on European energy policy. Environmental Science and Policy. 2012;

[4] IAEA. The Fukushima Daiichi Accident: Description and Context of the Accident. The Fukushima Daiichi Accident Vol. 1/5. 2015.

[5] Director General of International Atomic Energy Agency (IAEA). The Fukushima Daiichi Accident Report. IAEA. 2015.

[6] Hatamura Yotaro, Abe Seiji, Fuchigami Masao, Kasahara Naoto, and Iino Kenji. The 2011 Fukushima Nuclear Power Plant Accident: How and Why It Happened. The 2011 Fukushima Nuclear Power Plant Accident: How and Why It Happened. 2014.

[7] Tokyo Electric Power Company Inc. Fukushima nuclear accident analysis report. Press Corporation Limited. 2012;

[8] Lee Chang Jae, Baek Seung Min, and Lee Sang Jeong. Setpoint methodology improvement considering beyond design basis events for safety-related instrumentation. IEEE Transactions on Nuclear Science. 2014;

[9] Kutkov VA, Tkachenko VV, and Saakian SP. Basic strategies of public protection in a nuclear power plant beyond—Design basis accident. Nuclear Energy and Technology. 2016;

[10] Kasahara Naoto, Nakamura Izumi, Machida Hideo, Okamoto Koji, and Sato Takuya. Structural analysis approach for risk assessment under BDBE. American Society of Mechanical Engineers, Pressure Vessels and Piping Division (Publication) PVP. 2016.

[11] Viktorov Alex, and Harwood Christopher. Design extension conditions concept and its

application to operating reactors in Canada. International Nuclear Safety Journal. 2015;4:13–23.

[12] International Atomic Energy Agency. Nuclear Power Plant Operating Experience from the IAEA/NEA International Reporting System for Operating Experience 2012–2014. Vienna: IAEA; 2018.

[13] Kasahara Naoto, Sato Takuya, Wakai Takashi, and Nakamura Izumi. Application of Fracture Control to Nuclear Components for Mitigation of Accident Consequence. SMiRT 25. Charlotte, USA: IASMiRT; 2019.

[14] Kasahara Naoto, and Sato Takuya. Difference of strength evaluation approach between for DBE and for BDBE. Proceedings of the ASME 2017 Pressure Vessels and Piping Conference. Waikoloa, Hawaii, USA: ASME; 2017. p. Volume 3B: Design and Analysis.

[15] International Atomic Energy Agency. Safety of nuclear power plants: Design. IAEA Safety Standards Series No. SSR-2/1 (Rev. 1). IAEA Safety Standards. Vienna: IAEA; 2016.

[16] Galiev Ilnar I, Chernyaev Alexey N, and Bibik Stanislav V. Development of seismic protection system for design extension conditions. Nuclear Energy and Technology. 2018;4:43.

[17] International Atomic Energy Agency. Safety of Nuclear Power Plants: Design, IAEA Safety Standards Series No. NS-R-1. Vienna: IAEA; 2000.

[18] Agency International Atomic Energy. Considerations on the Application of the IAEA Safety Requirements for the Design of Nuclear Power Plants, IAEA-TECDOC-1791. International Atomic Energy Agency Vienna; 2016.

[19] Lachaume Jean-Luc, Miller Douglass, Rzentkowski Greg, Lahtinen Nina, Valtonen Keijo, Foucher Laurent, Harikumar Shri S, Yamada Tomoho, Sharafutdinov Rashet, and Kuznetsov Mark. Implementation of Defence in Depth at Nuclear Power Plants. Lessons Learnt from the Fukushima Daiichi Accident. Organisation for Economic Co-Operation and Development; 2016.

[20] Kasahara Naoto, and Sato Takuya. Necessity of best estimate strength evaluation considering failure modes for BDBE. 2017;

[21] Kammerer AM, Whittaker AS, and Constantinou MC. Technical considerations for seismic isolation of nuclear facilities. United States Nuclear Regulatory Commission, Office of Nuclear Regulatory …; 2019.

[22] Burby Raymond J, Deyle Robert E, Godschalk David R, and Olshansky Robert B. Creating hazard resilient communities through land-use planning. Natural Hazards Review. 2000;

[23] Lindell Michael K, and Prater Carla S. Assessing community impacts of natural disasters. Natural Hazards Review. 2003;

[24] Humar Jag Mohan, and Mahgoub Mohamed A. Determination of seismic design forces by equivalent static load method. Canadian Journal of Civil Engineering. 2003;

[25] Basu Prabir C, Ravindra MK, and Mihara Yoshinori. Component fragility for use in PSA of nuclear power plant. Nuclear Engineering and Design. 2017;

[26] Al Bari Md Abdullah, Sakemi Ryota, Katsura Yamato, and Kasahara Naoto. Proposal of Failure Mode Map Under Dynamic Loading - Ratcheting and Collapse. Journal of Pressure Vessel Technology, Transactions of the ASME. 2018;

[27] Kasahara Naoto, Al Bari Md Abdullah, and Sakemi Ryota. Failure modes of piping under seismic loads which have both load and displacement controlled characteristics. International Journal of Pressure Vessels and Piping. 2020;179:103938.

[28] IAEA. Seismic hazards in site evaluation for nuclear installations SSG-9. IAEA SSafety Standards. 2010;

[29] ASME Standard. 2017 Boiler and Pressure Vessel Code, An International Code BPVC17. ASME Boiler and Pressure Vessel Code. 2017;

[30] Electric Power Research Institute. Guidelines for Nuclear Power Plant Response to an Earthquake. 2015.

[31] Kasahara Naoto, Nakamura Izumi, Machida Hideo, and Nakamura Hitoshi. Research plan on failure modes by extreme loadings under design extension conditions. American Society of Mechanical Engineers, Pressure Vessels and Piping Division (Publication) PVP. 2014;1:1–8.

[32] ICHIHASHI Ichiro. Sine collapse tests for the large scale models of the nuclear reactor

facilities by shaking table. Journal of JAEEJournal of Japan Association for Earthquake Engineering. 2004;

[33] Tagart Sam W, Tang YK, Guzy Daniel J, and Ranganath Sam. Piping dynamic reliability and code rule change recommendations. Nuclear Engineering and Design. 1990;123:373–385.

[34] Nakamura Izumi, Otani Akihito, and Shiratori Masaki. Comparison of failure modes of piping systems with wall thinning subjected to in-plane, out-of-plane, and mixed mode bending under seismic load: An experimental approach. Journal of Pressure Vessel Technology, Transactions of the ASME. 2010;132:0310011–0310018.

[35] Varelis George E, Karamanos Spyros A, and Gresnigt Arnold M. Pipe elbows under strong cyclic loading. Journal of Pressure Vessel Technology, Transactions of the ASME. 2013;135:1–9.

[36] Ravikiran A, Dubey PN, Agrawal MK, Reddy GR, Singh RK, and Vaze KK. Experimental and numerical studies of ratcheting in a pressurized piping system under seismic load. Journal of Pressure Vessel Technology, Transactions of the ASME. 2015;137.

[37] Nakamura Izumi, and Kasahara Naoto. Discussion on failure behavior of piping systems subjected to excessive seismic loads. In: SMiRT 25, editor. Charlotte, USA: IASMiRT; 2019.

[38] Mahbadi H, and Eslami MR. Cyclic loading of beams based on the Prager and Frederick–Armstrong kinematic hardening models. International journal of mechanical sciences. 2002;44:859–879.

[39] Shi Hongrui, Chen Gang, Wang Yong, and Chen Xu. Ratcheting behavior of pressurized elbow pipe with local wall thinning. International Journal of Pressure Vessels and Piping. 2013;

[40] Yazdani H, and Nayebi A. Continuum damage mechanics analysis of thin-walled tube under cyclic bending and internal constant pressure. International Journal of Applied Mechanics. 2013;

[41] Chen Haofeng, Chen Weihang, Li Tianbai, and Ure James. On shakedown, ratchet and

limit analyses of defective pipeline. Journal of Pressure Vessel Technology, Transactions of the ASME. 2012;

[42] Boiler ASME, and Code Pressure Vessel. Section III, Division 1, Subsection NH. American Society of Mechanical Engineers. 2007;

[43] Bree J. Elastic-plastic behaviour of thin tubes subjected to internal pressure and intermittent high-heat fluxes with application to fast-nuclear-reactor fuel elements. Journal of Strain Analysis. 1967;2:226–238.

[44] Yamashita T, Tsukimori K, Nakamura M, Iwata K, and Imazu A. A simplified method of evaluating ratcheting in bellows and a test of its validation. International Journal of Pressure Vessels and Piping. 1990;42:263–285.

[45] Meyer Jimmy E, and Frey Joe. ASME Piping Code: B31.1, Power Piping. In: Rao KR, editor. Companion Guide to the ASME Boiler and Pressure Vessel Code, Volume 2, Fourth Edition. ASME Press; 2012. p. 0.

[46] JSME. Design and Construction for Nuclear Power Plants. JSME; 2009.

[47] Association française pour les règles de conception de construction et surveillance en exploitation des matériels des chaudières électro-nucléaires. RCC-MR: Design and Construction Rules for Mechanical Components of Nuclear Installations. AFCEN; 2007.

[48] Abdel-Karim Mohammad. Shakedown of complex structures according to various hardening rules. International Journal of Pressure Vessels and Piping. 2005;82:427–458.

[49] Chen Xiaohui, Chen Xu, Yu Dunji, and Gao Bingjun. Recent progresses in experimental investigation and finite element analysis of ratcheting in pressurized piping. International Journal of Pressure Vessels and Piping [Internet]. 2013;101:113–142. Available from: http://dx.doi.org/10.1016/j.ijpvp.2012.10.008.

[50] ASME. ASME Boiler and Pressure Vessel Code Section VIII: Division 1 & 2. The American Society of Mechanical Engineers. 2018;

[51] Nakamura Izumi, Demachi Kazuyuki, and Kasahara Naoto. AN EXPERIMENTAL INVESTIGATION ON FAILURE MODES OF PIPING COMPONENTS UNDER EXCESSIVE SEISMIC LOAD. SMiRT-23. 2015.

[52] Nakamura Izumi, and Kasahara Naoto. Trial model tests with simulation material to

obtain failure modes of pipes under excessive seismic loads. American Society of Mechanical Engineers, Pressure Vessels and Piping Division (Publication) PVP. 2016.

[53] Nakamura Izumi, and Kasahara Naoto. Improved model tests to investigate the failure modes of pipes under beyond design basis earthquakes. Pressure Vessels and Piping Conference. American Society of Mechanical Engineers; 2018. p. V03AT03A048.

[54] Corporation ITOCHU Techno-Solutions. FINAS/STAR r 160826 user manual. ITOCHU Techno-Solutions Corporation; 2015.

[55] Siemens Product Lifecycle Management Software Inc. FEMAP User Guide Version 10. Siemens Product Lifecycle Management Software Inc, Munich–Germany. 2009.

[56] Rao S Singiresu, and Yap Fook Fah. Mechanical vibrations, 5th Edittion. New York: Addison-Wesley; 2011.

[57] Yagi Yuji, Okuwaki Ryo, Enescu Bogdan, Kasahara Amato, Miyakawa Ayumu, and Otsubo Makoto. Rupture process of the 2016 Kumamoto earthquake in relation to the thermal structure around Aso volcano. Earth, Planets and Space. 2016;

[58] Resilience National Research Institute for Earth Science and Disaster. NIED K-NET, KiK-net, National Research Institute for Earth Science and Disaster Resilience. 2019;

[59] Rao KR. Companion guide to the ASME boiler & pressure vessel code: criteria and commentary on select aspects of the boiler & pressure vessel and piping codes. ASME Press; 2006.

[60] Ju Bu Seog, Tadinada Sashi Kath, and Gupta Abhinav. Fragility analysis of threaded T-joint connections in hospital piping systems. American Society of Mechanical Engineers, Pressure Vessels and Piping Division (Publication) PVP. 2011.

[61] Celebi Mehmet. Design of Seismic Isolated Structures: From Theory to Practice . Earthquake Spectra. 2000;

Publication Lists

Peer-Reviewed Journal Paper

1. **Jinqi Lyu**, Masakazu Ichimiya, Ryunosuke Sasaki, and Naoto Kasahara. Frequency effect on the occurrence of ratcheting. Journal of Pressure Vessel Technology, ASME. (Preparing)
2. **Jinqi Lyu**, Masakazu Ichimiya, Ryunosuke Sasaki, and Naoto Kasahara. Ratcheting occurrence conditions of piping under sinusoidal excitations. Mechanical Engineering Journal, JSME (2020): 20-00167.
3. **Jinqi Lyu**, Eun Hyun Ryu, and Joo Hwan Park. Innovative core design using cobalt-equipped bundles for cobalt-60 production in CANDU6 reactors. Annals of Nuclear Energy, 142 (2020): 107384.
4. **Jinqi Lyu**, Masakazu Ichimiya, Md Abdullah Al Bari, Ryunosuke Sasaki, and Naoto Kasahara. Study on ratcheting of beams under the combination of gravity and seismic load. Mechanical Engineering Journal, JSME,7(3) (2020): 19-00384.

Peer-Reviewed International Conference Paper

1. **Jinqi Lyu**, Masakazu Ichimiya, Ryunosuke Sasaki, Md Abdullah Al Bari, and Naoto Kasahara. Analytical and experimental study on ratcheting of beams under seismic loadings. University of Toronto, McMaster University, and the University of Tokyo Joint Workshop (postponed due to COVID-19).
2. Ryunosuke Sasaki, Masakazu Ichimiya, **Jinqi Lyu**, and Naoto Kasahara. Frequency Dependency of Beam Collapse Due to Vibration Loads. Pressure Vessels & Piping Conference 2020, Minneapolis, Minnesota, USA, July 19 – 24, 2020.
3. **Jinqi Lyu**, Md Abdullah Al Bari, and Naoto Kasahara. Fundamental Study on Ratcheting of Piping Systems under Seismic Loadings. 25th International Conference on STRUCTURAL MECHANICS in REACTOR TECHNOLOGY, Charlotte, NC, USA, August 4-9, 2019.
4. **Jinqi Lyu**, Md Abdullah Al Bari, and Naoto Kasahara. STUDY ON RATCHETING OF PIPES UNDER THE COMBINATION OF GRAVITY AND SEISMIC LOAD. The Proceedings of the International Conference on Nuclear Engineering (ICONE), Ibaraki, Japan, May 19-24, 2019.
5. Md Abdullah Al Bari, **Jinqi Lyu**, and Naoto Kasahara. Failure Modes of Piping Components Under Seismic Loading. 11th XJTU-UT-SJTU Joint International Symposium on Nuclear Science and Technology, Fukushima, Japan, August. 1-3, 2018.
6. **Jinqi Lyu**, Mohammad Abdul Motalab, and Yonghee Kim. A Reactor Physics Study on Production of Co-60 Using the CANDU Fuel. 5th International Workshop on "PHWR Challenging Issues and Long-term Sustainability" (CANSAS-2016), Gyeongju, Korea, October 12-14, 2016.

7. **Jinqi Lyu**, Mohammad Abdul Motalab, and Yonghee Kim. Neutronic Analysis of an In-core Co-60 Production Method in CANDU6 Reactors. 13th International Conference on CANDU Fuel, Kingston, Ontario, Canada, August 15-18, 2016.
8. **Jinqi Lyu**, Mohammad Abdul Motalab, Park Younwon, and Kim Yonghee. A Potential Way of Co-60 Production in CANDU6 Reactors. PBNC 2016, Beijing, China, Apr 5 - 9, 2016.
9. **Jinqi Lyu**, Donny Hartanto, Mohammad Abdul Motalab, and Yonghee Kim. Theoretical Potential of the CANDU Core for Transmutation of PWR TRU Nuclides. Proceedings of Reactor Physics Asia 2015 (RPHA15) Conference, Jeju, Korea, Sept 16 - 18, 2015.

Peer-Reviewed Domestic Conference Paper

1. **Jinqi Lyu**, Md Abdullah Al Bari, and Naoto Kasahara. Study on Failure Modes of Piping Structures under Realistic Seismic Waves. 2018 Fall Meeting of AESJ, Okayama University, Okayama, Japan, September 5 - 7, 2018.
2. **Jinqi Lyu**, Woosong Kim, Younwon Park, and Yonghee Kim. A New In-core Production Method of Co-60 in CANDU Reactors. KNS 2016, Jeju, Korea, May 12-13, 2016.

Patent

1. **Jinqi LYU**, Riping Ye, Jiajia Lu, "An Adding-oxygen System Driven by Wind-Solar Hybrid Power and Its Control Method," Granted on Jun 3, 2015 (CN103787519 A).

Award

1. Best Paper. Md Abdullah Al Bari, **Jinqi LYU**, and Naoto Kasahara. Failure Modes of Piping Components Under Seismic Loading. 11th XJTU-UT-SJTU Joint International Symposium on Nuclear Science and Technology, Fukushima, Japan, August. 1-3, 2018.

Acknowledgments

Firstly, I would like to thank my supervisor, Professor Naoto KASAHARA, for his insightful and patient guidance throughout my Ph.D. study and related research. He helped me all the time in the research and writing of this thesis. I quite appreciate that he gave me so many sincere suggestions and I could not have imagined having a better advisor and mentor. With his careful guidance and continuous encouragement, I gradually find my way to the fantastic research world. His suggestions on both research as well as on my life and career have been priceless.

I want to give my deep gratitude to Professor Kazuyuki DEMACHI, Dr. Takuya SATO, and Professor Masakazu ICHIMIYA for their excellent counsel and warm encouragement in this research and my life at the University of Tokyo. I would also to present my special thankfulness to Dr. Izumi NAKAMURA for allowing me to visit their experiments at the National Research Institute for Earth Science and Disaster Resilience.

My thanks also go to the members of my Thesis Defense Committee, Professor Naoto KASAHARA, Dr. Izumi NAKAMURA, Professor Kazuyuki DEMACHI, Professor Tsuyoshi TAKADA, and Professor Shunichi SUZUKI for reading through my thesis and giving insightful comments.

I would also thank my collaborators, Dr. Md Abdullah Al Bari, Dr. Shi CHEN, Mr. Satoru Kai, Mr. Yoshiki TSUNEMOTO, Mr. Ryunosuke SASAKI, and all other laboratory members for their detailed and helpful suggestions on my research and life. My thanks also go to our laboratory staff, Miss Mariko WADA and Miss Ritsuko MITSUBAYASHI for their kind help and support in three years.

My sincere thanks to all the faculty and staff members of the Department of Nuclear Engineering and Management, the University of Tokyo, for their kind patience and support.

My special thanks go to my wife, Dr. Min XIE, for her company, encouragement, and support. I also want to thank my dear parents and my family for their understanding for so many years. Their love and support always make me more than I can be.

2020 is a special year and all the world is under the shadow of COVID-19. I hope the world will push back against fear and isolationism and embrace hope and solidarity in the face of the coronavirus pandemic.

Thank you all.

Jinqi LYU

June 26, 2020